Testing and Modeling of Compressors for Low-Lift Cooling Applications.

by

Ryan Alexander Willingham
B.S. Mechanical Engineering
Georgia Institute of Technology, 2007
and
B.S. Applied Physics
Morehouse College, 2007

MASSACHUSETTS INSTITUTE OF TECHNOLOGY
JUN 16 2009
LIBRARIES

Submitted to the Department of Mechanical Engineering
in partial fulfillment of the requirements for the degree of

Master of Science in Mechanical Engineering

at the

MASSACHUSETTS INSTITUTE OF TECHNOLOGY

ARCHIVES

June 2009

© Massachusetts Institute of Technology 2009. All rights reserved.

Author .....
Department of Mechanical Engineering
May 22, 2009

Certified by .....
Leslie K. Norford
Professor of Building Technology, Department of Architecture
Thesis Supervisor

Certified by .....
Leon R. Glicksman
Professor of Building Technology and of Mechanical Engineering
Thesis Reader

Accepted by ...
David E. Hardt
Chairman, Department Committee on Graduate Students

Testing and Modeling of Compressors for Low-Lift Cooling Applications.

by

Ryan Alexander Willingham

Submitted to the Department of Mechanical Engineering
on May 22, 2009, in partial fulfillment of the
requirements for the degree of
Master of Science in Mechanical Engineering

Abstract

In this thesis, an inverter-driven variable speed scroll compressor is tested on a desuperheater test stand to determine its performance in areas of low-lift and low compressor speed. The goal is to adapt this test stand so that it could be used to test a reciprocating compressor in this region. A control program is written to maintain a constant saturated suction temperature, suction temperature, and saturated discharge temperature. The program was able to maintain control with errors of ± 0.2 °C at most points. At each test point, refrigerant mass flow rate, compressor input power, and discharge temperature is monitored. The amount of heat removed by the condenser was within 7% of the compressor input power and the inverter efficiency was within 5% of the compressor input power for all test points. The inverter efficiency is lowest at low speed. The isentropic efficiency is found to drop off significantly for low pressure ratios. A similar drop off is not expected for reciprocating compressors, so a model for reciprocating compressors is developed. The model is able to predict refrigerant mass flow rate and compressor input power as a function of shaft speed as well as suction and discharge pressures and temperatures. The model is able to accurately predict the mass flow rate with an RMS error within 0.5% and for the power model, the RMS errors are within 3.6%. The mass flow model is found to perform well when extrapolated into lower speed ranges with RMS errors remaining below 0.5%.

Thesis Supervisor: Leslie K. Norford
Title: Professor of Building Technology, Department of Architecture

Thesis Reader: Leon R. Glicksman
Title: Professor of Building Technology and of Mechanical Engineering

Acknowledgments

I would like to think everybody who helped me along the way. Appreciation is due to the MASDAR initiative for their financial support of this project. Steve Holden and Joseph Haller at Carrier Corporation were great resources. A special thanks to Professor Gerald Wilson and David Otten, who, generously, allowed us to use their test stand. Without them much of this thesis would not be possible.

Les–Your guidance and advice along the way was truly priceless. You've been instrumental in seeing that this document came to fruition. Thanks for providing words of encouragement, thoughtful criticism, and helping me throughout my matriculation.

Peter Armstrong–Thanks for insisting on perfection. A great deal of gratitude is owed for all of your support throughout this process. Your wealth of knowledge on, seemingly, every subject has made our many conversations invaluable to me. I learned a great deal working with you, and I am truly grateful.

To my fellow students in the Building Technology Lab, as well as other students within the MIT community (ACME, Heat Transfer Lab, LEES), I thank you for the enumerable times I've had to lean on you. You've helped me in ways, and in a magnitude, in which you probably will never realize.

To my friends and family, thanks for being there, even when I was not. Thanks for keeping me sane, and providing me with a distraction from my work. Your encouragement and belief in my abilities kept me going.

Many long days, and longer nights, but this has been a most rewarding experience.

For my mother: I love you, I miss you.

Contents

List of Figures

List of Tables

Chapter 1

Introduction

1.1 Energy Use in Buildings

Environmental effects, from carbon dioxide emissions to global warming, as well as supply concerns have resulted in a massive effort to greatly reduce our energy demands and utilize the energy we do consume more efficiently. On the supply side, the use of renewable energy sources is fast becoming a viable option. Sources such as photovoltaic (PV) power stations, wind turbines, hydro power and biomass are all being investigated to reduce our dependance on a declining supply of fossil fuels. However, in order to truly address this issue, we must take a serious look at the demand side. Figure 1-1 shows the primary energy consumption in the United States in 2006 [10]. Buildings consumed about 39% of the primary energy in the U.S. in 2006. This illustrates that energy use in buildings cannot be ignored when addressing the issue of energy efficiency. The building sector can be split into two major categories: residential and commercial. Commercial buildings consumed a little less than half of the energy consumed by the building sector; that is, 18% of the total primary energy used in the United States was consumed by commercial buildings.

The breakdown of energy use in buildings is not as clear. Figure 1-2 shows the end use of primary energy in U.S. buildings. However, climate has a great impact on the end use of primary energy in buildings. In hot climates, buildings may use little to no energy on space heating and, conversely, in really cold climates, building cooling

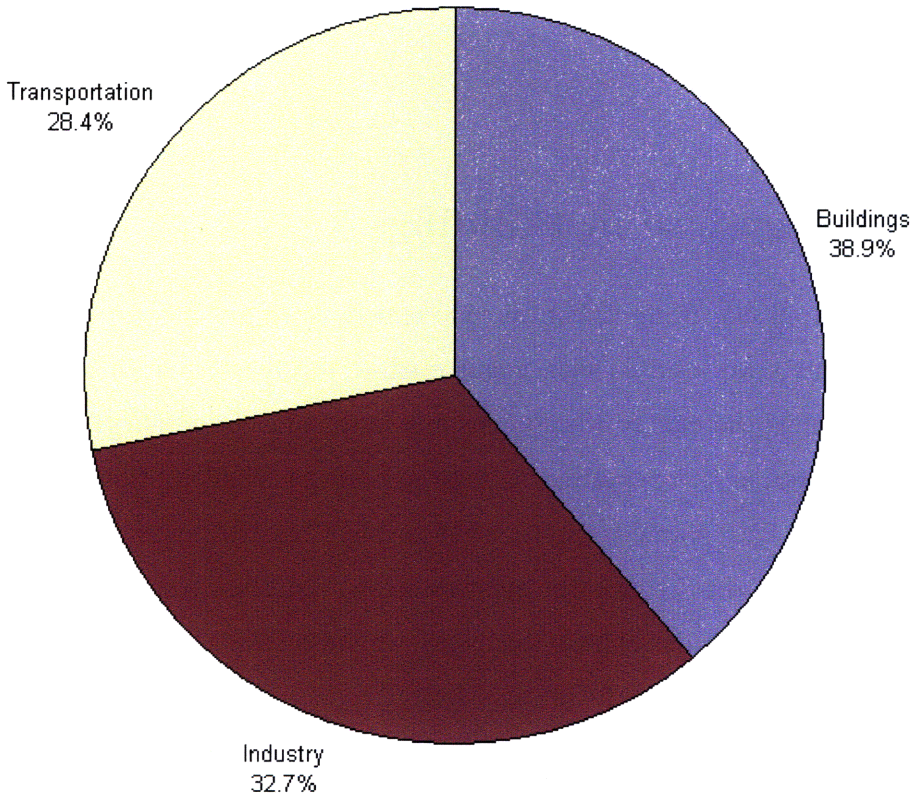

Figure 1-1: 2006 U.S. primary energy consumption by sector[10].

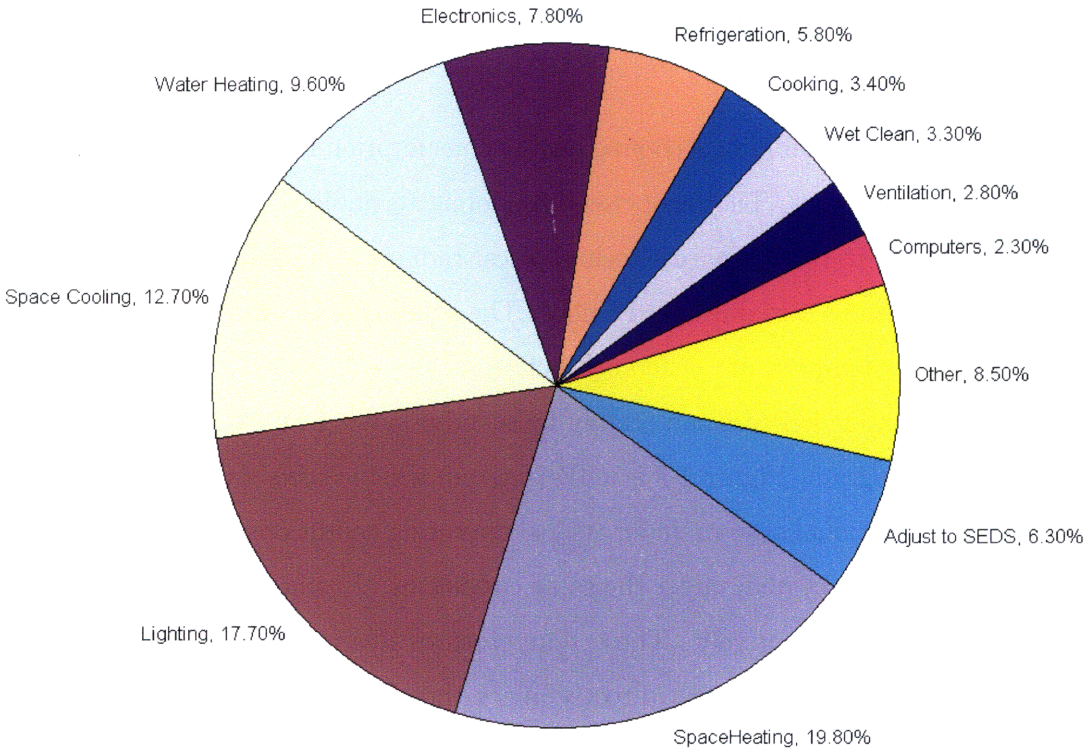

Figure 1-2: 2006 U.S. building end-use splits[10].

loads are significantly less. There are several ways to reduce a building's energy use. Occupancy sensors can be installed to ensure that lights are turned off when a space is not in use. With a properly designed building in certain climates, natural ventilation can be used to reduce the need for mechanically powered fans, while maintaining a comfortable space. There are also potential energy savings associated with appropriate system design as well as focusing on the performance of the major subsystems. Most buildings are cooled through the use of any combination of fans, pumps, chillers and cooling towers. Making the individual components of the system more efficient and making them work together in the most effective way could have significant impact on a building's overall energy consumption.

1.2 Low-Lift Cooling Technologies

One way to address a building's cooling energy consumption is through the use of low-lift cooling technologies. The term "low-lift cooling technologies", as described here, refers specifically to three separate technologies: radiant cooling subsystems, thermal energy storage, and a variable speed chiller. The primary goal of low-lift technologies is to reduce the temperature difference between the condenser and the evaporator. The thermodynamic benefits can readily be seen by looking at a temperature versus entropy (T-s) diagram. Figure 1-3 is a T-s diagram which shows a vapor-compression cycle for a conventional system under typical operating conditions as well as the cycle for a low-lift cooling system under the same conditions. T_z and T_x are the source and sink temperature, respectively. These temperatures determine the condensing and evaporating temperatures which directly affect the thermodynamic efficiency. The areas of the polygons represent the work done by the compressors in each system. The cooling capacity is represented by area under the polygons (i.e. extending the polygons down to 0 K). It is clear that the compressor work for the low-lift system is significantly smaller than the compressor work for the conventional system. Also, the cooling capacity is slightly larger for the low-lift system.

Radiant cooling subsystems are attractive because, for a given level of comfort, they allow the space to be maintained at a higher temperature than would be required for traditional air conditioning systems. With ceiling mounted radiant cooling panels, the heat radiated from the human body is increased from 35% to 50%, while the heat loss due to convection is decreased from about 40% to 30% [8]. This is because the human head, which emits most of the body's energy, can more effectively emit energy with a cool ceiling above. As a result, a space at 25.6 °C (78 °F) with ceiling mounted radiant cooling panels gives the perception of a room at 23.9 °C (75 °F) with a conventional cooling system. Consequently, the temperature difference across the building envelope is also decreased. Another advantage to using radiant cooling subsystems is that water is pumped through the building instead of blowing air. Water pumps transporting water through the building, with insulated pipes, are more

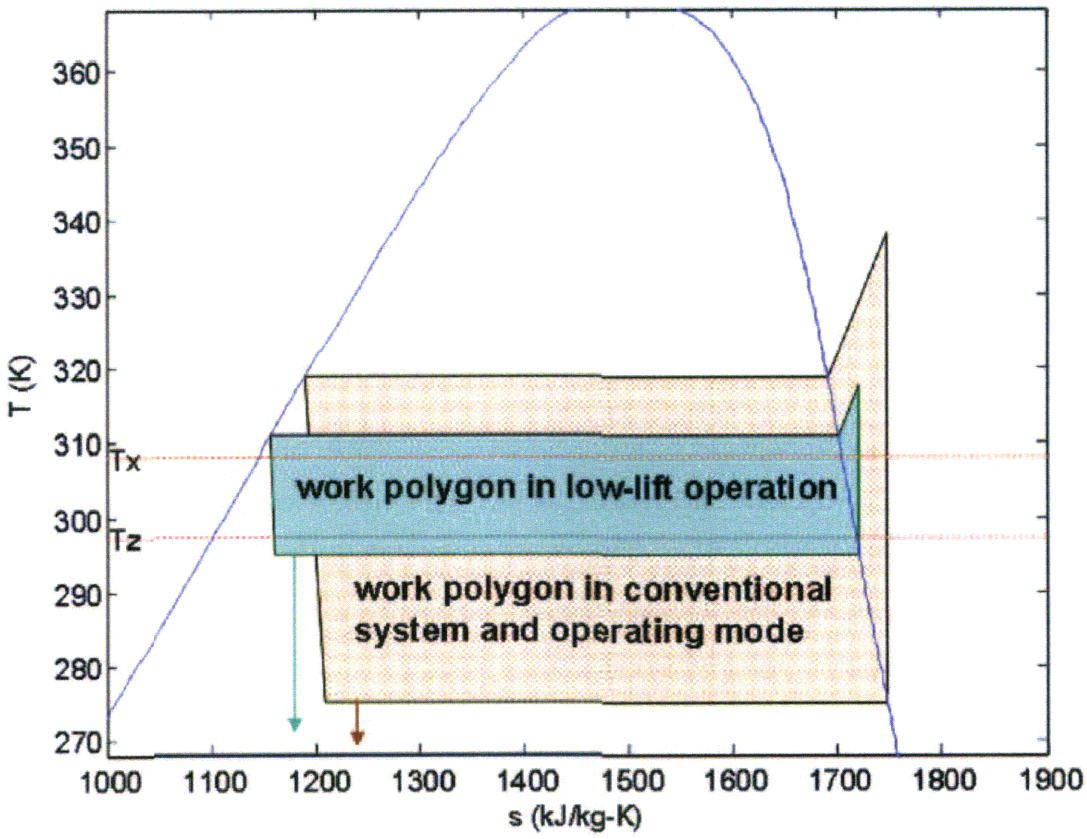

Figure 1-3: Typical work polygon for low-lift operation [4].

efficient than fans blowing air through ducts. Thus, the effect is a reduction in the amount of transport energy required. Also, radiant cooling subsystems require chilled water temperatures of 15 °C (59 °F) instead of 10 °C (50 °F) as typical all air systems need. This higher chilled water temperature means that the chiller does not have to work as hard, resulting in higher chiller efficiency. In order to use radiant cooling, a dedicated outdoor air system must be employed to provide dehumidification and meet minimum ventilation requirements. This results in splitting the sensible and latent portions of the cooling load. Sensible cooling is related to cooling by solely lowering or maintaining the temperature of a given space, while latent cooling is related to cooling by solely removing moisture content[18]. Latent cooling can also be thought of as dehumidification. Typically, a cooling load will require both sensible and latent cooling. Providing sensible cooling with radiant cooling subsystems and latent cooling with a dedicated outdoor air system results in better control of zone temperatures, humidity, and air quality. It can also result in better cooling efficiency[4].

Thermal energy storage (TES) involves storing energy in some medium (i.e. cooling it) and then using that energy to meet, or help meet a cooling load at a later time. This effectively allows the cooling load to be shifted to the night which saves money and energy. Money is saved because electricity is cheaper outside of peak time as the demand on the grid is much lower. Energy is saved because the outdoor ambient temperature is typically lower at night in most climates. This reduces the condenser temperature at the chiller. The use of thermal energy storage also allows for the cooling load to be spread over time. With modulation of the refrigerant mass flow in the compressor, spreading the cooling load over time will allow for a reduction in the average difference between condensing and evaporating temperatures. A good material for storing energy would have a high thermal capacitance. Water is commonly used today for energy storage because of its high heat capacity and relative ease of transport. Using water to store energy and then transporting that energy around the building is an example of an active thermal energy storage system. An intrinsic system uses the building itself to store the thermal energy. Such a system would require exposed building slabs that are cooled overnight. The building is cooler

at night than it would normally be which results in unwanted conduction heat gains, thus the storage efficiency is less than one. The slabs can be floors, ceilings, and/or walls. Consequently, the life span of most systems of this kind is expected to be the equivalent to the life span of the building [28].

A variable speed chiller can be used to modulate the compressor speed depending on the given cooling load. Chillers must be sized to meet the largest cooling load that the building is expected to see. However, for most of its lifetime a chiller will need to meet only a fraction of this load. The idea is to reduce the capacity of the chiller to meet the existing cooling load. A variable speed chiller consists of variable speed transport motor operation and a variable speed compressor. The amount of energy saved from running the compressor with a reduced difference between the condensing and evaporating temperatures is substantial. However per-unit compressor and motor losses can significantly affect the magnitude of these savings if they increase as the refrigerant mass flow rate is decreased[4]. Consequently, a compressor model at these low-lift conditions is needed to quantify just how much energy savings can be expected. Most manufacturers' data is not provided in this range, so experimental tests must be conducted to determine compressor savings under low-lift conditions.

Each of the three subsystems—radiant cooling, TES, and variable-speed chillers—has been used, and is being used, in buildings today in some form or fashion. However, it is the use of all three technologies together that is of particular interest. Armstrong [4] used DOE-2.2 to explore the effectiveness of using these three technologies in a building in five representative climates in the United States. For each climate, the effects of using one technology, all combinations of two technologies, and all three technologies were examined and compared against a baseline. For the baseline, conventional systems were used in place of each subsystem. In place of radiant cooling and dedicated outdoor air system, a variable air volume (VAV) distribution system was used for the baseline. VAV systems are the most efficient all-air systems that are used extensively in the United States. The variable speed chiller replaces a two-speed chiller (capable of operating at full speed and half speed) in the baseline. This is effectively the same as having a chiller with two equally sized, constant speed

compressors. In the baseline case there is no thermal energy storage. The low-lift technologies were compared to the baseline for a standard-performance building, a mid-performance building, and a high-performance building. It was found that in each climate there is a significant advantage (in regards to energy savings) in using the three low-lift cooling technologies, concurrently, instead of the baseline. For the standard-performance building, the energy savings associated with using radiant cooling subsystems, thermal energy storage, and a variable speed chiller instead of a 2-speed chiller with a VAV system and no thermal energy storage ranges from 74% to 70%. For mid-performance buildings the savings range from 73% to 45.5 %. The energy savings range from 71% to 34.5% for the high-performance building. In all cases, the biggest savings were seen in the hot climate (Houston, TX) while the lowest savings were seen in the mild climate (Los Angeles, CA).

This study indicates a theoretical potential for major energy savings. However, more extensive modeling is needed to give a more realistic picture. Central to a model for a variable speed chiller is a model for a variable speed compressor. Simulation results [4] show that much of the cooling energy savings potential comes from efficient operation well below 50% capacity fraction. Therefore, a variable speed compressor model must be capable of accurately determining the refrigerant mass flow rate and input power as a function of the pressure of the refrigerant entering and exiting the compressor as well as the temperature of the refrigerant entering the compressor. This must be a a robust model that is valid at low speed and low compression ratios. An effective way to develop a model is to fit it to a given data set. Compressor manufacturers run many tests to accurately characterize the performance of their compressors. However, most compressor manufacturers are unwilling to share such primary data. Also, since most cooling systems do not operate in the low-lift region, few, if any, manufacturers take data that includes this region. Therefore, it will be necessary to run tests to characterize compressor performance in the low-lift region.

1.3 Compressors

This thesis will focus on the modeling and testing of compressors. This section will provide an idea on the type of compressor technologies available in today's market. Compressors are one of the central parts of conventional refrigeration systems, along with the condenser, the evaporator and the thermal expansion valve. Compressor technology has evolved over the last century, and there are presently several different types compressors available. Generally, compressors can be split into two broad categories; positive displacement and dynamic compressors[2]. Positive displacement compressors achieve compression through the reduction of the compression chamber volume. Low pressure refrigerant vapor enters the compression chamber through the suction port of the positive displacement compressor, and mechanical work decreases the volume of the chamber causing the vapor pressure to rise. This high pressure refrigerant is then allowed to escape the chamber through the discharge port. Positive displacement compressors are typically driven by an electric motor. Reciprocating compressors, orbital compressors, and rotary compressors are the main classes of positive displacement compressors. Orbital compressors include scroll and trochoidal compressors, while rolling piston, rotary vane, single screw and twin screw compressors are types of rotary compressors. In addition to positive displacement compressors there are also dynamic compressors. Dynamic compressors achieve compression of refrigerant vapor through kinetic energy transfer to the vapor. This energy is then converted into a pressure rise. Centrifugal compressors are dynamic compressors because they have a mechanical element which is rotating at a high speed. Angular momentum is then exchanged from this element to the steadily flowing refrigerant liquid. This thesis will focus on reciprocating and scroll compressors, which are discussed below in more detail.

1.3.1 Reciprocating Compressors

A reciprocating compressor is, quite simply, a piston in a cylinder. It is, essentially, the opposite of the internal combustion engine. In an internal combustion engine, a

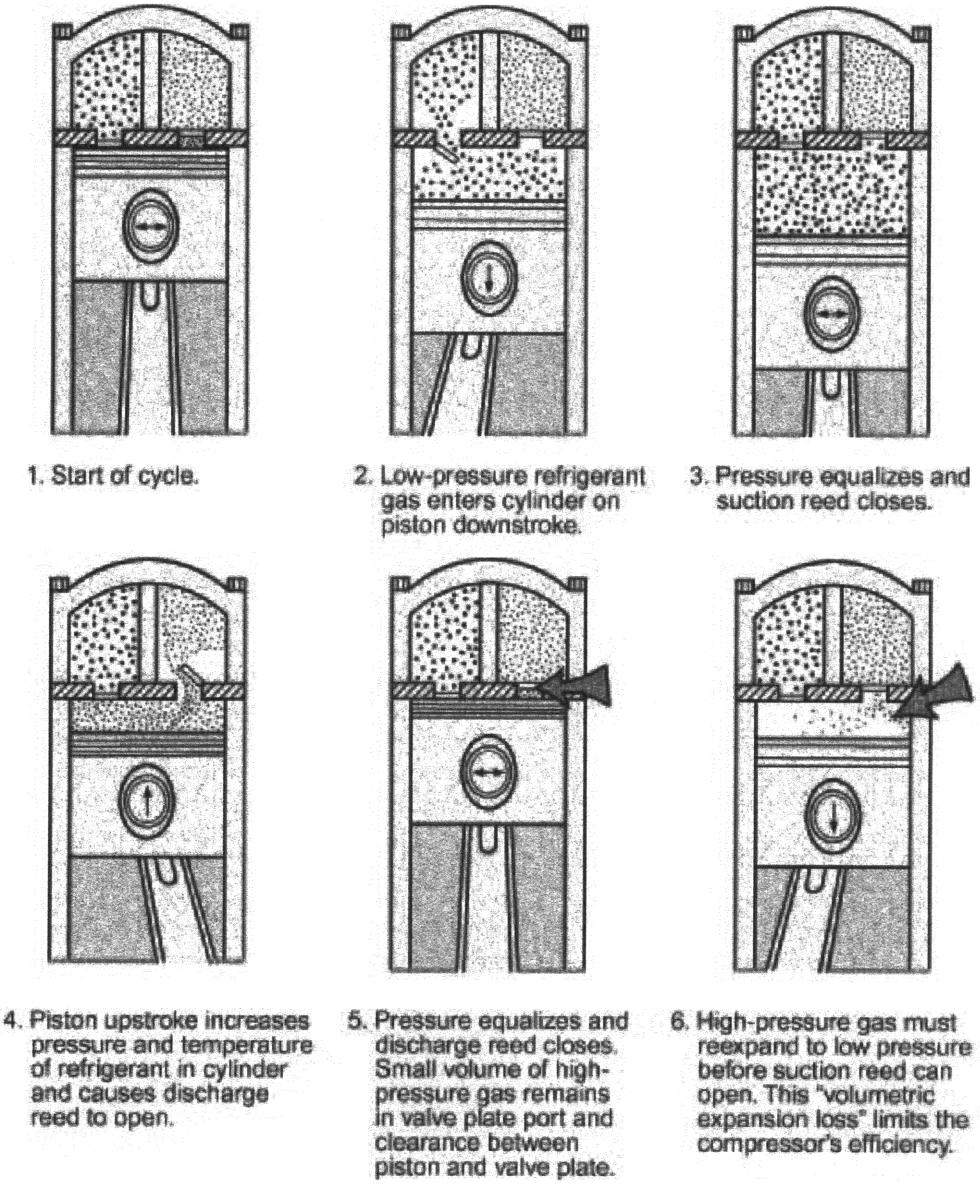

Figure 1-4: Compression cycle for a reciprocating compressor[2].

petroleum-air vapor mixture is ignited to raise its temperature and pressure which drives the piston downward causing the crankshaft to rotate. Thus, it is the expanding vapor that provides the power in the system. For reciprocating compressors, external power is used to drive the crankshaft which pushes the piston upward in the cylinder, compressing the trapped refrigerant vapor. This energy is then used to meet the cooling load. Typically, an electric motor is used to power the compressor. Figure 1-4 shows the compression cycle for a typical reciprocating compressor. The cycle begins with the piston at the top of the cylinder. The suction valve, along with the suction plenum, is on the left side while the discharge valve and plenum are on the right side in the cross-sections shown in Figure 1-4. The suction valve opens allowing the low pressure refrigerant vapor to flow into the cylinder. As the piston goes through its down stroke, the refrigerant vapor expands. Once the piston reaches its lowest point, the suction valve closes. The piston, which is connected to a motor driven crankshaft, is then driven upward. The trapped refrigerant vapor is then compressed as the piston goes through its upstroke. This volumetric reduction causes both the pressure and temperature of the refrigerant vapor to rise. Towards the end of the up stroke, the discharge valve is opened and most of the high pressure refrigerant escapes the cylinder. The volume of the cylinder at the completion of the upstroke is called the clearance volume. The clearance volume is very significant in terms of modeling the compressor and is discussed in more detail in Chapter 4. After the completion of the upstroke, there is some amount of high pressure refrigerant left in the cylinder. In order to allow the low pressure refrigerant in the suction plenum to enter the cylinder and begin the next compression cycle, this high pressure refrigerant must be re-expanded until it is brought down to a low pressure. This re-expansion is a loss that limits the efficiency of the compressor. It is important that only refrigerant vapor is allowed to enter the compression cylinder. Liquid refrigerant is essentially incompressible, so, again, like the internal combustion engine, if liquid reaches the cylinder catastrophic damage, such as bent piston rods, may take place. There is particular danger during startup, where slugging can occur if liquid refrigerant was allowed to migrate back to the compressor after shutdown. Floodback can occur if

an appropriately sized accumulator is not used. An accumulator is a device used to ensure liquid refrigerant is not continuously returned with the suction gas.

Reciprocating compressors can be single-, or multi-cylinder devices. Crankshafts are typically used to translate the motion of a rotating shaft into linear motion of a piston, but swashplates may also be used. A swashplate consisists of a disk mounted on a shaft. If the disk is not perpendicularly attached to the shaft, then as the shaft rotates, the swashplate edges will move back and forth in linear motion. Reciprocating compresssors may be hermetic or semi-hermetic devices. Hermetic compressors are completely welded devices so that the inner parts of the compressor are not serviceable. The motor is also housed within the hermetic housing. Consequently, the heat dissipated by the motor operation is then allowed to be transferred to the refrigerant gas which has an adverse affect on the overall efficiency of the refrigeration system. Semi-hermetic compressors are assembled with bolts, flanges, and gaskets. Semi-hermetic compressors allow many of the parts of the compressor (i.e. piston, connecting rod, crankshaft, valves, etc.) to be accessed and replaced as needed. Semi-hermetic compressors may have the motor within the accessible enclosure or they may be an open-drive compressor. Open-drive compressors have the crankshaft exposed and allows for the motor to be decoupled from the unit. An advantage to this configuration is that it dramatically reduces the amount of waste heat generated from the motor that ends up being absorbed by the refrigerant. This waste heat has an adverse affect on the performance of the compressor. From a testing standpoint, an open-drive compressor is appealing because it provides an easy and accurate method for measuring shaft speed and torque. With reflective tape attached to a portion of the shaft, a photoelectric sensor can be used to measure the rotational speed of the shaft. The motor can be mounted on a torque arm with a strain gauge attached which would allow for simple, accurate shaft torque measurements. From these shaft torque measurements shaft power can be derived.

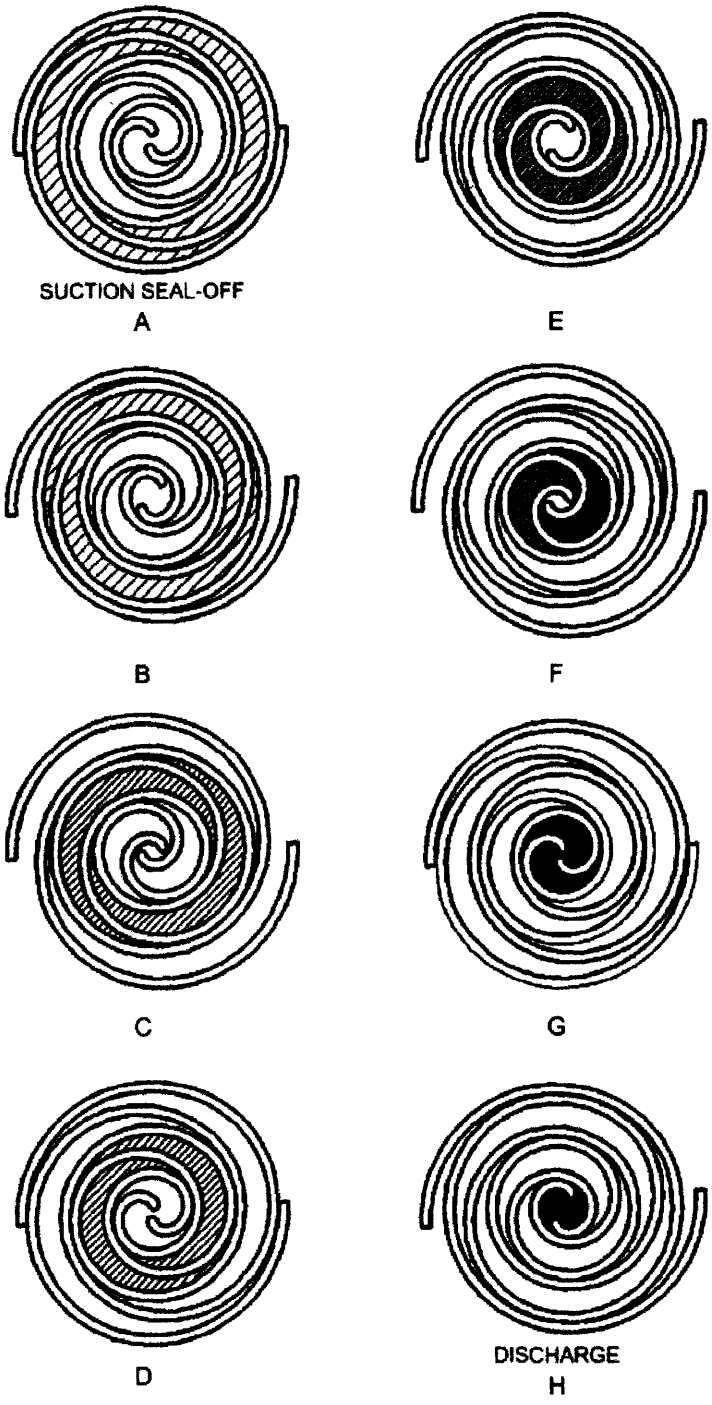

Figure 1-5: Compression cycle for a scroll compressor[26].

1.3.2 Scroll Compressors

Scroll type compressors are positive displacement compressors which are members of the more broad orbital class of compressors. Compression is achieved with the use of two spiral-shaped scroll members; a fixed scroll and an orbiting scroll. As their names suggest, the orbiting scroll rotates around the fixed scroll during the compression process. These members are geometrically identical, closely machined, and assembled 180° out of phase. Figure 1-5 shows the compression cycle for a scroll compressor. The scroll members are oriented in such a way that there are various points of contact, resulting in a pockets which are filled with refrigerant vapor. There are several pockets filled with refrigerant vapor at any given time, but Figure 1-5 focuses on the compression of one pocket, for clarity. As the orbiting scroll moves in relative motion with respect to the fixed scroll it remains in contact with the fixed member. However, the point of contact is moved closer and closer to the center thus decreasing the volume of the pocket and consequently increasing the vapor pressure and temperature of the refrigerant. The suction port is along the circumference while the discharge port is located at the center. At point G, the high pressure gas has reached the discharge port. The compressor index volume is the ratio of the vapor trapped on the suction side to the discharge side. It is clear that aside from the highlighted pocket, there are several other pockets full of refrigerant that are being compressed concurrently. As a result, nearly right after the high pressure refrigerant at point G is discharged, another pocket is ready to be discharged. This results in a nearly continuous discharge process. Scroll compressors can be either high-side or low-side devices. With a low-side scroll compressor, the entire shell is kept at suction pressure while the high pressure discharge gas is routed out of the shell through a plenum. A high-side scroll compressor has the entire shell at discharge pressure while the low pressure suction vapor is piped in.

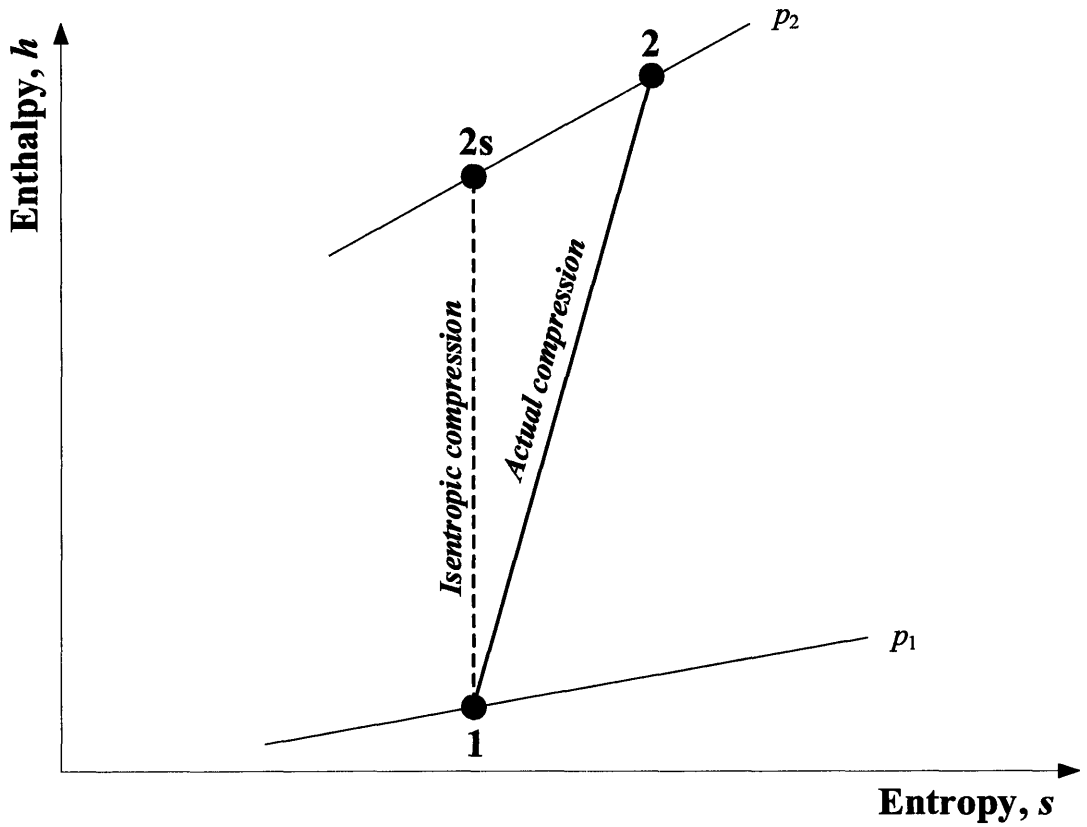

Figure 1-6: Isentropic compression versus actual compression.

1.3.3 Isentropic Efficiency

One measure of compressor performance is the isentropic efficiency, $\eta_{\text{isentropic}}$. By definition, an isentropic process is an adiabatic process of constant entropy. Such a process is considered *reversible*, because the fluid can be returned to its original state with no net work. The second law of thermodynamics prohibits any adiabatic process from taking place that would reduce the entropy of a fluid. Consequently, an *irreversible* process is one in which the entropy of the fluid is increased. It is called irreversible because once the entropy of the fluid has been increased it cannot be returned to its original state as this would require a reduction in entropy and be in violation of the second law of thermodynamics. Figure 1-6 shows two possible paths for compression on an enthalpy-entropy diagram. The dotted line represents reversible, isentropic compression while the solid line represents the actual compression process, complete with irreversibilities. The isentropic efficiency is a comparison of the isentropic process, which represents the least amount of work it take to compress the fluid, to the actual process. For the compression of a fluid from p_1 to p_2 in Figure 1-6, the isentropic efficiency is given by Equation 1.1,

$$\eta_{\text{isentropic}} = \frac{h_{2,\text{s}} - h_1}{h_2 - h_1} \tag{1.1}$$

where h_x is the enthalpy of the fluid at state x. Note that $h_{2,\text{s}}$ is the enthalpy of the fluid at pressure, p_2, but with the same entropy as the fluid before compression (at state 1). In Figure 1-6, the "actual" compression line is drawn to an arbitrary state 2; in fact, this state may lie anywhere on the constant pressure line for p_2 as long as it is to the right of point 2s, so as to not violate the second law of thermodynamics.

1.4 State of Compressor Modeling

There exist several models for reciprocating compressors. The Air Conditioning and Refrigeration Institute proposes a method which uses a bivariate cubic polynomial with cross terms to describe mass flow rate and compressor power[3]. This method

involves ten coefficients and depends solely on the evaporating and condensing temperatures. The ten coefficients make the formula more complex than what is desired for this work. Also, this method makes no distinction on compressor speed so it couldn't be used to describe a variable speed compressor. The method is not based on physics, but rather is an empirical model fitted to data. Consequently, interpolation and extrapolation with this model often yields erroneous results.

Qureshi and Tassou[24] provide an overview of capacity control in refrigeration systems. They show that inverter-based variable speed compressor technology offers significant potential energy savings. Most of the research involving inverter-based variable speed compressors has focused on scroll compressors. Scroll technology became very popular in the latter part of the 20^{th} century mainly because of several performance advantages. Large suction and discharge ports which result in lower pressure losses, the absence of valves and re-expansion volumes as well as a nearly continuous discharge process all result in high volumetric efficiency over a wide range of conditions[2]. Cuevas and Lebrun[6] performed tests using an inverter-based based variable speed scroll compressor. They found that inverter losses resulted in a decrease of COP between 2% and 5% for output powers ranging from 1.5 kW to 6.5 kW. Afjei[1] observed that the mass efficiency and isentropic efficiency decreased substantially for decreasing suction quality for liquid injection in inverter-driven scroll compressors. However, a major drawback of scroll compressors, in terms of low-lift cooling applications, is a drop off in isentropic efficiency for low pressure ratios[6, 32], as this is a key region. Reciprocating compressors are not expected to have a drop off of isentropic efficiency of the same magnitude, thus reciprocating compressor show great promise for low-lift cooling applications.

Popovic and Shapiro[25] as well as Jahnig, Reindl, and Klein[15] formulated models for a reciprocating compressor based on the volumetric efficiency. These models are based on the actual thermodynamics of the compression process, and as a result have much better interpolative and extrapolative properties. These models are considerably less complex with five or fewer coefficients, as compared with ten for the ARI model. Also, these models are not limited to a single suction superheat. The draw-

back to both models, however, is that they have not been applied to variable-speed compressors. In order to be useful for low-lift applications a model for a reciprocating compressor must be valid over a wide range of speeds.

1.5 Structure

This thesis is split into to two main parts: testing and modeling. Chapters 2 and 3 cover the compressor testing. The tests were carried out on a Carrier scroll compressor. The test stand was donated, but needed to be modified to make it useful for the current work. It was desired to generate a set of test points at various pressure ratios while focusing on the low-lift regime: points with high saturated suction temperatures and low saturated discharge temperatures. Also, it was desired to run the compressor at a variety of different speeds by installing a variable frequency drive. The goal of the first part of the this thesis was to adapt the test stand so that it could be used to test a reciprocating compressor. The compressor modeling aspect is discussed in Chapter 4. A model for a semi-hermetic, open-drive, reciprocating compressor is developed. Reciprocating compressors appear to be quite promising for use with low-lift cooling technologies. It was desired to develop a model that could be extended over various pressure ranges and, most importantly, over a variety of different shaft speeds. This thesis concludes with a summary of results as well as recommendations for future work.

Chapter 2

Description of Test Stand

This chapter will describe the compressor test stand in detail. The goal was to be able to impose a discharge pressure, suction pressure and suction temperature on the system and record the mass flow rate of refrigerant and compressor input power at each point. Also, the discharge temperature and condenser water temperatures must be recorded for heat balance checks as well as determination of the isentropic efficiency. An attempt will be made to get a data set that contains points at several pressure ratios and speeds. It was extremely beneficial to receive a test stand that was used on a previous project. This meant that the plumbing had already been done. Also, many of the necessary parts (i.e. control valves, pressure transducers, thermocouples, the flow meter and the condenser) had already been appropriately sized and installed. Data from the previous project could be used to ensure that the measurements obtained are accurate. Many changes were needed to adapt the test stand for use in the current research. There is a complete overhaul of the data acquisition system and, consequently, the control valves needed to be re-tuned, as they are controlled by the new datalogger. Other systematic changes, such as increasing line sizes, replacing components, and adding ball valves and additional sensors, also were needed to adapt this system for the current research.

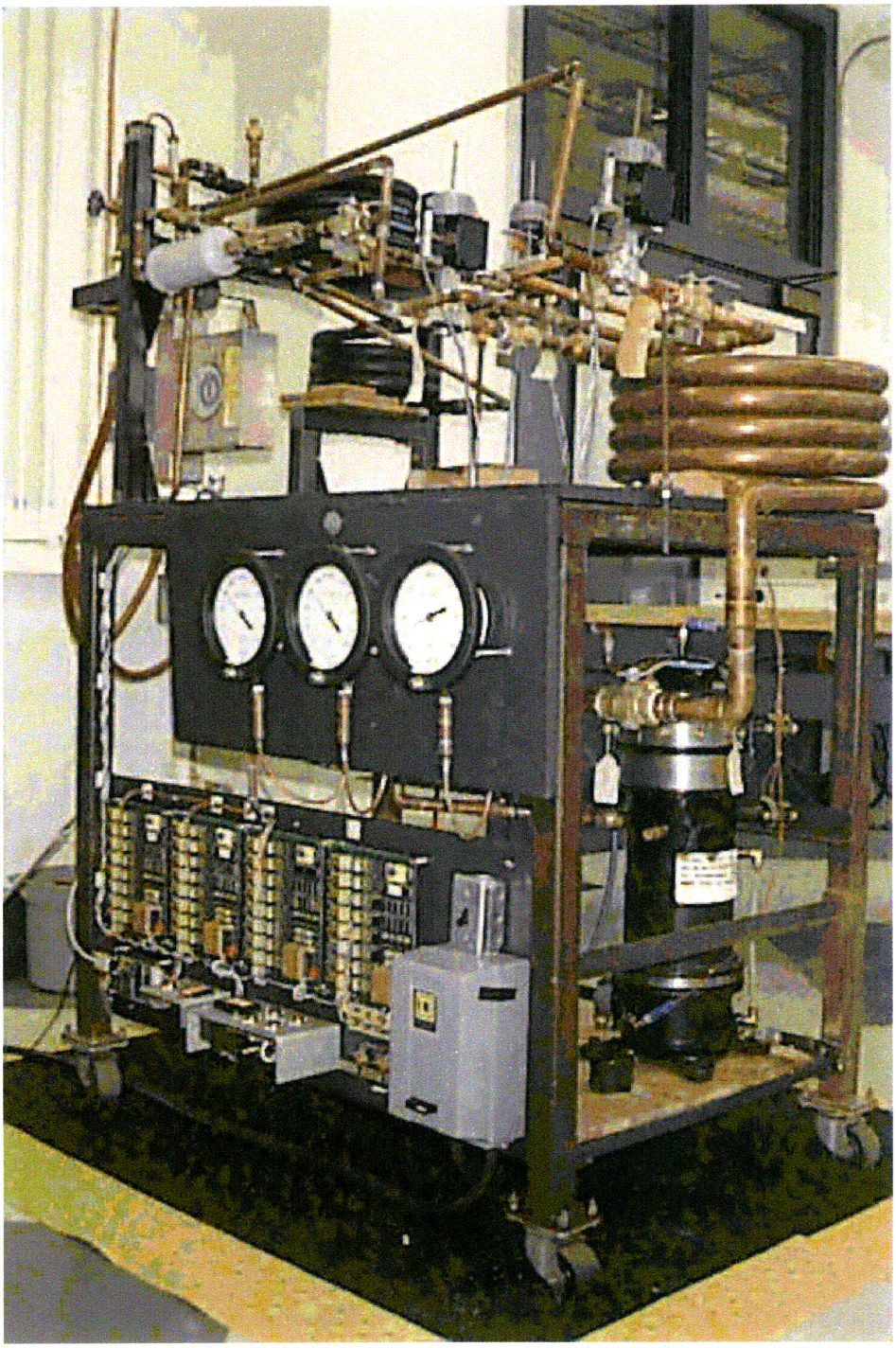

Figure 2-1: Otten/Wilson calorimeter [23].

2.1 Otten and Wilson De-superheater

In the spring of 2008, David Otten and Prof. Gerald Wilson donated a compressor calorimeter to be used to characterize the performance of a variable speed compressor. The calorimeter consisted of a fixed speed scroll compressor, two coaxial, water cooled heat exchangers, two Micro-Motion mass flow meters, 4 stepper-motor controlled valves, a 64 channel data acquisition system, as well as numerous thermocouples and pressure transducers. The calorimeter is shown in Figure 2-1. The compressor used in this test stand is a specially modified semi-hermetic refrigeration compressor from Carrier Corporation. The modifications allowed for extra monitoring points (such as motor winding temperatures) which are not found on traditional scroll compressors. Consequently, manufacturer's ratings and other specific information about the compressor are not readily available. The scroll compressor stands two feet tall with a diameter of 8 inches. The suction line is 3/4" nominal copper tube, while the discharge is 5/8" nominal copper tube.

The calorimeter is a desuperheater loop. Refrigerant gas exits the discharge port of the scroll compressor and is split into two streams. A portion of the gas flows through the condenser and then through the a filter drier and onto the thermal expansion valve. The other stream bypasses the condenser and flows directly back to the suction port. Heat is not removed from the latter stream and the amount of hot gas that bypasses the condenser is controlled by the appropriately named hot gas bypass valve. Traditional air conditioning systems have a condenser and an evaporator, which is designed to meet the cooling load of a given space. This test stand, however, does not have an evaporator. Instead the modulation of the thermal expansion valve and the hot gas bypass valve controls the conditions of the refrigerant at the suction port (i.e. the suction pressure and suction temperature) to simulating a cooling load. To control the conditions at the discharge port (pressure), the condenser water valve is modulated as needed to respond to changes in discharge pressure. Figure 2-2 illustrates the schematic for the modified system.

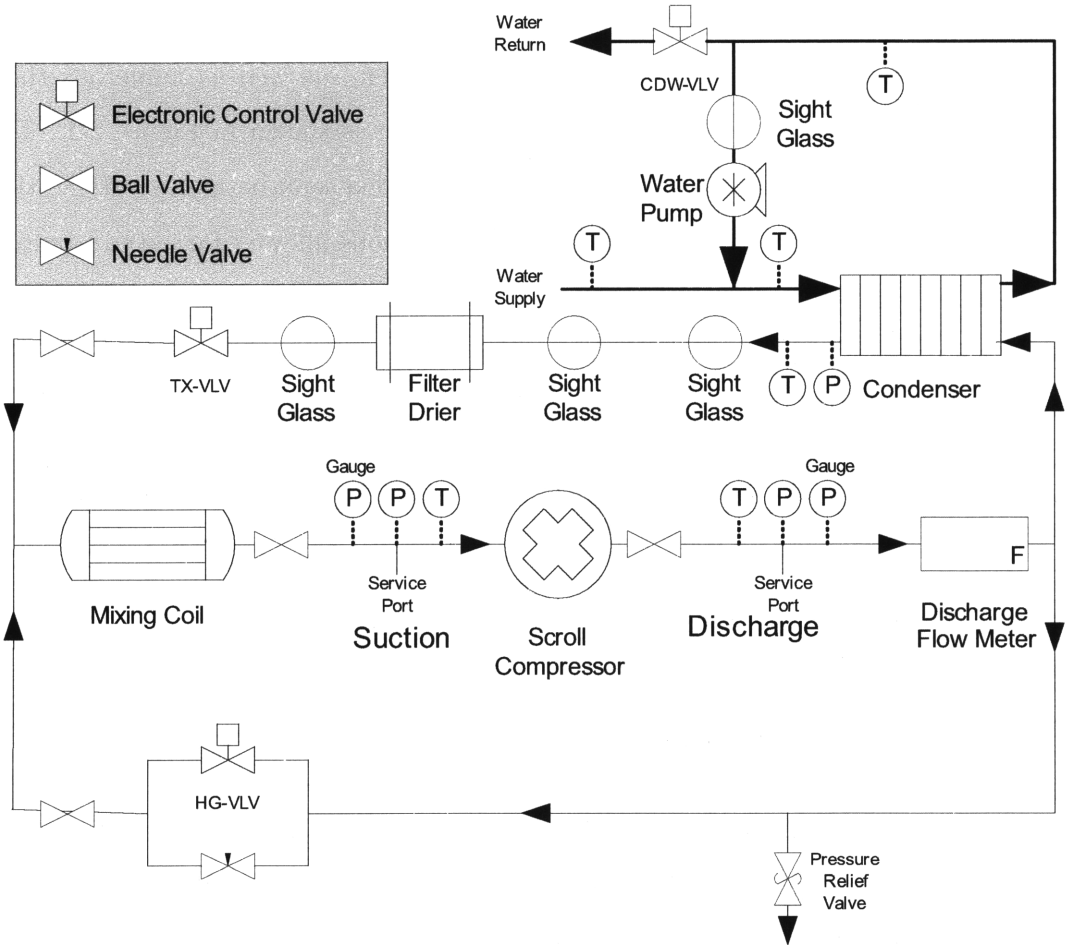

Figure 2-2: Flow diagram of the modified system.

2.2 Modifications to the Test Stand

2.2.1 Data Acquisition

An IBM PC AT was used to run the calorimeter and collect data from the 64 channel data acquisition board. This computer runs MS-DOS 6.0 and does not support NTFS, which most new computers use. Accordingly, it became prudent to switch to a new data acquisition system. A Campbell Scientific CR1000 in conjunction with an AM25T solid state multiplexer is used to collect the desired data. The heat capacity of the grounding bar and an insulated aluminum cover reduce thermal gradients along the length of the multiplexer. Reducing thermal gradients provides better reference temperature performance (0.01 K between channels) than the A/D boards provided with the original calorimeter. The program code used to control the test stand can be found in Apppendix D. The goal of the program is to provide stable control of the system and to log the relevant quantities of interest. Stable control is constant discharge and suction conditions (suctions and pressures). The quantities of interest are refrigerant mass flow rate, compressor power, condenser water temperatures, as well as the discharge and suction conditions.

2.2.2 Additional Sensors

The Otten/Wilson desuperheater had an abundance of thermocouples, with many measuring temperatures at various spots in the compressor. For the new tests, the temperatures of interest are given in Table 2.1, along with their terminations on the AM25T. The suction temperature (ST) thermocouple is wired to channel 5 of the CR1000. This is to ensure that the suction temperature, which is needed to control the motorized valves, is read each scan. The other thermocouples are put on a lower priority than the control variables. All of the thermocouples were type T (copper-constantan junctions) except for the discharge temperature which is type E (chromel-constantan junctions). The temperature range for a type T thermocouple is from -270 °C to 400 °C, while the range for Type E is -270 °C to 1000 °C.

AM25T Ch.	Description
1	$CWT_{\text{out,stream}}$ (Condenser Water outlet stream Temp)
2	$CWT_{\text{out,stream}}$ (Condenser Water outlet stream Temp)
3	$CWT_{\text{out,surf}}$ (Condenser Water outlet Temp)
4	$CWT_{\text{in,surf}}$ (Condenser Water inlet Temp)
5	CWT_{mix} (Condenser Water mix Temp)
7	DT (Discharge Temp)
8	CET (Condenser Exit Temp)
9	Comp. Dome Temp
10	Oil Sump Temp
12	Motor Temp 1
13	Motor Temp 2
14	Motor Temp 3

Table 2.1: Thermocouple points list.

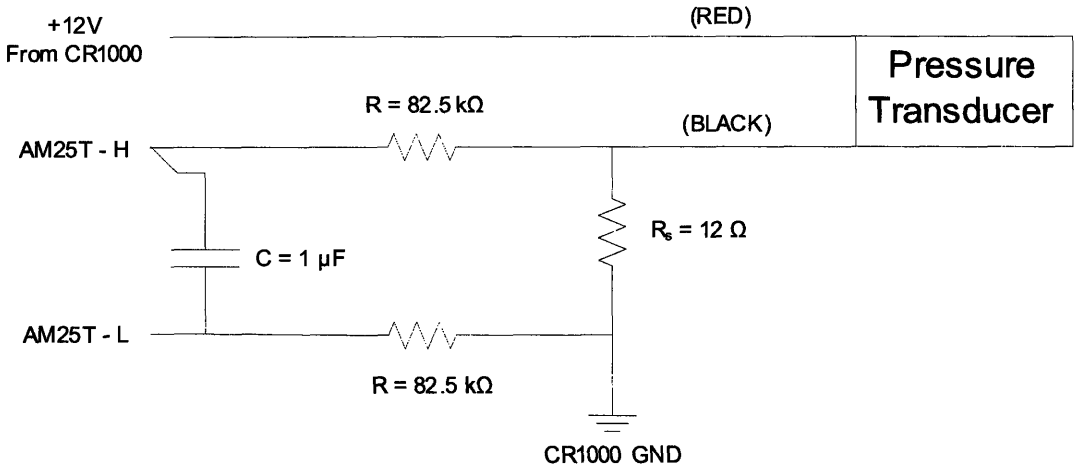

Figure 2-3: Typical pressure transducer circuit diagram.

CR1000 Ch.	Description	Range	R_s
6	*SP* (Suction Pressure)	0-100 psig	12.02 Ω
7	*DP* (Discharge Pressure)	0-1000 psia	12.11 Ω
8	*CEP* (Condenser Exit Pressure)	0-500 psig	12.09 Ω

Table 2.2: Pressure transducers points list.

The pressure transducers are terminated directly on the CR1000. Table 2.2 shows the points list for the relevant pressure transducers. All of the pressure transducers are loop powered and output a 4 to 20 mA signal proportional to the pressure of the fluid. A wiring diagram is shown in Figure 2-3. The pressure transducers pass through an RC filter which is in place to eliminate the noise from the measurement signal. The filter cutoff frequency was chosen to have 60 Hz noise rejection since the primary power is delivered at this frequency. When the VFD is used at lower frequency, the signal noise becomes apparent for the motor winding temperatures, but not for any of the other thermocouples or transducers. The CR1000 measures a voltage proportional to the current output from the sensor (through Ohm's Law). Equation 2.1 is used to determine the pressure for a given voltage reading,

$$P = (mV - 4R_s)\frac{P_{max}}{16R_s}\left|\frac{10^6 \text{ MPa}}{147.0337 \text{ psi}}\right| \tag{2.1}$$

where mV is the measured differential voltage in millivolts, R_s is the sensing resistor in ohms, P_{max} is the maximum pressure for the given transducer in psi, and P is the measured pressure in MPa. The differential voltage is measured at the CR1000 logger on a ± 250 mV scale. With a 4 to 20 mA output, a sensing resistance of about 12 Ω would allow for the entire range to be detectable. The discharge pressure transducer has an accuracy of ±1% of full scale pressure, while the condenser exit pressure transducer has an accuracy of ±0.4% full scale and the suction pressure has an accuracy of ±0.25% full scale.

A MicroMotion coriolis mass flow meter is used to measure the refrigerant mass flow rate. The flow meter is an externally powered device, and its wiring diagram is shown in Figure 2-4. The signal from the mass flow meter also passes through an RC

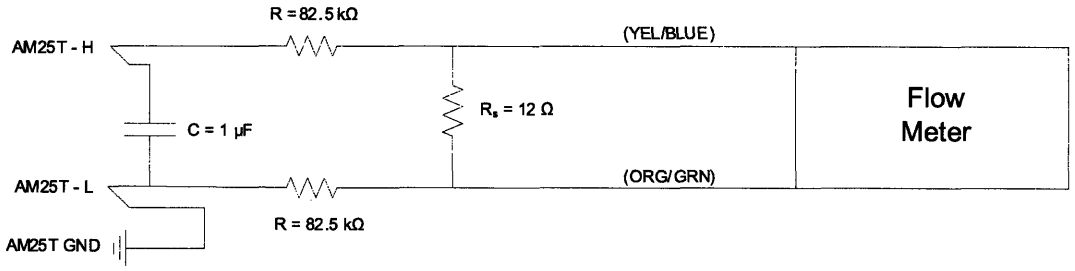

Figure 2-4: Mass flow meter wiring diagram.

filter. The mass flow is calculate by Equation 2.2 below,

$$\dot{m} = (mV - 4R_s)\frac{\dot{m}_{\max}}{16R_s}\left|\frac{1 \text{ kg}}{2.205 \text{ lb}}\right|\left|\frac{60 \text{ min}}{1 \text{ h}}\right| \tag{2.2}$$

where $\dot{m}_{\max}$ is the maximum flow rate through the flow meter in lbm/min and $\dot{m}$ is the measured mass flow in kg/h. The flow meter also outputs 4-20 mA signal. The sensing resistor for the flow meter is 35.93 Ω, which is about 3 times larger than the sensing resistor which would be needed to see the entire range of the flow meter. This is because, in running the compressor, the flow rate never gets anywhere close to the 125 lb/min (3400 kg/h) maximum. The largest flows initially observed are on the order of 300 kg/h, which corresponds to a current of about 5.4 mA. Increasing the sensing resistor provides more resolution but also decreases the maximum detectable flow rate. With a sensing resistor equal to 35.93 Ω, the maximum detectable flow rate is approximately 630 kg/h, corresponding to a current output of about 7 mA. The mass flow meter has an accuracy of ±0.2% of the measured mass flow rate. A full parts list can be found in Appendix A with model numbers and manufacturers.

2.2.3 Plumbing Changes

It is imperative that the liquid refrigerant leaving the condenser does not flash to vapor upstream of the thermal expansion valve (TX-VLV). The magnitude of the pressure drop in the liquid line has a direct impact on this. To ensure that flashing upstream

of the thermal expansion valve does not take place several plumbing changes were made. The line size on the liquid line was increased from 1/2" copper tubing to 5/8" tubing. The number of elbows was minimized and the filter drier was changed from a standard hermetically sealed horizontally orientated type to an upright replaceable core type (See Figure 2-5). With the new filter drier liquid flows from the condenser into the side of the filter drier. It then passes through the core material, which absorbs any water in the refrigerant, and flows out the bottom of the filter drier. With this construction, the filter drier also acts as a reservoir for the liquid refrigerant, providing enough liquid head to ensure that the pressure drops will not cause flashing upstream of the thermal expansion valve. The level of the liquid within the filter drier shell was a characteristic that also needed to be monitored to ensure that there is not flashing upstream of the TXV and to aid in determining the correct charge for the system. It also provides an early sign for loss of refrigerant in the system in the case of a major leak. When the system is shut down, most of the refrigerant is kept in the filter drier, so if there is a noticeable drop in in filter drier liquid level when the system is left idle, there is likely a leak that needs to be sealed. To facilitate this, the filter drier was modified so that a side-arm liquid level indicator was installed as seen in Figure 2-5. Also, for visualization, one sight glass was installed just downstream of the condenser, another was installed just upstream of the filter drier, and one was installed just upstream of the thermal expansion valve. In addition to the sight glasses, a ball valve was installed on the discharge line, just downstream of the compressor. This extra valve (in conjunction with the previously installed suction line ball valve) allows for complete isolation of the compressor, which was a source for many of the leaks within the system.

2.2.4 Condenser Subsystem

There is significant concern that for low water flow rates through the condenser, the response of the condenser water valve would be sluggish. To ensure that the flow of water remains at an acceptable level, a Grundfos non-submersible circulation pump was installed. The installed circulation pump is shown in Figure 2-6. The pure

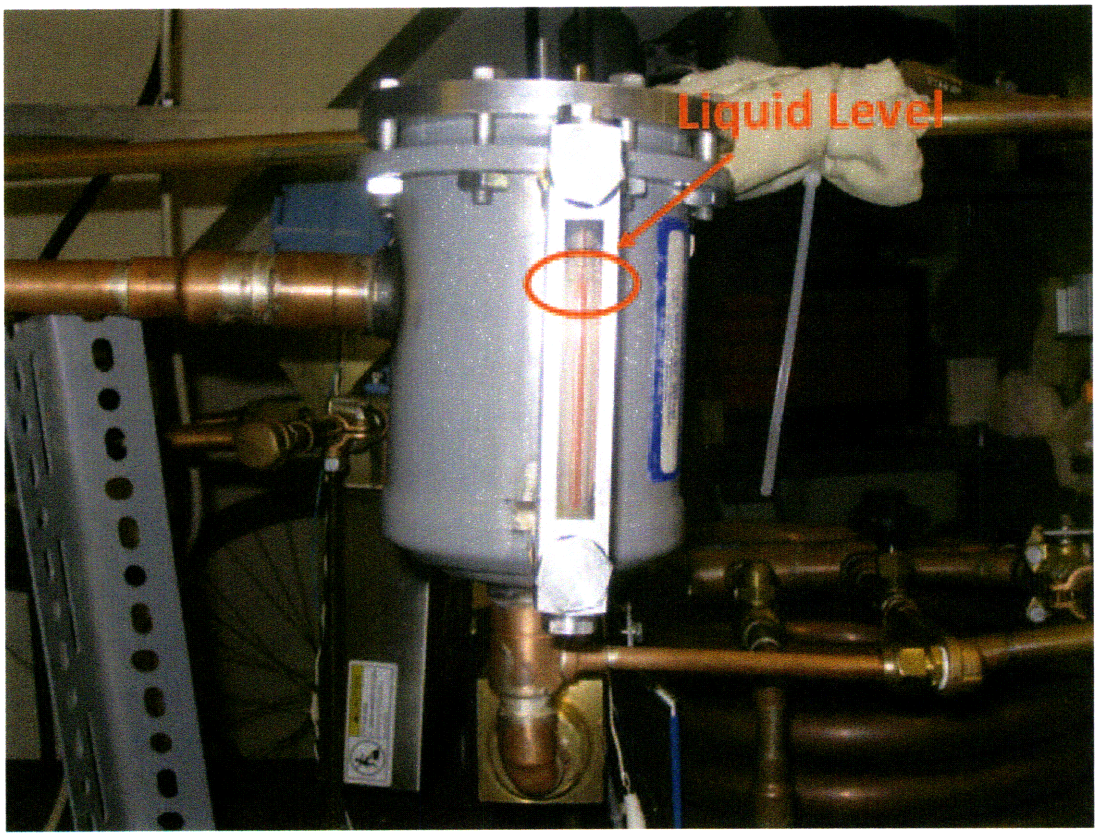

Figure 2-5: New filter drier with liquid level indicator.

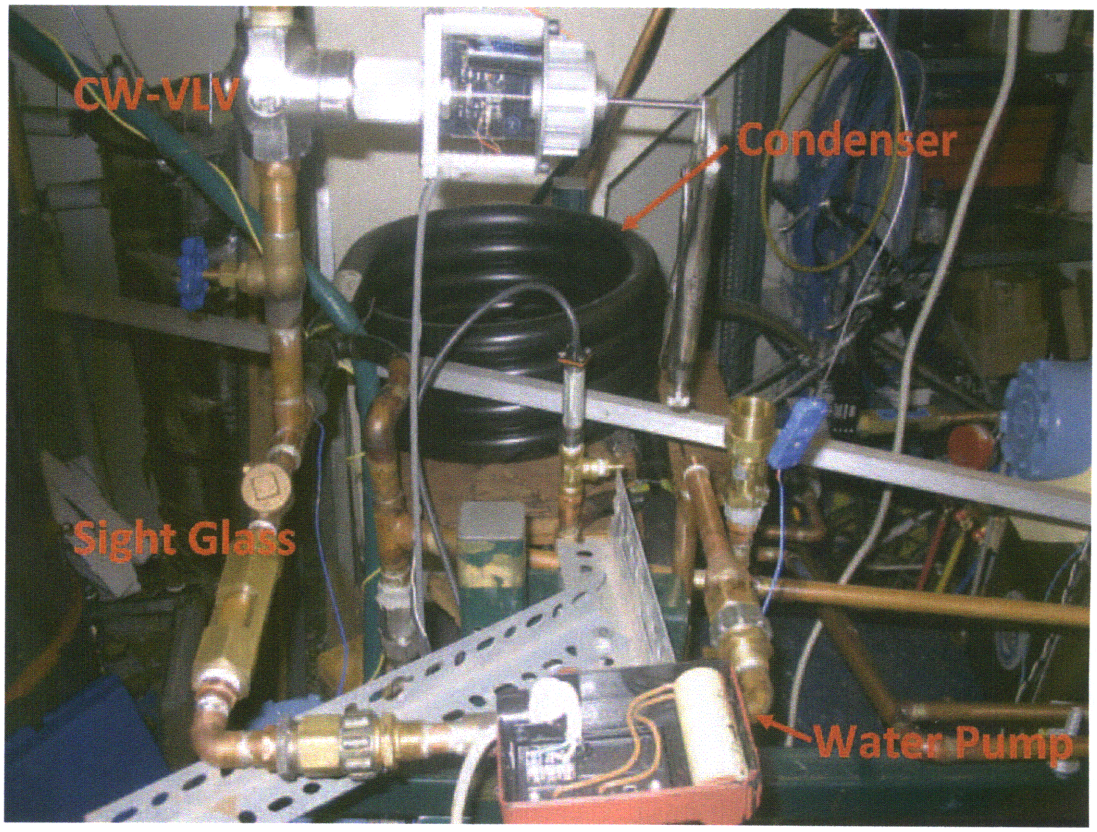

Figure 2-6: Condenser and water circulation pump.

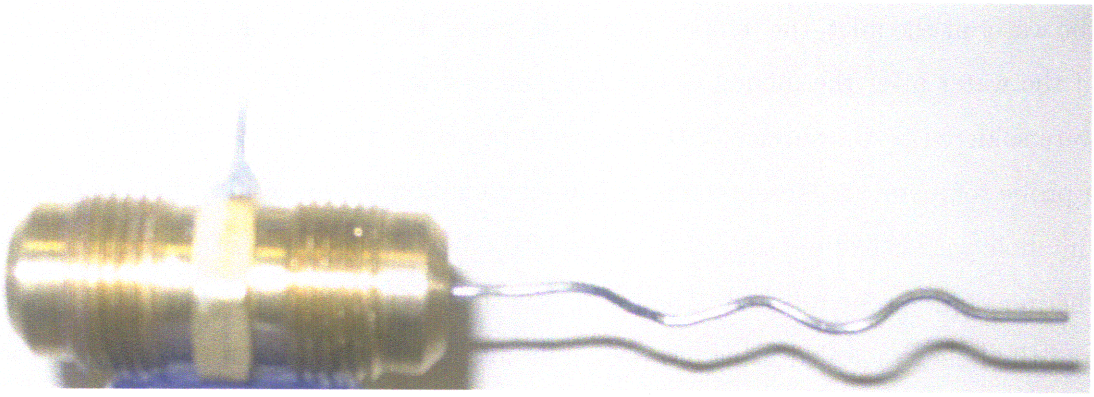

Figure 2-7: Condenser water inlet stream temperature probe.

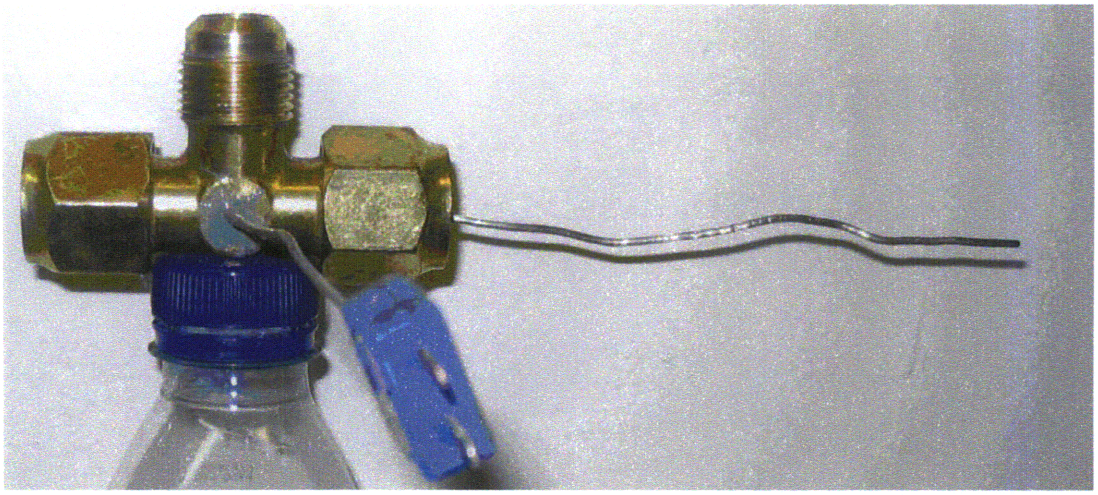

Figure 2-8: Condenser water outlet stream temperature probe.

delay characteristics of the condenser heat exchanger becomes the dominant (and troublesome) plant dynamic at low flow rate. This makes tuning the condenser water control valve difficult as the controller gains at low flow rates would need to be less aggressive, which would result in sluggish control at higher flow rates. Consequently, inlet water is mixed with recirculated water before entering the condenser. With the pump in the loop it became necessary to flip the condenser water valve so that water flowed upward to exit the loop. This ensured that there was no air trapped inside of the system. To obtain a heat balance, it was necessary to know the temperature of the water at the inlet, the temperature of the water at the outlet and the temperature of the water after the mixing of the inlet and recirculated streams. Thermocouples were soldered to the surface of the copper tubes at all three locations. At the inlet, a probe temperature measurement is made by modifying a male-male flare union. A tiny hole was drilled into one of the faces of the hex at the center of the union and a thermocouple probe inserted. The probe was then gently tapped to form a 90° bend and the hole was sealed using 3M 3501 adhesive, as shown in Figure 2-7. The probe for the condenser water outlet temperature, shown in Figure 2-8, was fabricated in a similar fashion as the inlet temperature, except a flare tee is used instead of a flare union.

2.3 Control Valves and Valve Tuning

Perhaps the most challenging aspect of adapting the test stand to this research was the actuation and tuning of the control valves. Since the data acquisition and computer control from the previous project will not be used, the valves must now be actuated by the CR1000. This section focuses on the task of actuating and controlling the three control valves: the hot gas bypass valve (HG-VLV), the thermal expansion valve (TX-VLV) and the condenser water valve (CDW-VLV).

A single test point is defined by the pressure of the refrigerant entering the suction side of the compressor, p_{in} or SP, the temperature of the refrigerant entering the suction side of the compressor, ST, and the pressure of the refrigerant exiting the discharge of the compressor, p_{out} or DP. Instead of using the discharge pressure, the pressure of the refrigerant leaving the condenser (CEP) is used; in the control algorithm this pressure is converted into saturated temperature ($SCET$) by using the saturation curve for R-134a. REFPROP 8.0 (see Appendix B) is used to generate the saturation curve. Conversion to saturation temperature is done primarily for consistency and simplicity of data presentation; so that all of the control parameters have the same units. $SCET$ is used as the control variable instead of SDT (saturated discharge temperature) mainly because at the time the valves were tuned, the discharge pressure transducer was not working. The discharge pressure does not equal the condenser exit pressure; there are pressure drops as the refrigerant flows through the mass flow meter and through the condenser. However, for a steady $SCET$, SDT will also be steady. By the time compressor tests were actually performed, the discharge transducer was working, so the actual discharge pressure is being recorded and is used in the results section of this thesis (Chapter 3). The $SCET$ is controlled by modulating a control valve on the condenser water loop (CDW-VLV in Figure 2-2). This is a single-input single-output control loop, as shown in Figure 2-9. By controlling the flow rate of water through the condenser, this valve is controlling the amount of heat removed by the condenser. The heat removed by the condenser, Q_{cond}, is defined as $\dot{m}_{\text{water}} [h_{\text{out}} - h_{\text{in}}]_{\text{water}}$. If there is a need to increase the $SCET$, the amount of

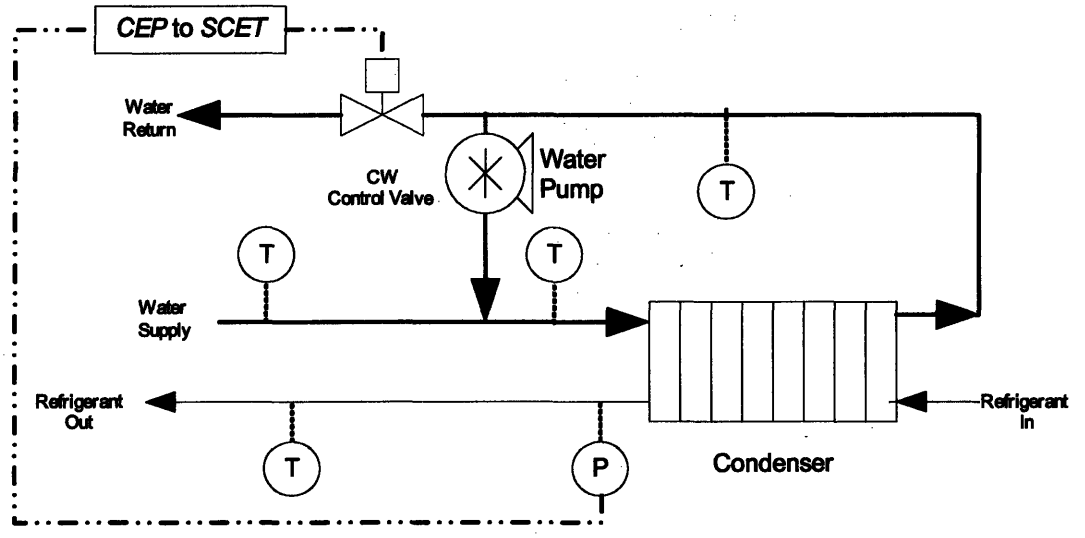

Figure 2-9: Condenser water control loop.

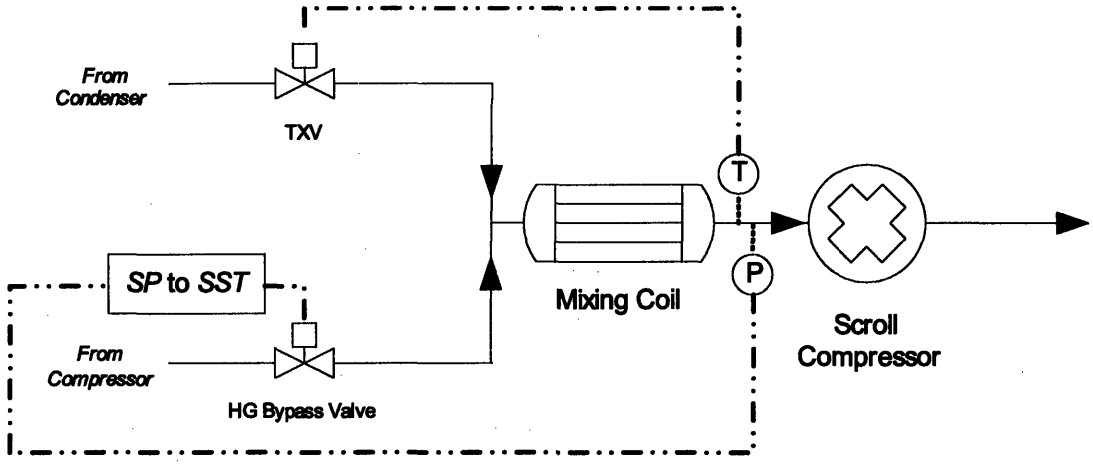

Figure 2-10: Hot gas bypass and thermal expansion valve control loop.

heat the rejected by the condenser must be reduced and the condenser water valve is closed.

On the suction side, the temperature (ST) and pressure (which is, again, converted to a saturated temperature, SST) are maintained by modulating two control valves. A thermal expansion valve (TXV) downstream of the condenser is typical of refrigeration systems, but since there is no evaporator, refrigerant gas from the discharge side of the compressor is allowed to bypass the condenser and mix with the stream of liquid flowing through the TXV. The hot gas bypass valve is modulated to maintain a

constant SST while the TXV is modulated to maintain a constant ST. This control loop is shown in Figure 2-10. Controlling the hot gas bypass valve just on the suction pressure and the thermal expansion valve just off of suction temperature is a notable difference from the way these two valves were previously controlled. The previous project controlled both valves on both pressure and temperature.

The interactions between the control loops make this an especially difficult control problem. It is clear that allowing more refrigerant to pass through the hot gas bypass valve not only affects the pressure at the compressor inlet, but also the temperature. A change in position of any of the three valves has some non-negligible effect on all of the control variables (ST, SST, and $SCET$). The fastest responding control loop is the hot gas bypass loop. The reason for this is two-fold. First, the hot gas bypass directly controls the pressure source. That is, it is modulating the amount of high pressure refrigerant coming from the discharge side of the compressor that is introduced directly back to the suction side of the compressor. Secondly, pressure changes in response to valve position changes happen almost instantaneously; approximately at the speed of sound. The next fastest loop is the condenser water control loop. It is controlling pressure, so a change in $SCET$ is noticed immediately; however it is not directly modulating the pressure source. This valve is modulating the amount of water that is flowing through the condenser. It is controlling the amount of heat rejected by the condenser, Q_{cond}. Decreasing the flow rate of water through the condenser, decreases the amount of heat rejected, thus increasing the $SCET$. The slowest control loop, then, is the TXV. This is mainly due to the transient nature of the temperature it is controlling. The ST is measured by a thermocouple at the inlet to the compressor. In between this thermocouple and the TXV is a large mixing coil which is in place to ensure that all of the liquid that exits the TXV flashes to vapor as it mixes with the hot gas bypass stream. Once the TXV position has been changed there is some natural lag time before the ST thermocouple reacts to this change and fully makes its change to a new state. Because of mixing coil mass and consequently slow open loop response of the suction temperature sensor, TXV control is the slowest of the three control loops. The slow nature of this loop is quite problematic and will

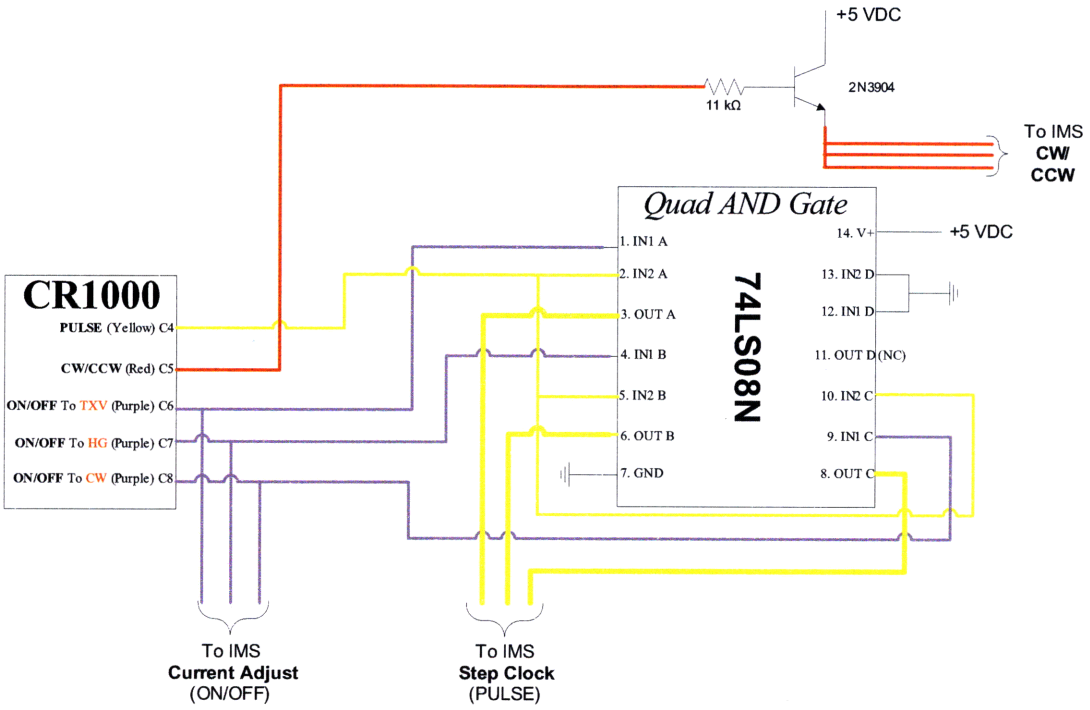

Figure 2-11: Control valve wiring diagram; CR1000 side.

be discussed further in the Section 2.3.2.

2.3.1 Valve Actuation

Each valve is a Research Control Valve actuated by an Airpax stepper motor and an IMS stepper motor controller. The wiring diagrams for the control valves are shown in Figures 2-11 and 2-12. The IMS stepper motor controller for each valve is operated by sending high or low signals to 3 different pins. The "Step Clock" pin receives the pulses and actuates the valves. The "CW/CCW" pin determines the direction in which the motor will actuate the valve. A low signal corresponds to clockwise, or opening the valve, while a high signal corresponds to counter clockwise, or closing the valve. The "Current Adjust" pin effectively acts as an ON/OFF switch for the controller. That is, when this pin is high, the valve will be actuated; when it is low it will not be actuated. It should be noted that the "H/F" pin is not connected. This means that the controller is being operated in half-step mode. Thus it takes 96 pulses to result in a full revolution instead of 48 pulses. This increases the resolution

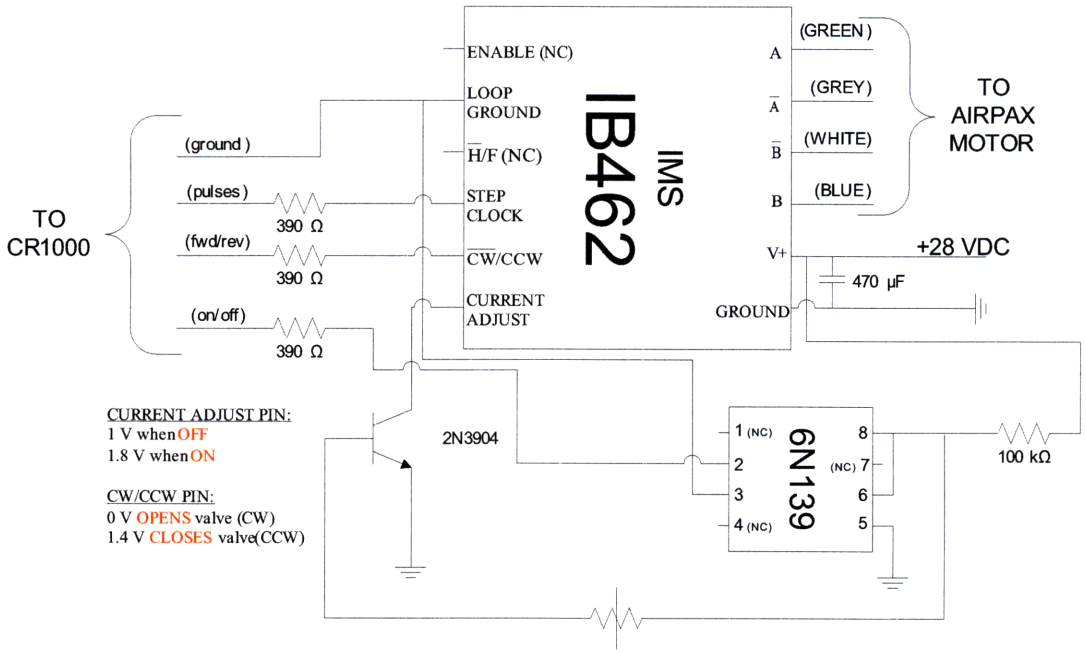

Figure 2-12: Control valve wiring; valve side (*typical of 3*).

of the actuator, allowing for tighter control on each valve. For each valve, there are three pins; thus, there are 9 pins that need to be sent either a high or low signal. However the CR1000 only has 8 logic control ports and one of those ports is used by the AM25T which is used to read temperature, pressure, and flow measurements. Thus, a set of "AND" gates and a transistor was employed so that only 5 logic control ports on the CR1000 are used. As shown in Figure 2-11, control port 4 is used to send pulses to all valves, control port 5 is used to set the direction of motion for all valves, and control ports 6, 7 and 8 are used to turn "ON" the TXV, hot gas bypass valve, and the condenser water valve, respectively. To ensure that there is enough current reaching the "FWD/REV" pins at each valve, this signal is sent through a common transistor before going to each valve. To ensure that only the desired valve is actuated, the pulse signal is sent through AND gates. Only if there is a high signal sent to the "Current Adjust" pin is a pulse sent to a particular valve. In order to maintain proper control of the valves it is necessary to ensure that there are no skipped pulses, and each pulse carries the same amount of linear motion by the valve stem. To do this, the rotor on the Airpax motor was marked and it was confirmed

that 96 pulses equaled one full revolution; whether each pulse was sent one at a time or all at once. It was also confirmed that pulses sent in the clockwise direction equaled those sent in the counter clockwise direction. It was determined that 2140 pulses (half steps) were needed to fully open the TXV from a fully closed state, while 2160 pulses were needed for the hot gas bypass valve and 1160 pulses were needed for the condenser water valve. Knowing the number of pulses needed to send a valve fully open enables position tracking which is essential for control.

2.3.2 Valve Control

A proportional plus integral plus derivative (PID) controller is implemented to control each valve. In classical control[16], a PID controller is described by Equation 2.3,

$$u(t) = K_{\mathrm{c}} \left[e(t) + \frac{1}{T_{\mathrm{i}}} \int_0^t e(t)\, dt + T_{\mathrm{d}} \frac{de(t)}{dt} \right] \tag{2.3}$$

where $u(t)$ is the controller input, $e(t)$ is the setpoint error (i.e. for the TXV, which controls the suction temperature, $e(t) = ST_{\mathrm{set}} - ST(t)$), K_{c} is the controller gain, T_{i} is the integral time, and T_{d} is the derivative time. For valve control, the controller input is valve position. Equation 2.3 is continuous and while the process variables (ST, SST, and $SCET$) are continuous, the CR1000 can only read their values and actuate the valves at discrete intervals. Thus the equation must be approximated through discretization. The derivative mode is approximated by the backward-difference approximation and the integral mode is approximated by the backward integration rule[13], leading to Equation 2.4,

$$u(k) = K_{\mathrm{c}} \left[e(k) + \frac{1}{T_{\mathrm{i}}} S(k) + \frac{T_{\mathrm{d}}}{T} \{ e(k) - e(k-1) \} \right] \tag{2.4}$$

where $u(k)$ is the controller input at sample k, $e(k)$ is the setpoint error at the k-th sample, T is the sample interval, and $S(k)$ is the integrator, or the sum of the errors at sample k; $S(k) = S(k-1) + Te(k)$. The sample interval is one second; that is, the CR1000 scans and reads the control temperatures and pressures and appropriately

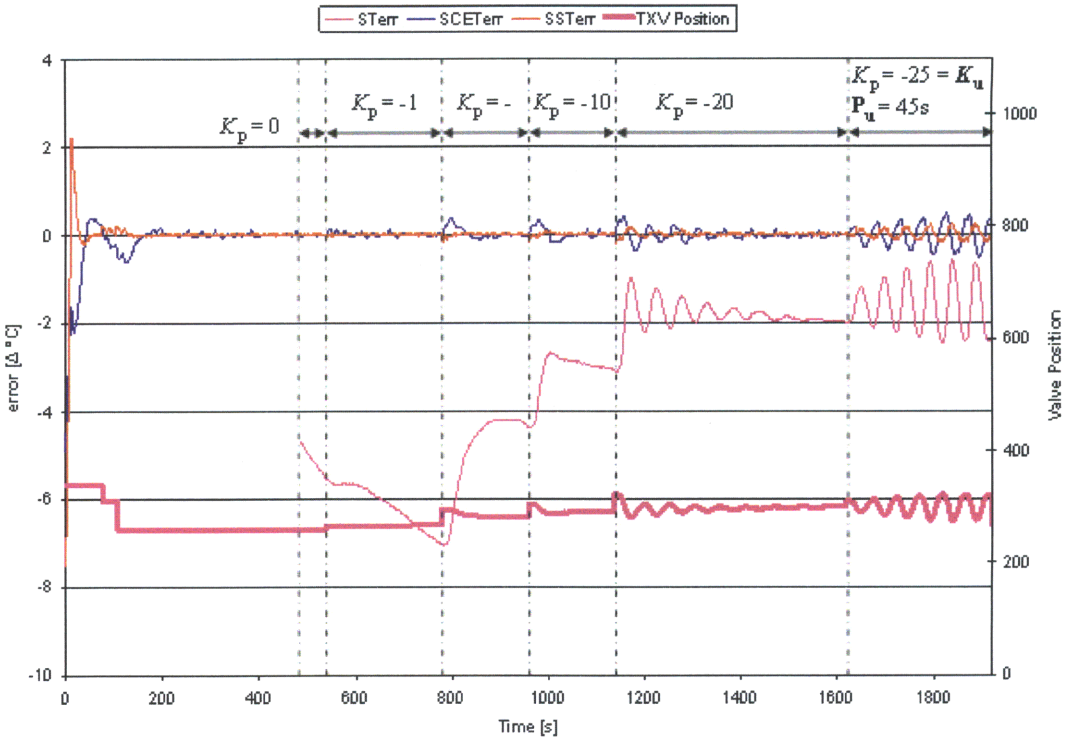

Figure 2-13: Ziegler-Nichols tuning of the thermal expansion valve.

actuates the valves each second. There is certainly some limit to just how much reading and actuating the CR1000 can process in one second. If the CR1000 takes more than one second to perform these tasks, then a scan (or more) is skipped. When a scans are skipped, the actual period is longer than T. This can wreak havoc on the controls as Equation 2.4 depends on this interval. To prevent skipped scans, a limit was placed on how far each valve could be actuated during a sample period. Valves were limited to a maximum of 50 pulses per a scan. The number of pulses sent to a valve is simply the difference between $u(k)$ and the current valve position. Also, not only is the scan rate discrete, but the control input (valve position) is also discrete. Thus, the resulting $u(k)$ must be rounded.

Ziegler-Nichols Tuning

To obtain appropriate values for K_c, T_i, and T_d for each valve the Ziegler-Nichols tuning method based on the ultimate gain and ultimate period of the response is

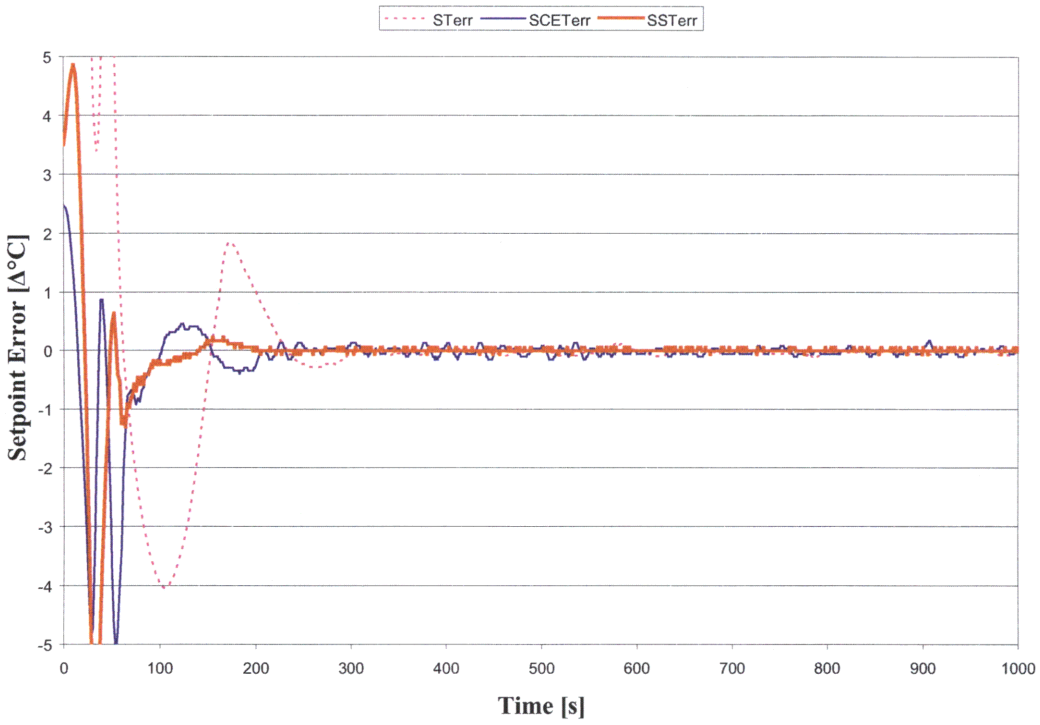

Figure 2-14: Example of PID controller performance.

used[16]. This is a closed loop control tuning method in which the plant is put under proportional control (i.e. T_d is set to zero and $T_i \rightarrow \infty$). The magnitude of the value of K_c is increased until sustained oscillations are observed. This value of K_c is taken to be the ultimate gain, K_u, and the period of oscillation is taken to be ultimate period, P_u. The Ziegler-Nichols gains for both PI and PID control are given in terms of K_u and P_u in Table 2.3. Ziegler and Nichols developed this method nearly 70 years ago, yet it is still quite useful. The resultant gain relations were developed empirically and they do not provide optimal (i.e. fastest settling time with the lowest overshoot) control parameters, but rather, serve as a good starting point. The loops have non-negligible effects on each other. Therefore the loops are tuned in the following sequence. First, the hot gas bypass valve is tuned because it has the fast response time, while the condenser water valve and TXV are in a fixed positions. Then, with the hot gas bypass valve under control, the condenser water valve is tuned, and, finally, the TXV is tuned with both the hot gas and the condenser water valves under control. The

	K_c	T_i	T_d
P	$0.5K_u$	n/a	n/a
PI	$0.45K_u$	$0.83P_u$	n/a
PID	$0.6K_u$	$0.5P_u$	$0.125P_u$

Table 2.3: Recommended Ziegler-Nichols gains[16].

hot gas bypass valve can then be re-tuned with the other valves under control. Figure 2-13 shows the Ziegler-Nichols tuning process for the thermal expansion valve. Since this loop is the last to be tuned, the hot gas bypass and condenser water valves are under control during the tuning process. First the controller gain is set to zero, then -1, and then the magnitude is increased until sustained oscillations are observed. Note that the controller gain on the TXV loop is negative; this is due to the way the error is defined on the TXV loop ($e_{\text{TXV}}(t) = ST_{\text{set}} - ST(t)$). A positive error means that the suction temperature is cooler than setpoint. In order to raise the temperature, the TXV must be modulated closed, thus the negative controller gain. The controller gains on the hot gas bypass ($e_{\text{HG}}(t) = SST_{\text{set}} - SST(t)$) and the condenser water ($e_{\text{CW}}(t) = SCET(t) - SCET_{\text{set}}$) valves are positive. When the controller gain is increased to -20, oscillations begin, but dampen out over approximately 5 minutes. When the gain is increased to -25, the oscillations become steady, so this is taken to be the ultimate gain, K_u, and the ultimate period, P_u, is about 45 s. The recommended Ziegler-Nichols PID gains are then found (using Table 2.3) to be -15, 22.5, and 5.625, for K_u, T_i, and T_d, respectively. As previously mentioned, these gains served as a starting point. The aim was to get a single set of gains that were robust enough to work under various conditions. Table 2.4 shows the gains used for all three valves. The controller gain on the TXV must be dramatically reduced (sometimes as low as -1) when taking points with low suction super heat ($ST - SST$), but other than this gain, this set of gains provides the ability to bring the system under control within a reasonable amount of time and to provide reasonably tight control. Figure 2-14 shows an example of how well the PID controller was able to meet setpoint. In this example, all errors are reduced to ± 0.2 °C within 5 minutes.

An important issue regarding PID control is that of integrator wind up. When

	K_c	T_i	T_d
	[position/°C]	**[s]**	**[s]**
HG-VLV	35	5	0.1
CW-VLV	80	14	1
TX-VLV	-15	30	7.5

Table 2.4: PID gains for each valve.

a valve is saturated (either fully open or fully closed) while setpoint is not met, the integrator term will simply keep growing in magnitude. Subsequently, when the sign of the error changes and the valve actually needs to start opening (if it were saturated close), it could take too long for the magnitude of the integrator term to decrease to a level that would result in the valve being commanded to open. This could be problematic for almost any system and result in a catastrophic failure. For instance, if the there is a large setpoint change in the $SCET$, this could cause the condenser water valve to saturate closed. If the condenser water valve does not open in time, this could result in dangerously high discharge pressures. To prevent such integrator 'wind-ups,' the integrator is stopped once the valve reaches saturation. Integration is not resumed until the error changes sign. Also, because integration action is moving towards a specific setpoint, the integrator is zeroed if the setpoint is changed.

2.4 Replication of Previous Data Points

One of the major benefits to using this calorimeter is that the previous project provides data for comparison purposes. Two data points were chosen, one with a high compressor input power and one with a fairly low compressor input. The compressor input power as well as the refrigerant mass flow were measured at each point and compared with the data from the previous project. Figures 2-15 and 2-16 show the power and mass flow rate as measured by the CR1000 with $SCET_{\text{set}} = 55.83°\text{C}$; $SST_{\text{set}} = -6.67°\text{C}$; and $ST_{\text{set}} = 4.44°\text{C}$. Table 2.5 shows the average power and mass flow rates at this test point. Both the mass flow rate and the compressor power agree to within 2%.

Figures 2-17 and 2-18 show the power and mass flow rate as measured by the

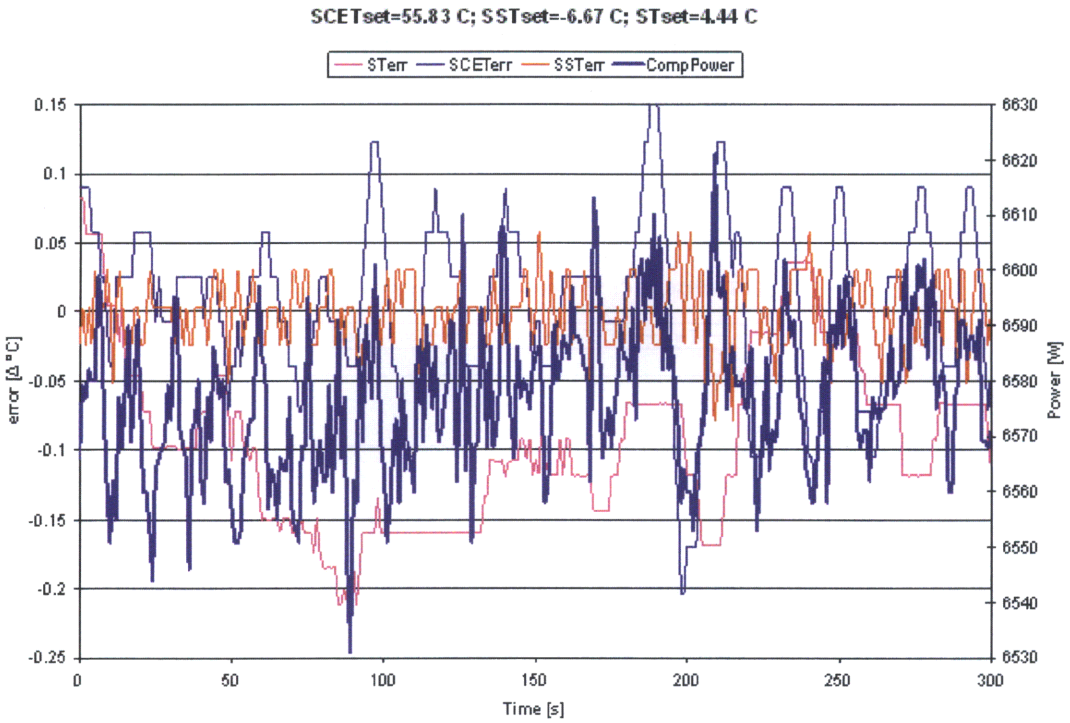

Figure 2-15: Errors and power at first replicated data point.

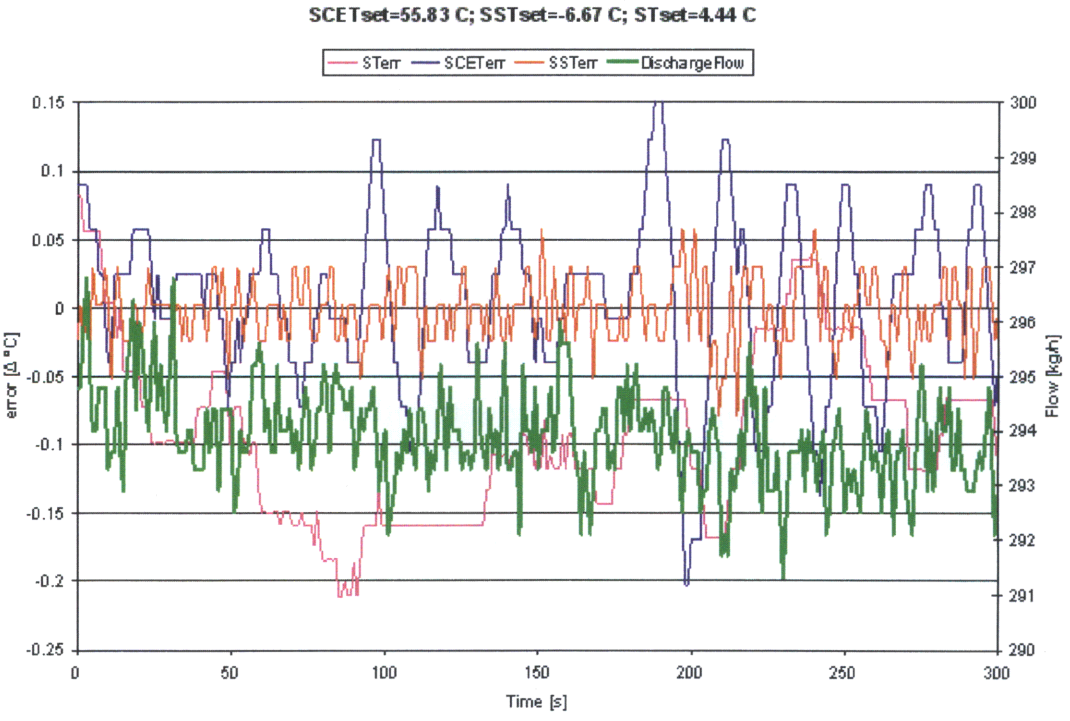

Figure 2-16: Errors and mass flow at first replicated data point.

	Power	Flow
	[W]	[kg/h]
Otten's Value	6514	298
AVG	6577	294

Table 2.5: Comparison of measured data and previous data for first replicated data point.

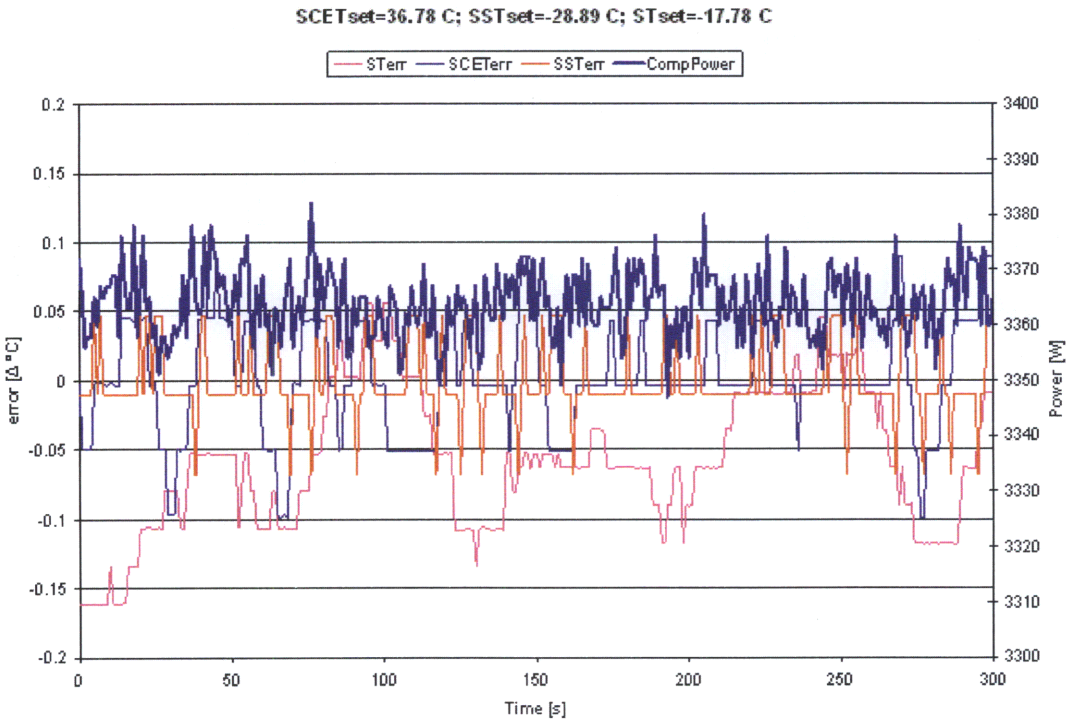

Figure 2-17: Errors and power at second replicated data point.

CR1000 with $SCET_{\text{set}} = 36.78°\text{C}$; $SST_{\text{set}} = -28.89°\text{C}$; and $ST_{\text{set}} = -17.78°\text{C}$. Table 2.6 shows the average power and mass flow rates at this test point. Again, both the mass flow rate and the compressor power agree to within 2%.

2.5 Variable Frequency Drive

One of the central changes made to the system was the installation of the variable frequency drive (VFD). A Baldor AC closed vector control VFD is used for this test stand. The VFD takes primary three phase power supply running at 60 Hz and uses a pulse width modulation (PWM) scheme to feed three phase power to the motor at

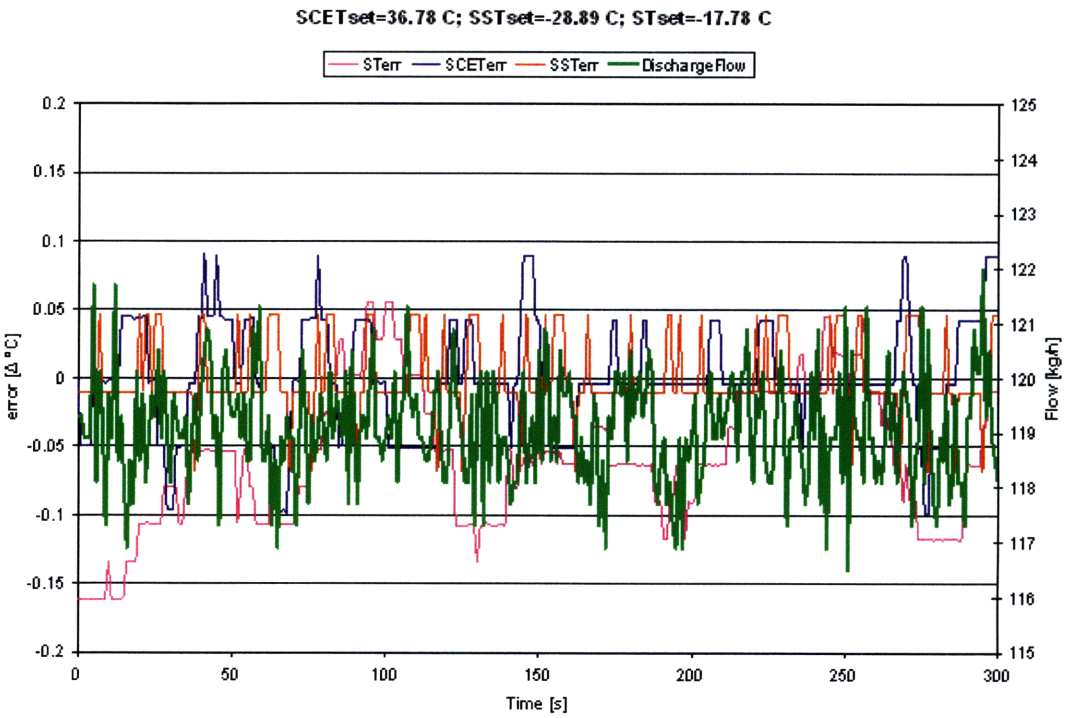

Figure 2-18: Errors and mass flow at second replicated data point.

	Power	**Flow**
	[W]	**[kg/h]**
Otten's Value	3303	118
AVG	3364	119

Table 2.6: Comparison of measured data and previous data for second replicated data point.

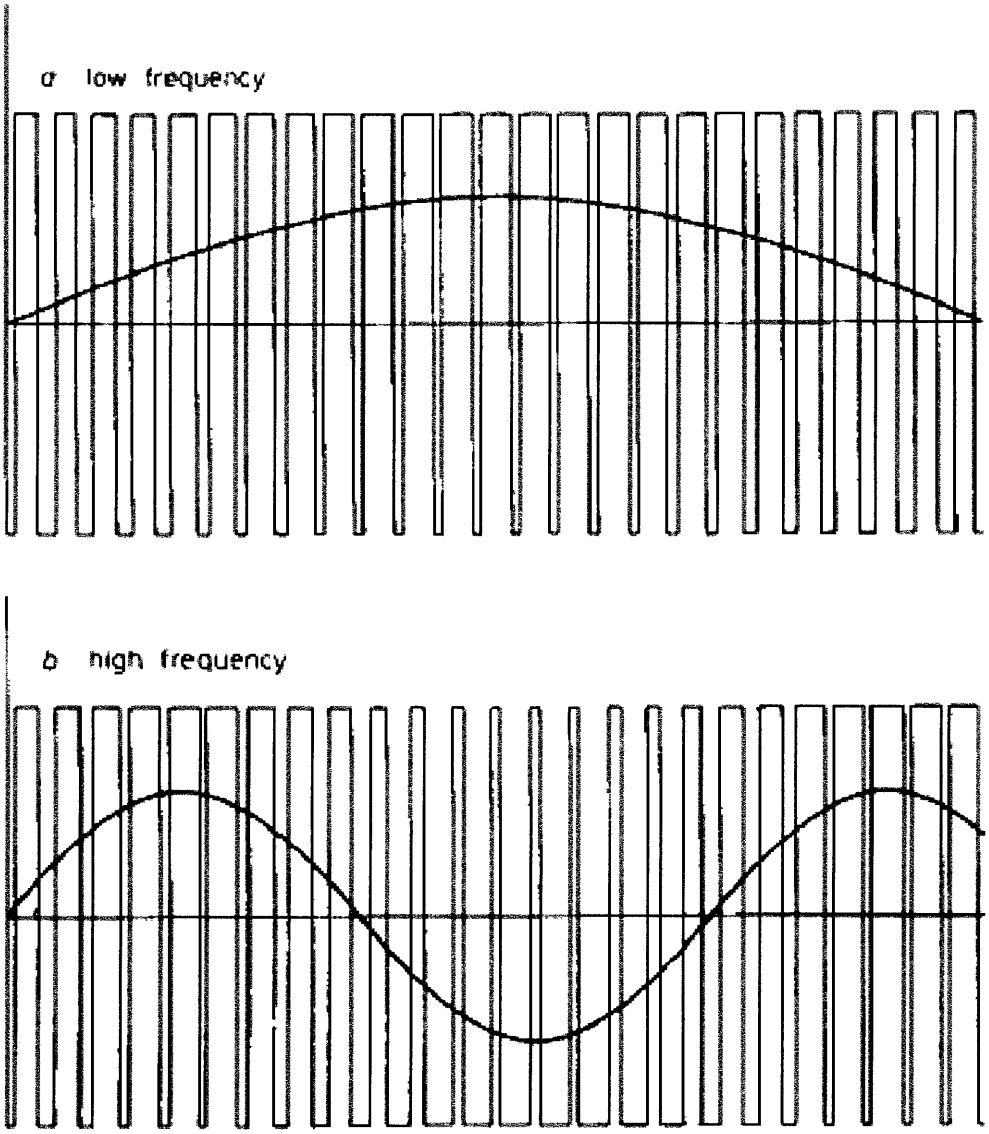

Figure 2-19: Frequency variation using PWM[11].

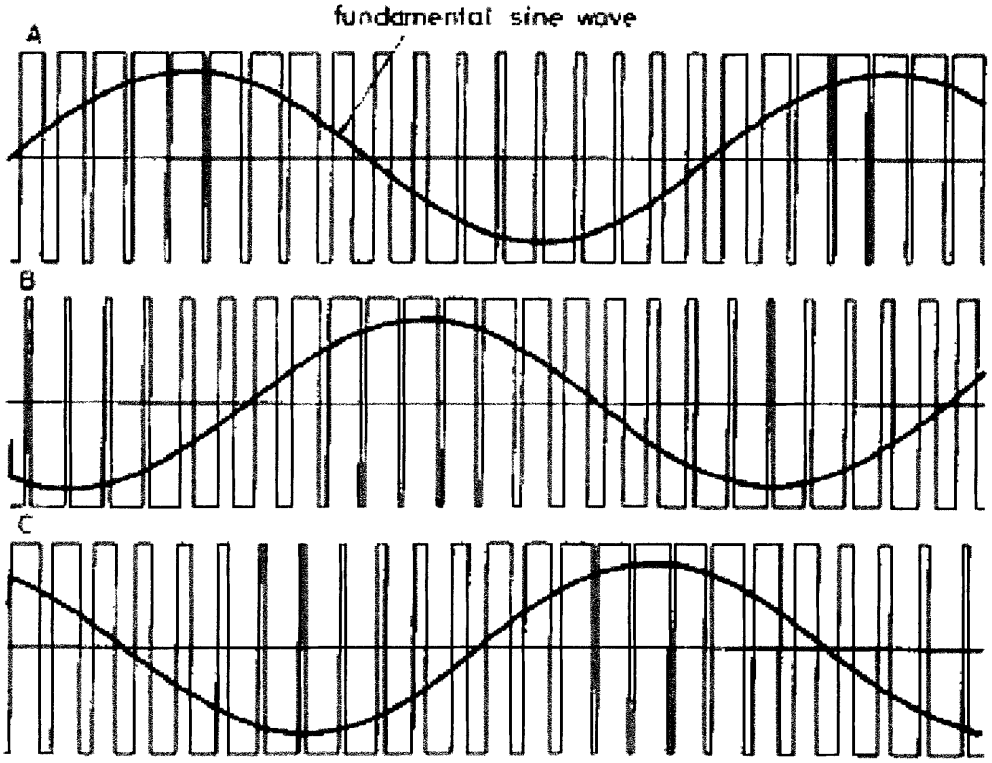

Figure 2-20: 3 Phase operation of PWM scheme[11].

a lower (or higher) frequency. This is a DC link inverter system in which the primary power is rectified to produce a DC (direct current) voltage which is then inverted to supply AC (alternating current) to the motor. Essentially, with a PWM scheme, the voltage is switched on and off (pulsed) onto the motor many times during each half cycle. The voltage is switched between the positive and negative values of the DC voltage. The frequency and duration (width) of the 'ON' pulses are varied with respect to those of the 'OFF' pulses over the desired half cycle. As a result, the magnitude and the frequency of the sine wave can be varied. Figure 2-19 shows the PWM frequency variation, achieved by changing the time between high frequency pulses or by changing the number of pulses which occur in a half cycle. Voltage variation can also be achieved by changing the width of the pulses. The maximum peak voltage is equivalent to the DC voltage level. To reduce the voltage by some proportion, the widths of all the pulses must be reduced by that same proportion. All three phases of the inverter are being pulsed, continuously, at the switching frequency so that the motor gets the correct supply voltage to turn at the desired speed. Figure 2-20 shows the three-phase operation of the PWM principle. Note that the voltages are 120° out of phase.

2.6 Other Considerations

2.6.1 Refrigerant Charge and Leakage

Refrigerant charge is the amount of refrigerant that is used in the system. It is important to have the correct amount of refrigerant in the system. An improper refrigerant charge can affect system performance and lead to equipment failure. An overcharged system can lead to increased power consumption as the effective condenser area is reduced, leading to a higher condensing temperature and pressure and higher compression ratio[7]. An overcharged system also may lead to excess liquid refrigerant finding its way to the compressor. Liquid refrigerant in the compressor could lead to catastrophic failure of the compressor as it attempts to compress a nearly incompress-

ible fluid[33]. Both undercharged and overcharged systems have an adverse effect on energy efficiency as well as cooling capacity. The energy efficiency ratio (EER) of the system can be reduced by 16% for an undercharged system and by as 11% for an overcharged system[27]. The cooling capacity can be reduced by as much 24% for undercharged systems while overcharging the system has a less dramatic effect on the cooling capacity with a 4.5% reduction[7]. The charge used for this system was 7 lbs. Enough refrigerant was used so that the system could meet the most extreme condition in the Otten/Wilson dataset, but the charge was kept low enough so that liquid refrigerant was not backed up all the way to the condenser during operation.

Refrigerant leakage is also of great concern with any refrigeration system. This project used the hydrofluorocarbon (HFC) refrigerant R-134a. While the absence of chlorine in R-134a (as opposed to hydrochlorofluorocarbon refrigerants, such as R-22) means that it does not contribute to the degradation of the ozone layer, it is still important not to unnecessarily vent this refrigerant to atmosphere. It still contributes to global warming, and because its vapor density is less than that of air, release of too much refrigerant in a confined space could lead to one being asphyxiated. To prevent leaks, all joints must be properly sealed during normal operation as well as charging and recovery operations. This system had many leaks which needed to be sealed. Some leaks were so large that one could hear the refrigerant leaking out, but most of the time some other method of leak testing and detection was employed. To check if a system had a leak, it is useful to observe how well it hold a vacuum. The system is pulled down, using a vacuum pump, to very low pressures (500 microns) and then left idle. If the system is not properly sealed, the pressure in the system will rise. If a leak is suspected, an electronic leak tester may be used to fin the location of a leak. Alternatively, a leak testing fluid may also be used. With this method, the fluid is applied to joints suspected of leaking. If a leak exists at that joint, bubbles should form.

Refrigerant recovery must also take place anytime modifications are made to the system which would result in a chance for the refrigerant to be vented to atmosphere. Recovery involves pumping the refrigerant through a recovery machine and into a

recovery tank. The refrigerant is then stored in the recovery tank until the system is used again.

2.6.2 Electromagnetic Interference and Grounding

The chopped waveform output from the VFD results in a substantial concern regarding electromagnetic interference (EMI). EMI can wreak havoc on low voltage lines in the system. These include the wires used to actuate the valves as well as the signal wires from sensor, such as the pressure transducers and flow meter. Consequently, it is imperative that these wires are properly shielded. For example, failure to properly shield the control valve wires results in the multiple valves being actuated upon the command to actuate a single valve. This, naturally, makes the system uncontrollable and unstable. This was a major source of problems for this work. Shielding is achieved by wrapping the control wires in some conductive material and providing a way for any excess current to find its way to ground. Control wires are typically purchased with a shield within the insulation. It is important that this shield is connected to ground, and not left *floating*, to EMI from disrupting the control signal. Grounding of the system is of particular importance for safety concerns as well. If the chassis ground potential is left *floating* at some higher potential than earth ground, this creates a potentially dangerous situation. A person touching the chassis and earth ground would feel the full effect of this voltage difference and could incur bodily harm. To prevent this system, all of the components from the CR1000 to the VFD were connected to the building's earth ground.

Chapter 3

Experimental Results

The goal of the experimental section of this thesis is to get compressor performance data at a wide range of pressure ratios and over various speeds with an emphasis on the low-lift region (high suction pressures and low discharge pressures). SSH is the suction superheat; it is the difference between suction temperature, ST, and saturated suction temperature, SST. The goal was to record data at four speeds (60, 50, 40 and 30 Hz), three saturated condenser exit temperatures (50, 40, and 30 °C), three saturated suction temperatures (-10, 0, and 10 °C) and two levels of superheat (3 and 10 °C). This would have resulted in 72 data points, as shown in Table 3.1, however not all points were attainable. The points which were not achievable are struck out in the table. Particularly at high speeds, reaching low discharge pressures while having high suction pressures was problematic. For points which could not be achieved, the most extreme points were taken. That is, if a $SCET_{\text{set}}$ of 30 °C is not possible, then the set point might be changed to 33 °C. The scroll compressor would not run at frequencies less than 40 Hz, and had trouble controlling at this frequency. Therefore, the frequency range was changed to include test points at 60, 50, and 45 Hz. There was focus on getting points at low speed and low pressure ratios. The pressure ratios in this data set range from 7 to 1.3.

Freq	*SCET*	*SST*	*SSH*		**Freq**	*SCET*	*SST*	*SSH*
[Hz]	[°C]	[°C]	[°C]		**[Hz]**	[°C]	[°C]	[°C]
60	50	-10	10		~~40~~	~~50~~	~~-10~~	~~10~~
60	50	-10	3		~~40~~	~~50~~	~~-10~~	~~3~~
60	50	0	10		~~40~~	~~50~~	~~0~~	~~10~~
60	50	0	3		~~40~~	~~50~~	~~0~~	~~3~~
60	50	10	10		~~40~~	~~50~~	~~10~~	~~10~~
60	50	10	3		~~40~~	~~50~~	~~10~~	~~3~~
60	40	-10	10		~~40~~	~~40~~	~~-10~~	~~10~~
60	40	-10	3		~~40~~	~~40~~	~~-10~~	~~3~~
60	40	0	10		~~40~~	~~40~~	~~0~~	~~10~~
60	40	0	3		~~40~~	~~40~~	~~0~~	~~3~~
~~60~~	~~40~~	~~10~~	~~10~~		~~40~~	~~40~~	~~10~~	~~10~~
~~60~~	~~40~~	~~10~~	~~3~~		~~40~~	~~40~~	~~10~~	~~3~~
~~60~~	~~30~~	~~-10~~	~~10~~		~~40~~	~~30~~	~~-10~~	~~10~~
~~60~~	~~30~~	~~-10~~	~~3~~		~~40~~	~~30~~	~~-10~~	~~3~~
~~60~~	~~30~~	~~0~~	~~10~~		~~40~~	~~30~~	~~0~~	~~10~~
~~60~~	~~30~~	~~0~~	~~3~~		~~40~~	~~30~~	~~0~~	~~3~~
~~60~~	~~30~~	~~10~~	~~10~~		40	30	10	10
~~60~~	~~30~~	~~10~~	~~3~~		40	30	10	3
50	50	-10	10		~~30~~	~~50~~	~~-10~~	~~10~~
50	50	-10	3		~~30~~	~~50~~	~~-10~~	~~3~~
50	50	0	10		~~30~~	~~50~~	~~0~~	~~10~~
50	50	0	3		~~30~~	~~50~~	~~0~~	~~3~~
50	50	10	10		~~30~~	~~50~~	~~10~~	~~10~~
50	50	10	3		~~30~~	~~50~~	~~10~~	~~3~~
50	40	-10	10		~~30~~	~~40~~	~~-10~~	~~10~~
50	40	-10	3		~~30~~	~~40~~	~~-10~~	~~3~~
50	40	0	10		~~30~~	~~40~~	~~0~~	~~10~~
50	40	0	3		~~30~~	~~40~~	~~0~~	~~3~~
50	40	10	10		~~30~~	~~40~~	~~10~~	~~10~~
50	40	10	3		~~30~~	~~40~~	~~10~~	~~3~~
~~50~~	~~30~~	~~-10~~	~~10~~		~~30~~	~~30~~	~~-10~~	~~10~~
~~50~~	~~30~~	~~-10~~	~~3~~		~~30~~	~~30~~	~~-10~~	~~3~~
~~50~~	~~30~~	~~0~~	~~10~~		~~30~~	~~30~~	~~0~~	~~10~~
~~50~~	~~30~~	~~0~~	~~3~~		~~30~~	~~30~~	~~0~~	~~3~~
~~50~~	~~30~~	~~10~~	~~10~~		~~30~~	~~30~~	~~10~~	~~10~~
~~50~~	~~30~~	~~10~~	~~3~~		~~30~~	~~30~~	~~10~~	~~3~~

Table 3.1: Originally proposed test matrix.

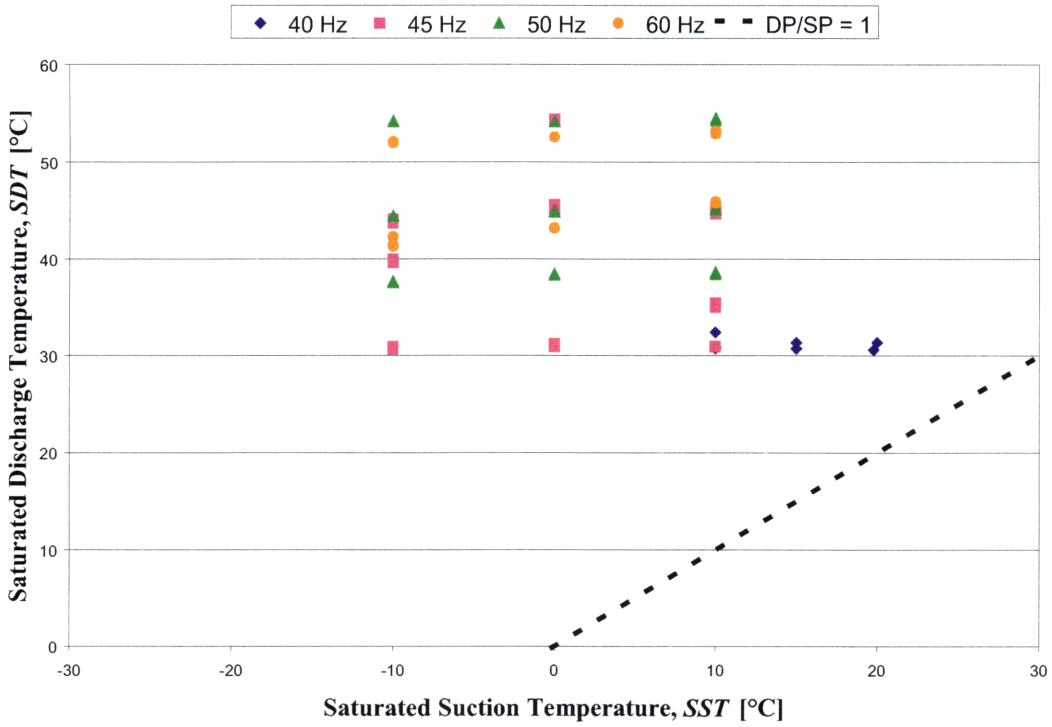

Figure 3-1: Location of test points with respect to saturated suction and discharge conditions.

3.1 Test Data

	Freq	DT	ST	SST	SDT	$\dot{m}_{\mathrm{r}}$	$\dot{W}_{\mathrm{primary}}$	Q_{cond}	$\dot{W}_{\mathrm{VFD}}$
#	**[Hz]**	**[°C]**	**[°C]**	**[°C]**	**[°C]**	**[kg/hr]**	**[W]**	**[W]**	**[W]**
1	60	77.28	3.03	0.00	52.59	384.61	6835.86	6420.15	6561.67
2	60	69.13	13.00	10.00	52.90	545.95	7485.64	7067.82	7189.24
3	60	77.71	20.00	10.00	53.23	520.78	7525.17	7025.71	7238.28
4	60	88.24	-7.00	-10.00	51.98	262.27	6081.64	5720.63	5842.17
5	60	85.11	10.02	0.00	52.57	368.48	6885.95	6391.36	6617.83
6	60	94.33	0.01	-10.00	52.12	261.72	6138.61	5694.11	5900.83
7	60	70.72	20.01	10.00	45.96	514.79	6706.23	6378.56	6458.46
8	60	62.19	13.00	10.00	45.78	537.47	6683.20	6432.03	6482.02
9	60	64.48	3.06	0.00	43.17	391.97	5779.39	5474.47	5558.50

Table 3.2 – Continued on next page

	Freq	DT	ST	SST	SDT	$\dot{m}_r$	$\dot{W}_{primary}$	Q_{cond}	$\dot{W}_{VFD}$
#	**[Hz]**	**[°C]**	**[°C]**	**[°C]**	**[°C]**	**[kg/hr]**	**[W]**	**[W]**	**[W]**
10	60	77.16	0.03	-10.00	42.35	259.58	5085.75	4699.03	4892.50
11	60	72.05	-6.99	-10.00	42.30	266.13	5104.34	4831.64	4906.67
12	60	71.67	10.02	0.00	43.24	378.52	5740.99	5386.50	5517.50
13	60	69.49	-6.96	-10.01	41.50	266.48	4990.43	4934.29	4833.65
14	60	74.00	0.02	-10.00	41.32	260.06	4937.16	4790.50	4779.47
15	50	95.06	-5.49	-10.00	54.25	225.02	5548.83	5093.34	5319.39
16	50	80.47	4.51	0.00	54.15	320.81	5833.44	5449.52	5591.00
17	50	84.36	9.99	0.00	54.15	313.84	5865.38	5386.24	5620.66
18	50	96.57	0.00	-10.00	54.13	225.93	5589.33	5113.00	5349.17
19	50	80.67	20.05	10.00	54.53	423.83	6491.63	5955.08	6219.09
20	50	74.24	14.09	10.00	54.26	438.71	6404.44	5926.74	6139.28
21	50	77.74	0.01	-10.00	44.41	223.86	4459.17	4187.44	4274.37
22	50	68.47	14.01	10.00	45.10	389.10	5442.38	5116.01	5218.79
23	50	75.44	19.98	10.00	45.20	368.67	5489.14	5061.27	5274.52
24	50	67.79	4.53	0.00	44.87	323.57	4872.74	4594.63	4676.10
25	50	71.56	9.96	0.00	44.94	318.28	4868.47	4579.49	4662.17
26	50	75.01	-5.45	-10.00	44.47	227.32	4463.78	4212.84	4286.79
27	50	67.39	0.04	-10.01	37.67	228.87	3877.71	3768.06	3719.60
28	50	64.20	14.55	10.00	38.66	360.76	4746.89	4527.31	4562.65
29	50	69.08	20.01	10.00	38.42	345.66	4674.44	4435.17	4478.04
30	50	64.36	-5.46	-10.00	37.53	231.30	3882.19	3693.65	3726.10
31	50	66.26	10.07	0.00	38.46	306.31	4390.17	4166.93	4218.35
32	50	62.21	4.53	0.00	38.33	311.37	4400.15	4293.79	4230.30
33	45	92.25	10.04	0.00	54.45	254.72	5664.96	5149.43	5428.02
34	45	87.06	3.01	0.00	54.31	263.70	5640.36	5163.40	5403.13
35	45	70.60	3.01	0.00	45.07	274.24	4469.75	4214.21	4283.29

Table 3.2 – Continued on next page

	Freq	DT	ST	SST	SDT	$\dot{m}_{\mathrm{r}}$	$\dot{W}_{\mathrm{primary}}$	Q_{cond}	$\dot{W}_{\mathrm{VFD}}$
#	**[Hz]**	**[°C]**	**[°C]**	**[°C]**	**[°C]**	**[kg/hr]**	**[W]**	**[W]**	**[W]**
36	45	72.97	13.13	10.00	45.08	300.01	4658.48	4293.87	4476.28
37	45	58.77	-6.99	-10.00	43.73	215.65	3977.27	3950.99	3808.43
38	45	78.75	19.97	10.00	44.69	282.33	4640.70	4225.29	4439.87
39	45	76.26	9.98	0.00	45.65	266.10	4576.75	4240.24	4375.49
40	45	80.27	0.00	-10.00	44.18	191.49	4167.48	3846.70	3994.59
41	45	54.21	-7.00	-10.00	40.02	215.22	3710.98	3735.03	3552.29
42	45	74.95	-0.05	-9.99	39.63	193.61	3868.21	3617.17	3714.39
43	45	67.59	19.99	10.00	35.01	262.28	3592.94	3308.15	3450.58
44	45	62.67	13.10	10.00	35.49	276.87	3680.98	3415.19	3523.98
45	45	61.92	20.06	9.99	30.97	266.25	3210.17	2960.54	3096.35
46	45	62.68	3.05	0.00	31.25	215.54	3379.49	3166.85	3244.14
47	45	58.94	-6.94	-10.00	30.63	196.14	3195.62	3051.72	3076.80
48	45	56.56	13.07	9.99	30.88	277.32	3263.85	3007.67	3126.99
49	45	63.53	0.02	-10.00	30.94	192.34	3205.07	3046.38	3070.50
50	45	66.19	9.99	0.00	30.91	211.75	3329.34	3144.83	3217.16
51	40	74.38	20.01	10.00	32.42	175.79	3001.07	2674.73	2864.14
52	40	63.30	24.97	15.00	31.33	230.08	2708.82	2419.57	2585.12
53	40	64.66	13.01	10.00	30.99	191.41	2821.67	2600.64	2692.07
54	40	58.52	30.01	20.00	31.35	298.44	2633.07	2356.15	2510.69
55	40	68.22	20.03	10.00	30.75	190.58	2820.90	2554.44	2691.00
56	40	56.63	17.96	15.00	30.72	243.84	2666.09	2472.02	2543.80
57	40	51.27	23.04	19.80	30.59	313.08	2597.42	2386.46	2492.42

Table 3.2: Experimental results: scroll compressor test data.

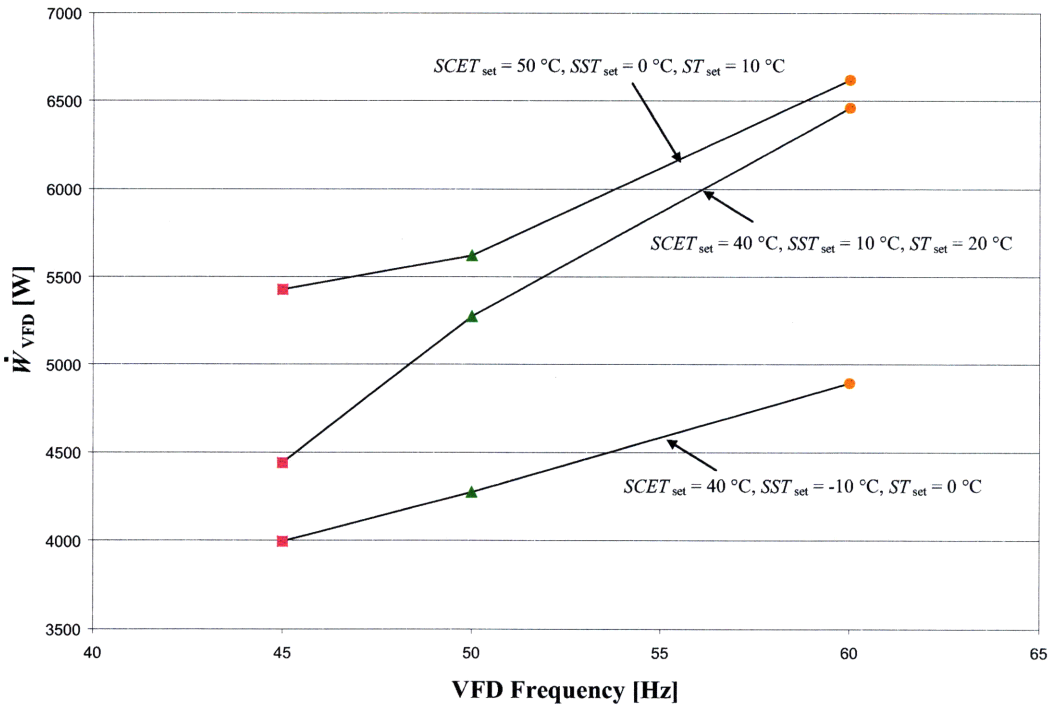

Figure 3-2: Compressor input power for three different conditions.

As shown in Figure 3-1, most of the test points were taken in the same region of pressure ratios. Tests were also conducted at 40 Hz, but these tests only focused on the low-lift regime (i.e. approaching the $DP/SP = 1$ line). The condenser water control valve was left fully open to maximize the amount of heat that was rejected by the condenser. This results in the lowest possible discharge pressure for a given suction condition (temperature and pressure). Saturated suction pressures (i.e., suction pressures) of 10, 15, and 20 °C were tested along with the two levels of superheat for each. A full collection of test data is shown in Table 3.2. There are 57 test points, and for each test point the frequency of the VFD output, the discharge temperature, DT, the suction temperature, ST, the saturated suction temperature SST, the saturated discharge temperature SDT, the refrigerant mass flow rate, $\dot{m}_{\mathrm{r}}$, the primary power, $\dot{W}_{\mathrm{primary}}$, the condenser heat rate (see Section 3.2.1), Q_{cond}, and the output power from the VFD, $\dot{W}_{\mathrm{VFD}}$, are listed. There are two advantages to running the compressor at lower speeds. First, lower motor speeds make lower pressure ratios

more attainable. A saturated suction temperature of 20 °C, a suction temperature of 30 °C, and a saturated discharge temperature of 31 °C was not attainable for speeds greater than 40 Hz. Secondly, even for the same set of conditions, operating the compressor at a lower speed will allow for lower power consumption. Figure 3-2 shows the effect that the VFD frequency has on the compressor input power for three different conditions ($SCET = 50°C$, $SST = 0°C$, $SST = 10°C$; $SCET = 40°C$, $SST = 10°C$, $SST = 20°C$; and $SCET = 40°C$, $SST = -10°C$, $SST = 0°C$). In each case, there is a drop in power. For the top curve, the compressor input power at 45 Hz is 18% less than the power consumption than at 60 Hz. This condition has a pressure ratio of about 5.4. For the bottom curve, the compressor input power at 45 Hz is 18.4% less than the power consumption than at 60 Hz. This condition has a pressure ratio of about 4.8. The greatest reduction in power is seen with the middle curve, which, not surprisingly, has the lowest pressure ratio, at about 2.8. At this test condition, the compressor input power at 45 Hz is about 31% less than the power consumption than at 60 Hz.

3.2 Heat Balances

3.2.1 Condenser Heat Balance

Whenever performing experimental tests, it is important to have some redundancy as a method of checking measurement calculations. If a control volume is draw around the entire system, there are only two points through which energy crosses the boundary. At the compressor, electrical power is fed from the VFD. This electrical power is measured directly by the Yokagawa WT230 Wattmeter. At the condenser, heat is removed through a continuous flow of water. Water, at a moderately cool temperature, flows through the condenser, and is heated by the hot refrigerant flowing through the outer concentric tube of the heat exchanger. The temperature rise of the water as well as the flow rate of water through the condenser determine the condenser heat rate, Q_{cond}. The condenser heat rate is the amount of energy removed by the

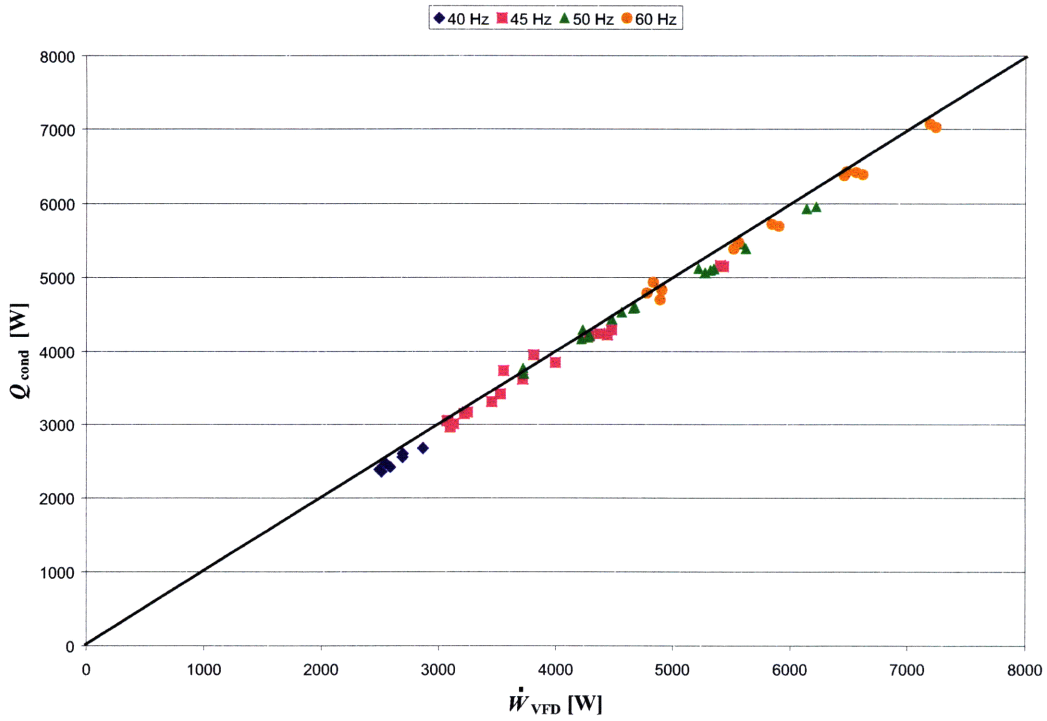

Figure 3-3: Compressor input power versus condenser heat rate.

condenser per unit time, in Watts, and is defined by Equation 3.1,

$$Q_{\text{cond}} = \dot{m}_{\text{water}} \left(h_{\text{water,out}} - h_{\text{water,in}} \right) \tag{3.1}$$

where $h_{\text{water,in}}$ and $h_{\text{water,out}}$ are the entering and exiting enthalpies and $\dot{m}_{\text{water}}$ is the mass flow rate of water through the condenser. Since this is a single input, single output energy balance, ideally, the condenser heat rate should equal the compressor input power. As a part of the experimental setup, condenser water temperatures are being measured, and logged, by the CR1000. The mass flow rate of the water through the condenser is measured manually at each test point. Once the system has reach a steady state, the mass of water that flows through the condenser during some prescribed amount of time is measured. For each of the 57 data points, 3 water mass flow measurements were taken. The measurements were taken while noting the time stamp on the CR1000 datalogger so that correct values of water temperatures

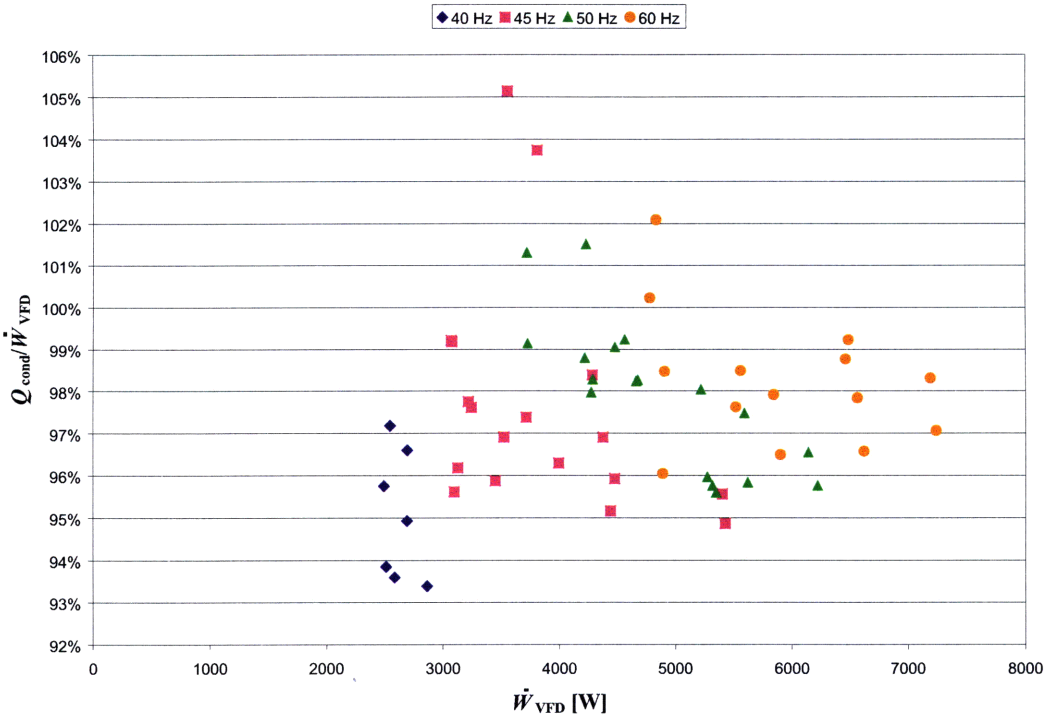

Figure 3-4: Ratio of condenser heat rate to compressor input power.

are used to calculate Q_{cond}. The timestamp resolution is 1 second, so to dampen any errors introduced to the water mass flow rate by the time difference measurement, it is desirable to have a longer test time, provided that the system is truly at steady state so that the compressor power and actual condenser heat rate are not changing with time. The water mass was measured by filling a 5 gallon water cooler bottle and measuring the change in mass, so the length of the mass flow measurement was limited by how fast the bottle was filled. For most test points it was possible to have test times of 3 or more minutes, but for test points with the highest condenser water flow rates, test times were limited to 60 seconds. Figure 3-3 shows the condenser heat rates versus the compressor input power for each test point. To say that energy only crosses the control volume at the condenser and the compressor is to say that the system is completely adiabatic. This, of course, is not accurate, as the refrigerant vapor flowing through the discharge line is often quite hot; sometimes 100 K hotter than the ambient temperature in the room. The discharge line is an extreme area, but any place on the

system that is at a different temperature than the surrounding ambient air is a place for potential "jacket" energy loss, as heat is exchanged with the surroundings. To mitigate the effects of these "jacket" losses, the condenser, mixing coil, flow meter, filter drier, and most of the piping was insulated. At one point, without insulation, the calculated condenser heat rate was about 89% of the compressor input power. With the addition of the insulation, the calculated condenser heat rate was about 96% of the compressor input power. All of the data in Figure 3-3 is with insulation. The condenser heat rate is always within 93% to 106 % of the compressor input power, with most of the data points being within 95% to 100%. Plotting the ratio of condenser heat rate to compressor input power(Figure 3-4) provides an even clearer view. There are two points with $\frac{\dot{Q}_{\text{cond}}}{\dot{W}_{\text{VFD}}}$ values over 103%. These values occurred at points with suction temperatures at -7 °C. These points were done back to back, so the system remained at this low suction temperature for several hours. As a result, frost started to cover much of the compressor shell, thus there was, realistically, some heat gained by the system at these points. While most of the piping and other equipment was insulated, the compressor shell itself was left uninsulated. There are 4 other points with $\frac{\dot{Q}_{\text{cond}}}{\dot{W}_{\text{VFD}}}$ values over 100%. For two of these test points the suction temperature was at 0 °C, while it was at -7 °C and 4.5 °C for the other two. For all of these test points the mass flow of water through the condenser was fairly high so that the time period over which these tests were taken was on the order of one minute. The shorter time period means that an error of one second has a greater effect on the mass flow measurement. Similarly, all of the points with $\frac{\dot{Q}_{\text{cond}}}{\dot{W}_{\text{VFD}}}$ values less than 95% occur at points where the test where the 5 gallon water bottle was filled in 60 seconds. Still, the heat balance provides good confirmation of the power and condenser water thermocouple measurements. The compressor shell itself was not insulated, so there was some amount of heat loss from the motor and compressor body. Accordingly, the differences between the input power and the condenser heat rate are due to both the heat loss from the compressor shell and any measurement error.

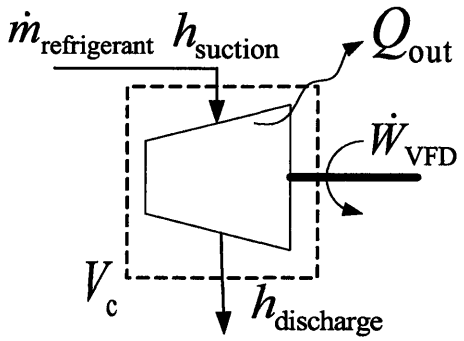

Figure 3-5: Compressor shell heat transfer.

3.2.2 Compressor Heat Balance

Drawing a control volume just around the compressor, as shown in Figure 3-5, provides another useful heat balance. Energy transfer is made in three modes. Electrical power, $\dot{W}_{\text{VFD}}$, is delivered to the compressor and most of this energy is transferred to the refrigerant in the form of an enthalpy rise while the rest of the energy exits the control volume in the form of heat losses. A simplified heat balance for this control volume can then be written as Equation 3.2,

$$\dot{W}_{\text{VFD}} = \dot{m}_{\text{r}} \left(h_{\text{discharge}} - h_{\text{suction}}\right) + Q_{\text{out}} = Q_{\text{comp,apparent}} + Q_{\text{out}} \tag{3.2}$$

where Q_{out} is the net energy loss from the compressor shell and $\dot{m}_{\text{r}}$. Typically, the top of the compressor shell (above the scroll crankcase) is near discharge temperature (well above ambient) while the lower half of the shell, through which the suction gas flows, is cooler. Thus, there is heat gained at the suction side and heat loss at the discharge side. The net effect is typically a heat loss (driven by the larger temperature difference between the discharge vapor and ambient), however there are a few points where heat is gained by the system. At these points, Q_{out} is negative. Using a method developed by Leung [17], Otten (for the previous project) estimated the magnitude of the heat loss to be, at its maximum, on the order of 400 W. Q_{out} is also present in the condenser heat balance and is part of the reason there are discrepancies between Q_{cond} and $\dot{W}_{\text{VFD}}$. Since most of the rest of the calorimeter is insulated, Q_{cond} should be equal

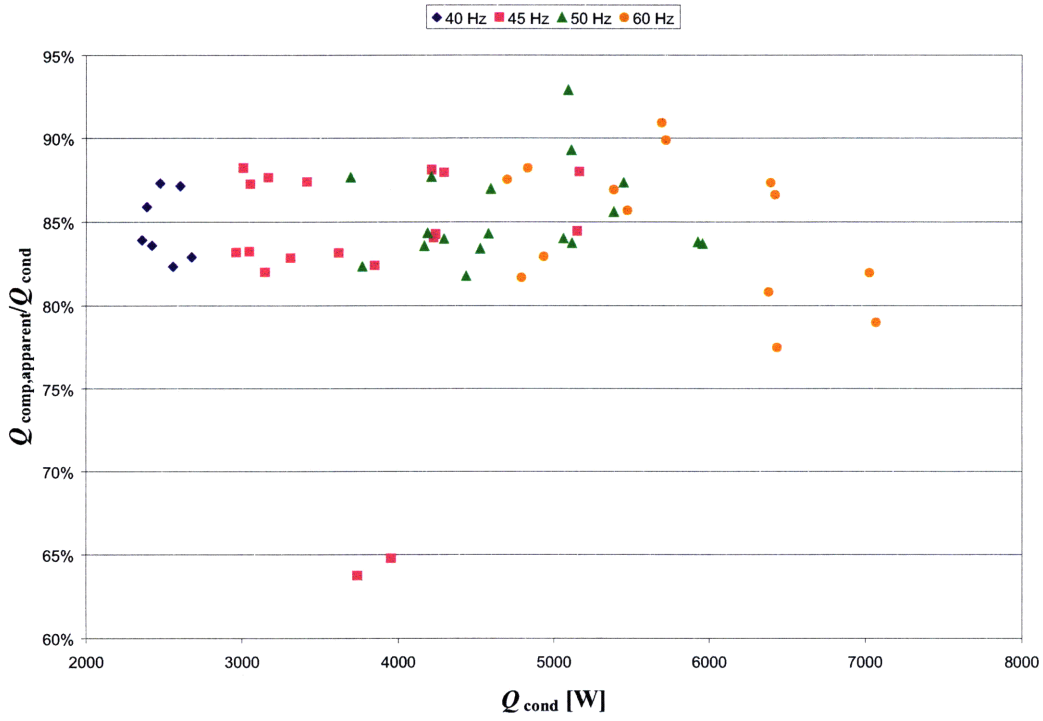

Figure 3-6: Apparent compressor heat rate normalize to and plotted against condenser heat rate.

$Q_{\text{comp,apparent}}$ Figure 3-6 shows a comparison of the condenser heat rate and apparent compressor heat rate, which is given by $Q_{\text{comp,apparent}} = \dot{m}_{\text{r}} \left(h_{\text{discharge}} - h_{\text{suction}}\right)$. The apparent compressor heat rate is, typically, 10-20% lower than the condenser heat rate. There are two likely causes for this error: neglected oil flow and measurement error.

Oil Flow

Equation 3.2 equates the compressor heat rate to the product of the mass flow rate of refrigerant through the compressor and its change in enthalpy. This a simplification. In addition to the refrigerant vapor that is flowing through the compressor, there also is liquid oil which is needed to lubricate the moving parts of the machinery. There is 2-phase flow going through the compressor; with refrigerant vapor and liquid oil. The MicroMotion flow meter is actually measuring the total mass flow, $\dot{m}_{\text{total}} = \dot{m}_{\text{r}} + \dot{m}_{\text{oil}}$.

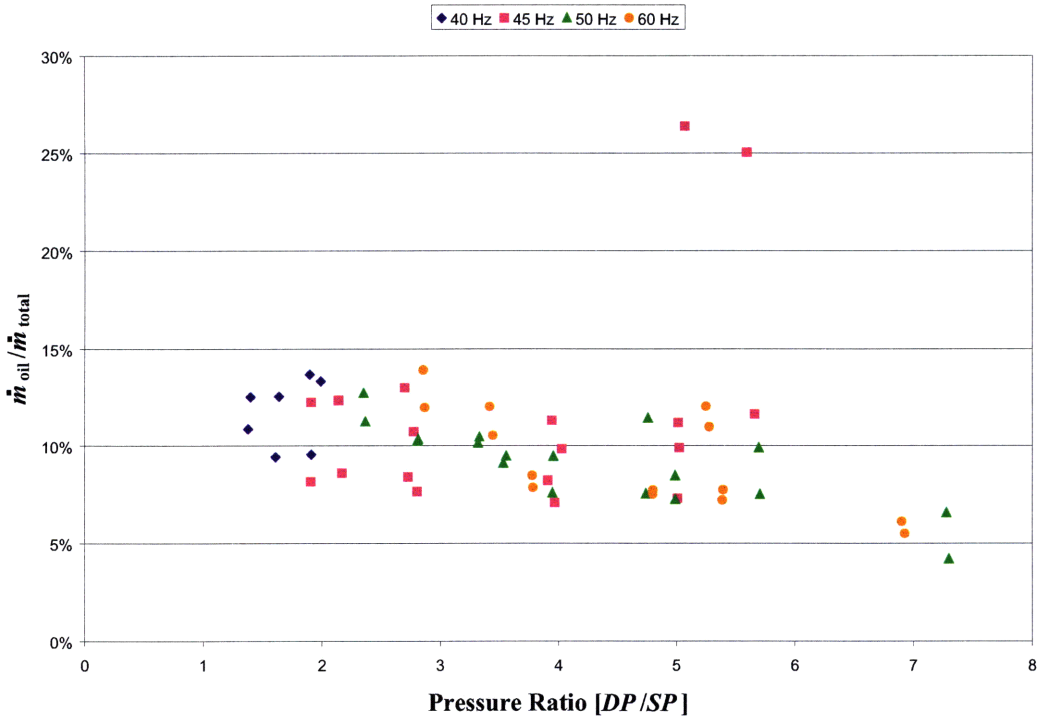

Figure 3-7: Inferred mass flow rate of oil as a percentage of total mass flow.

Therefore, the condenser heat rate is defined by Equation 3.3,

$$Q_{\text{comp}} = (\dot{m}_{\text{total}} - \dot{m}_{\text{oil}})\,(h_{\text{discharge}} - h_{\text{suction}}) + \dot{m}_{\text{oil}} c_{p_{\text{oil}}}\,(T_{\text{discharge}} - T_{\text{suction}}) \qquad (3.3)$$

where $\dot{m}_{\text{oil}}$ is the mass flow rate of oil through the compressor and $c_{\text{p}_{\text{oil}}}$ is the specific heat of the oil. Polyolester (POE) oil is used to lubricate the system. Thermodynamic properties for POE oil are not readily available, so the properties for engine oil are used instead[31]. The specific heat of engine oil, in J/kg*K, varies linearly with temperature, in degrees Celsius [$c_{\text{p}_{\text{oil}}}(T) = 3.094T + 1980.441$]. Equating Q_{cond} to Equation 3.3 (since they are both equal to the compressor input power minus Q_{out}), a mass flow rate for the oil can be inferred.

$$\dot{m}_{\text{oil}} = \frac{Q_{\text{cond}} - \dot{m}_{\text{total}}\,(h_{\text{discharge}} - h_{\text{suction}})}{c_{\text{p}_{\text{oil}}}\,(T_{\text{discharge}} - T_{\text{suction}}) - (h_{\text{discharge}} - h_{\text{suction}})} \qquad (3.4)$$

Figure 3-7 shows the inferred mass flow rate of oil as a function of refrigerant mass flow rate. The inferred oil mass flow rates are typically between 5 and 15% of the total mass flow rate. There were two notable exceptions, however, where the inferred oil mass flow rate is over 25%. This occurs at the same two points that are outliers on the other graphs. These outliers are discussed in section 3.7. These inferred mass flow rates assume there is no measurement error. However, these calculations do show that, in future work, a direct measurement of oil flow may be warranted. In the absence of a direct oil mass flow measurement, the MicroMotion measurement is used for the mass flow of refrigerant vapor in the calculation of the volumetric efficiency. It is also presented in Table 3.2.

Measurement Error

An immediate benefit to performing a heat balance on the compressor is that it highlighted a significant programming error. The thermocouple used to measure discharge temperature, DT, was a type E thermocouple, but the program was written to read a type T thermocouple. As a result, this was giving abnormally high discharge temperature readings. The discharge temperature is not used for control, but is used in the calculation of the isentropic efficiency as well as the compressor heat rate. Consequently, the discharge temperature had to be recalculated in post-test processing. Ultimately, the datalogger is converting a differential voltage into a temperature reading. Depending on what scale is being used, the datalogger calculates the reference temperature voltage and adds this voltage to the sensed voltage, as shown in Equation 3.5 (for a type T reading),

$$V_{\text{sense,T}} = V_{\text{ref,T}} + V_{\text{AM25T}} \tag{3.5}$$

where $V_{\text{sense,T}}$ is the voltage used to calculate temperature using a type T thermo-

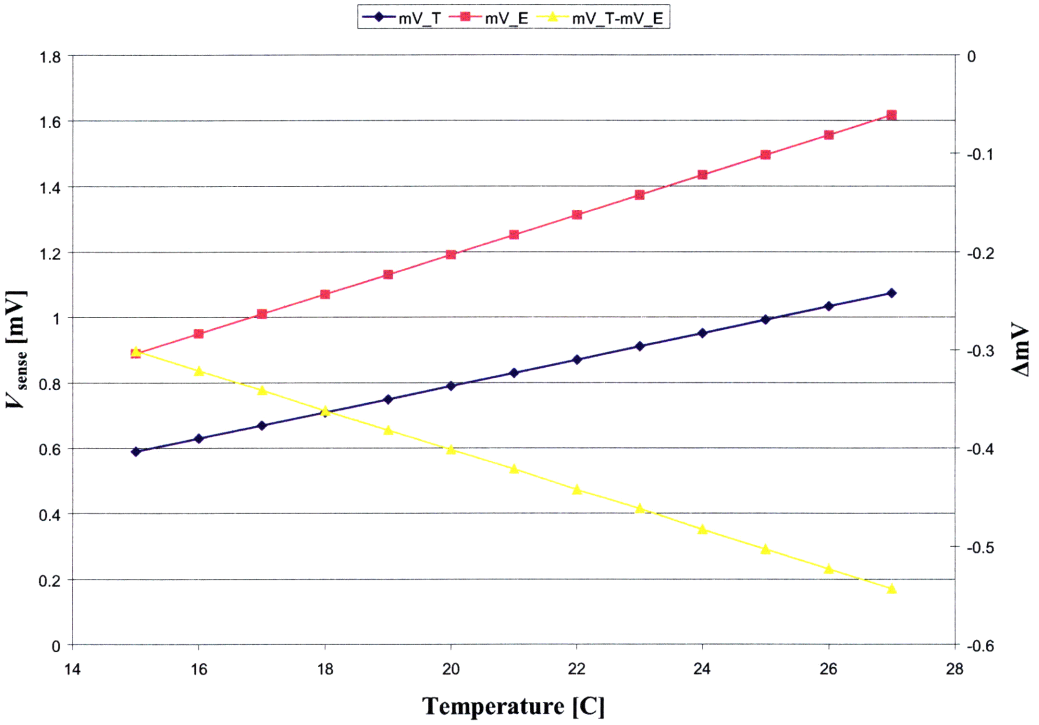

Figure 3-8: Voltage curves for type T and type E thermocouples in room temperature range.

couple equation, V_{AM25T} is the actual differential voltage measured at the AM25T channel, and $V_{\text{ref,T}}$ is the voltage, on the type T thermocouple scale, corresponding to reference temperature; there would be a different voltage ($V_{\text{ref,E}}$) if a type E thermocouple were being read. Unfortunately, the reference temperature was not being recorded. In order to take into account the difference between reference temperature an offset is used. Figure 3-8 shows the voltage curves for both the type T and type E thermocouples, as well as the difference between the two curves at temperatures near typical room temperature. It is clear that the difference is not constant in this range. Accordingly, the average difference was used as the offset. If the difference is defined as $x \equiv V_{\text{ref,T}} - V_{\text{ref,E}}$, then the voltage used to calculate temperature using a type E thermocouple equation, $V_{\text{sense,E}}$, is given by Equation 3.6.

$$V_{\text{sense,E}} = V_{\text{sense,T}} - x \tag{3.6}$$

$V_{\text{sense,T}}$ is calculated using Equation 3.7,

$$V_{\text{sense,T}} = \sum_{i=0}^{8} c_i (DT_{\text{meas,T}})^i \tag{3.7}$$

where c_i is the i^{th} coefficient in Table 3.3 and $DT_{\text{meas,T}}$ is the measured value of DT by the logger which is using the type T command. Then, $V_{\text{sense,E}}$ is calculated according to Equation 3.6, and then Equation 3.8 is used to calculate the real discharge temperature, $DT_{\text{calc,E}}$.

$$DT_{\text{calc,E}} = \sum_{j=0}^{9} d_j (V_{\text{sense,E}})^j \tag{3.8}$$

where d_j is the j^{th} inverse coefficient found in Table 3.4. Taking a constant offset is essentially assuming a constant reference temperature of about 21.5 °C (70.7 °F) , so there is certainly some error with this approach. To get an idea of how much error is introduced, the difference between assuming a reference temperature of 15 °C

c_0	0
c_1	3.87481E-02
c_2	3.32922E-05
c_3	2.06182E-07
c_4	-2.18823E-09
c_5	1.09969E-11
c_6	-3.08158E-14
c_7	4.54791E-17
c_8	-2.75129E-20

Table 3.3: Type T thermocouple coefficients.[22]

d_0	0
d_1	1.70570E+01
d_2	-2.33018E-01
d_3	6.54356E-03
d_4	-7.35627E-05
d_5	-1.78960E-06
d_6	8.40362E-08
d_7	-1.37359E-09
d_8	1.06298E-11
d_9	-3.24471E-14

Table 3.4: Type E thermocouple inverse coefficients.[22]

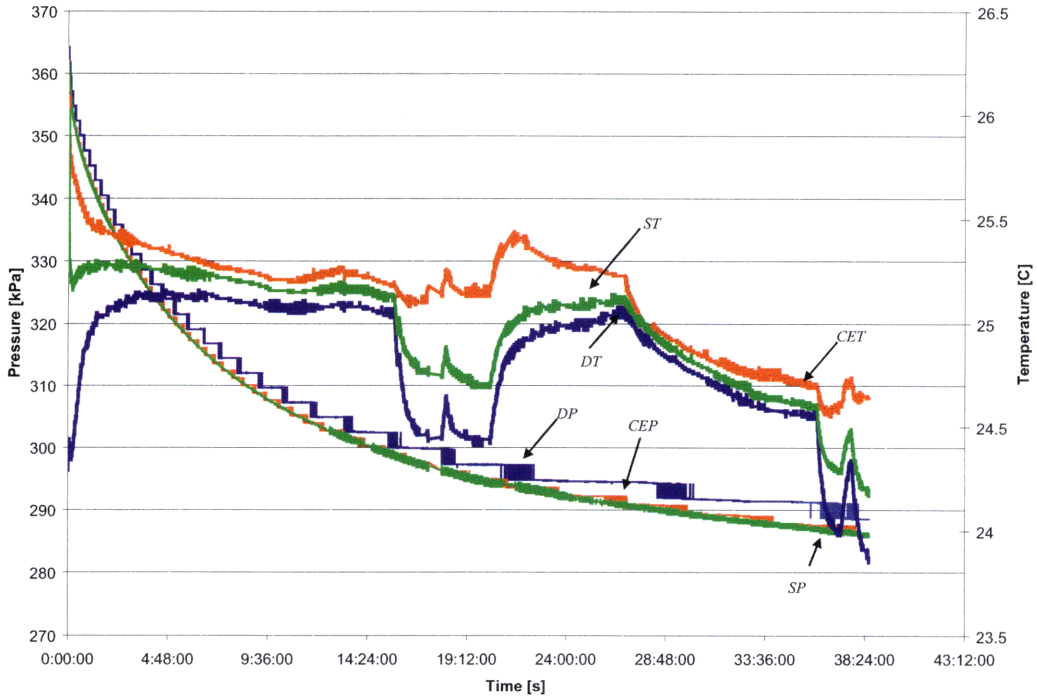

Figure 3-9: Sensor readings over a 38 hour idle period.

(59 °F) and 25 °C (77 °F) were compared for each point. The average difference in measured discharge temperature was 1.24 °C, and ranged from 1.20 °C to 1.28 °C. In addition to this programming error, the sensors themselves could be sources of error. Figure 3-9 shows how well each of pressure transducers as well as the thermocouples agree with each other over a 38 hour period during a leak testing experiment. The thermocouples are typically within 0.5°C of each other and the pressure transducers are typically within 3 kPa. Errors of this magnitude could results in errors in the calculation of the isentropic efficiency of about 9%. Errors in the compressor heat rate would be on the order of 2.3%. There is, however, no direct method to test the validity of the mass flow meter. It is clear from Equation 3.2 that the mass flow has a direct and substantial effect on the calculated compressor heat rate. It is believed that both measurement error and oil mass flow contribute to the discrepancies that are seen between the apparent compressor heat rate and the condenser heat rate measurements. These measurements (Figure 3-9) were taken months before the

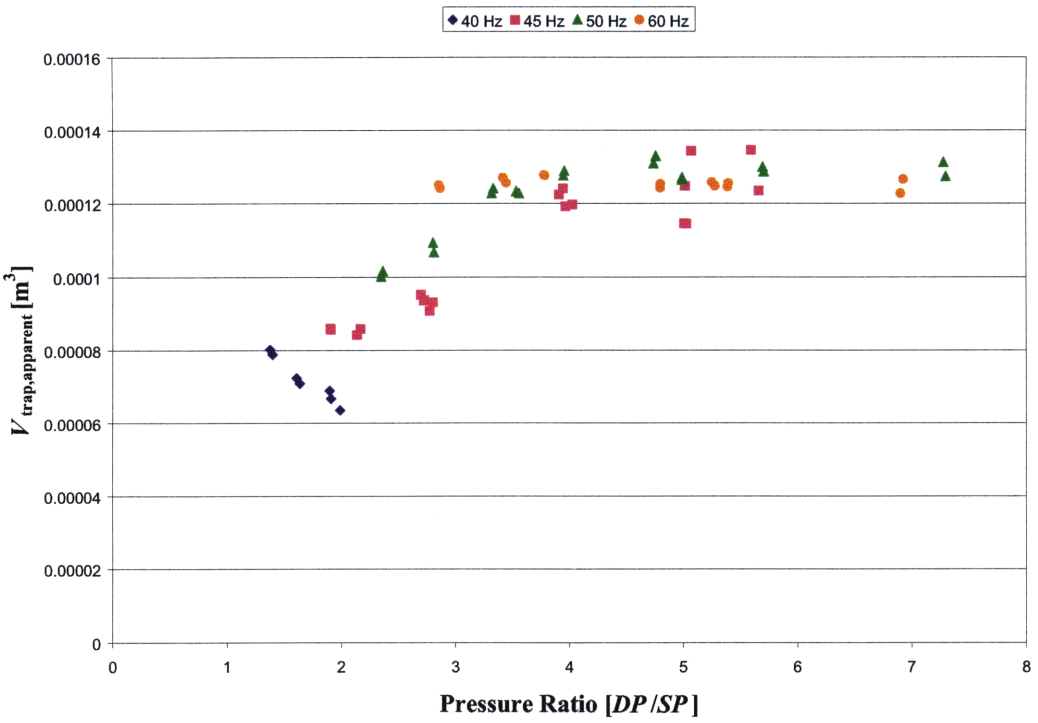

Figure 3-10: Volumetric efficiency for experimental data.

compressor tests were performed, and logged at low resolution (2-byte floating point); the actual compressor tests were take at a higher resolution (4-byte floating point).

3.3 Volumetric Efficiency

The volumetric efficiency of a compressor, η_v can be defined as the ratio of the mass of vapor actually pumped by the compressor to the mass of vapor that would be pumped if the compressor if there were no re-expansion losses[29]. The volumetric efficiency can be written as

$$\eta_v = \frac{\dot{m}_r \nu_{suction}}{V_{trap} f_{HZ}} \tag{3.9}$$

where $\nu_{suction}$ is the specific volume of the refrigerant at the suction state, f_{HZ} is the frequency of the motor, and V_{trap} is the trapped volume, which is the volume of the scroll pocket at discharge. Unfortunately, the trapped volume for this scroll

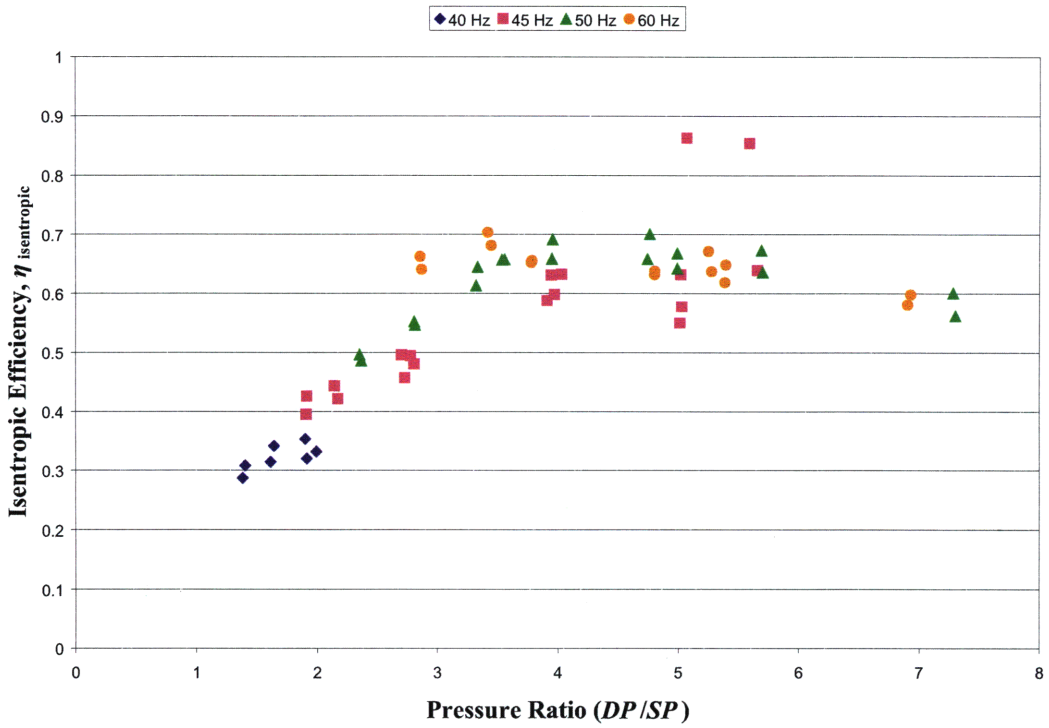

Figure 3-11: Isentropic efficiency for experimental data.

compressor is not known, but the apparent trapped volume can be calculated by Equation 3.10[32].

$$V_{\text{trap,apparent}} = \frac{\dot{m}_{\text{r}} \nu_{\text{suction}}}{f_{\text{HZ}}} \tag{3.10}$$

The apparent trapped volume for each speed is shown in Figure 3.10. This should be a constant parameter and, for high pressure ratios, the trapped volume is fairly constant[32], but for pressure ratios below 3 the apparent trapped volume is smaller. One possible explanation for this phenomenon is leakage between scroll members. Leakage has been shown to increase for certain gaps at low pressure ratio[30].

3.4 Isentropic Efficiency

As mentioned in Chapter 1, one measure of compressor performance is isentropic efficiency. For this process, the isentropic efficiency is defined as

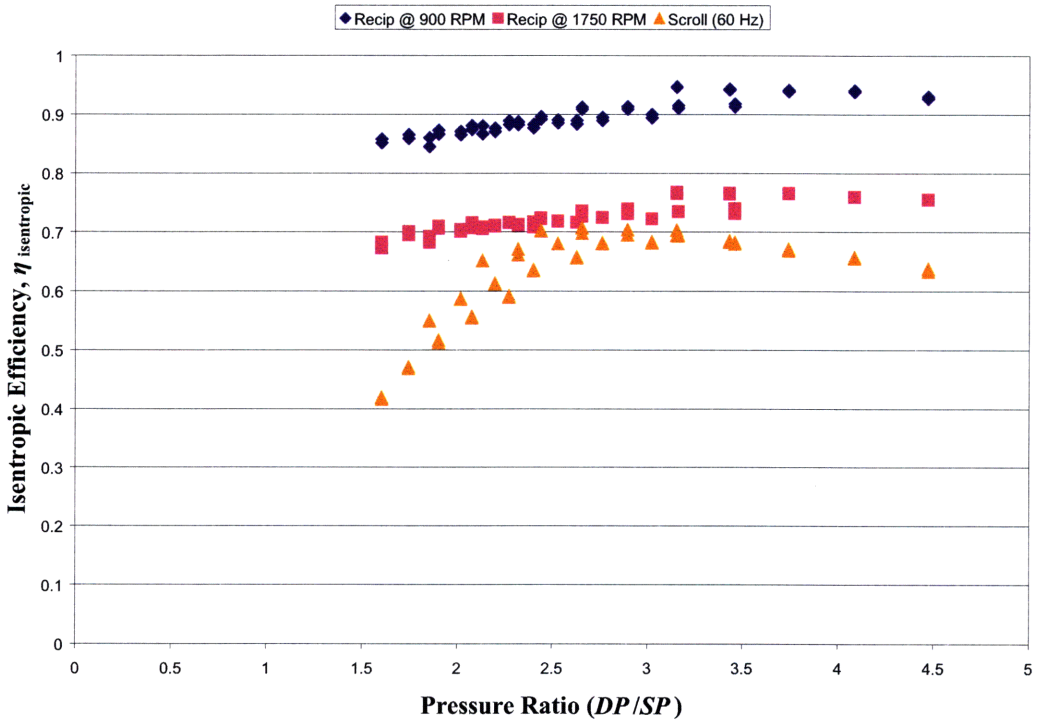

Figure 3-12: Isentropic efficiency for reciprocating compressor as well as a scroll compressor using Carwin tool.

$$\eta_{\text{isentropic}} = \frac{h_{\text{discharge,s}} - h_{\text{suction}}}{h_{\text{discharge}} - h_{\text{suction}}} \tag{3.11}$$

where $h_{\text{discharge,s}}$ is the enthalpy of the refrigerant vapor at pressure $p_{\text{discharge}}$ and entropy s_{suction}, while $h_{\text{discharge}}$ is the enthalpy of the refrigerant at the discharge of the compressor, and h_{suction} is the enthalpy of the refrigerant at the suction port. Figure 3-11 shows the isentropic efficiency as a function of pressure ratio. It is clear that as the pressure ratio decreases, the isentropic efficiency also decreases. This is an undesirable consequence because the goal of this work is operate within the regions of low pressure ratios. A similar drop off is not expected, at least theoretically, for reciprocating compressors, thus this result supports the idea of using a reciprocating compressor in place of a scroll compressor for low-lift, low speed operation. Figure 3-12 shows the isentropic efficiency for a Carlyle 5F60 (a reciprocating compressor) at two different speed as well as for Carlyle scroll compressor (SRH752AC). This data was generated using the Carlyle selection software, Carwin (see section 4.3). It is immediately apparent that the reciprocating compressor sees a much lower reduction in isentropic efficiency at lower pressure ratios than does the scroll compressor. Also, the scroll compressor curve looks similar to the curve generated with the experimental data. This drop off in isentropic efficiency could negate the gains in reduced power consumption. Since the isentropic efficiency drop off for reciprocating compressor is not nearly as dramatic, reciprocating compressors may be the better option for low-lift cooling applications.

3.5 Inverter Efficiency

Some power is loss the inverter. If these losses in the inverter overcome the energy efficiency gains from using the inverter in the first place then it would not be prudent to use a variable frequency drive at all. Inverter losses stem from several sources. There are conduction losses as the inverter itself heats up. The main losses are conduction losses and switching losses in the power electronics that produce the PWM

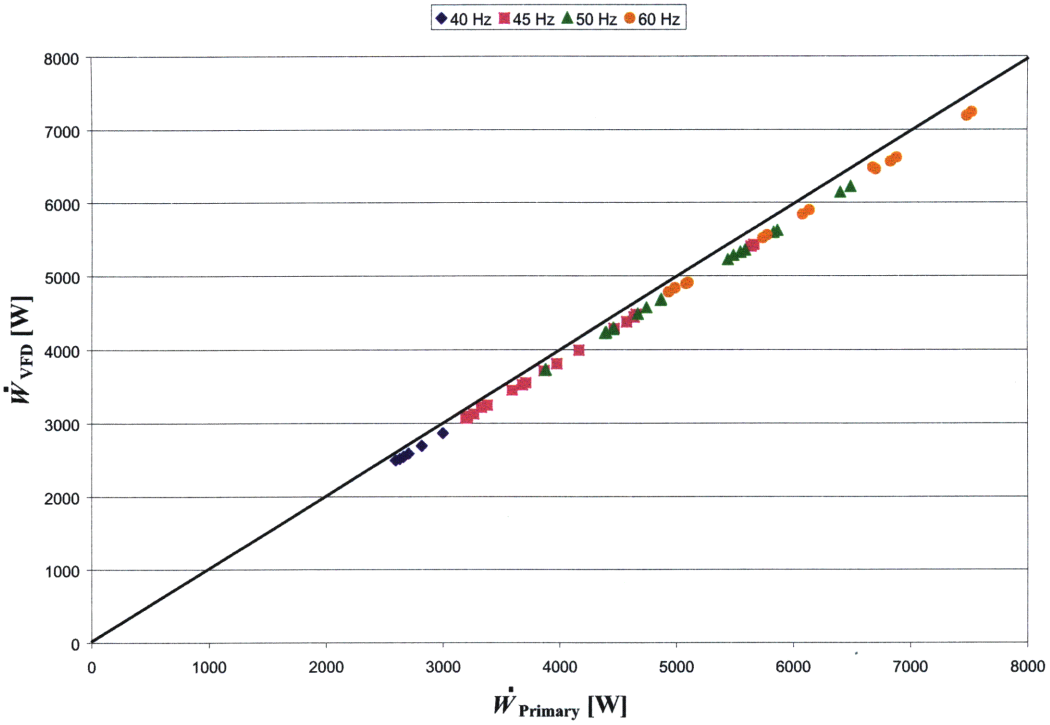

Figure 3-13: VFD output power as a function of primary power.

power delivered to the motor. Losses are produced in the switches every time they switch the current ON [11]. The magnitude of the inverter losses is indicated by Figure 3-13 which shows the power out from the VFD as a function of the primary power input to the VFD. At all test points, the power output of the VFD is lower than the power input, so there is some loss. Figure 3-14 shows the inverter efficiency ($\eta_{\text{VFD}} \equiv \frac{\dot{W}_{\text{VFD}}}{\dot{W}_{\text{Primary}}}$) plotted as a function of primary power, $\dot{W}_{\text{Primary}}$. This plot shows that, in general, the inverter efficiency is higher for higher frequencies. However, even for the lowest speed tested, the inverter efficiency remains over 95%. Over the entire test grid the inverter efficiency is always between 95% and 97%. Although the efficiency is lower at lower speeds, the magnitude of the power loss is less. Generally, lower speed corresponds to a lower power consumption.

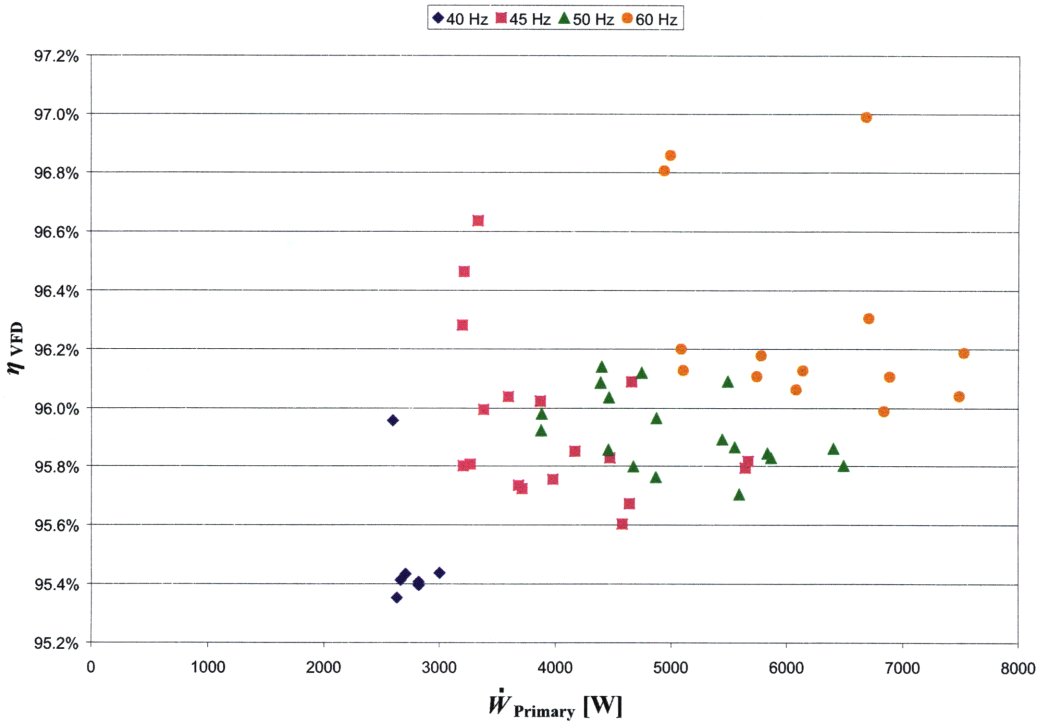

Figure 3-14: Inverter efficiency as a function of primary power.

3.6 Settling time

One issue that arose in testing the variable speed scroll compressor was the settling time. While the control is fairly fast, as the pressures and temperatures are typically brought to setpoint within minutes, it takes considerably longer for the entire system to reach a steady state. Figure 3-15 shows the settling time for a single test point. In this graph, the system is under control within minutes after the compressor has first started, however this long settling time is observed when setpoint is changed, regardless of how long the compressor has been running.

In Figure 3-15, there is an approximately 800 W difference between the initial power and the steady state power and the motor winding temperatures take several hours to reach a steady state value. This results in a long settling time for the compressor power. At lower speeds, each test point took two to three times longer to reach steady state. The cause of the long settling times is believed to be slow transient response of motor windings to the cooling effect that the suction gas provides. As the

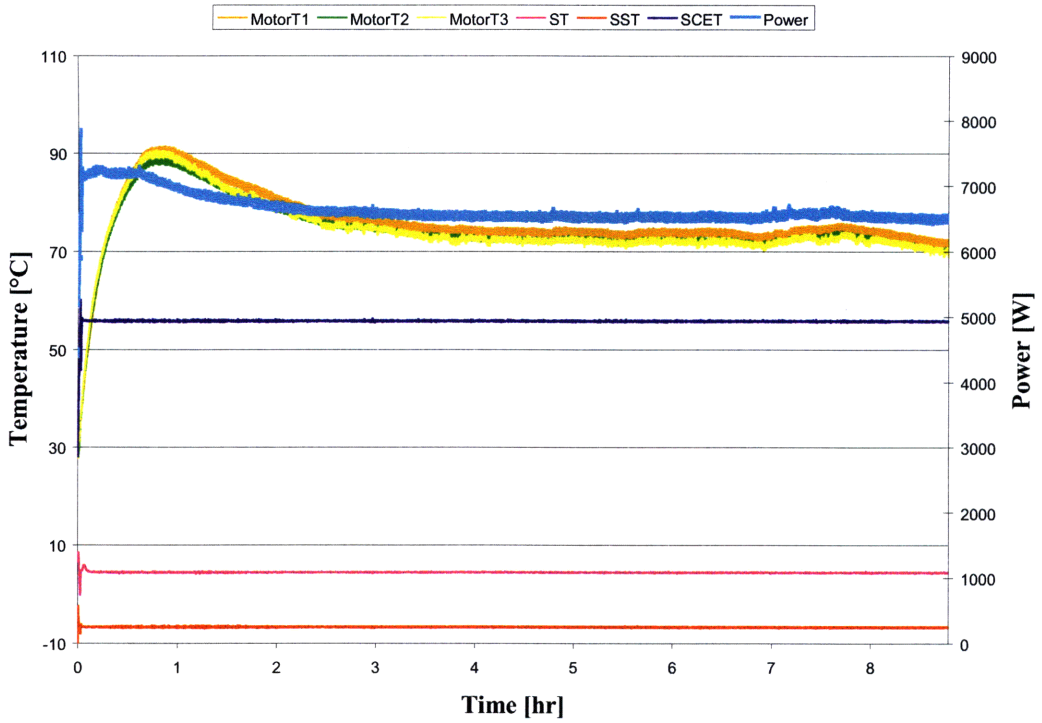

Figure 3-15: Settling time of the system for a single test point.

motor windings heat up (cool down) they are being cooled by the colder refrigerant vapor and at the same time the average temperature of the iron core is slowly rising (falling). So while the suction temperature is being kept constant by the control valves, there is transient heat transfer taking place between the motor windings, the iron core, and the refrigerant vapor. Not until this process has reached a steady state can the entire calorimeter system be said to have reached steady state. Therefore a test point was decided to be in steady state when the input power and mass flow rate remained constant (from visual inspection of realtime data) for over 30 minutes. Also, at low speeds, there was not enough motor cooling to keep the motor winding temperatures from rising asymptotically. In theses instances, steady state is never reached, because eventually the compressor draws too much current and a fuse is blown. An open-drive, semi-hermetic reciprocating compressor provides decoupling of the motor and the compressor. For purposes of compressor characterization, an open drive compressor should be easier to test because both the long settling time and

motor cooling problems are decoupled from the refrigerant thermodynamic process.

3.7 Outliers

There are two points (numbers 37 and 41 in Table 3.2) which are outliers in the plots for isentropic efficiency (Figure 3-11), condenser heat rate versus compressor power (Figures 3-3 and 3-4), compressor heat rate versus condenser heat rate (Figure 3-6), as well as the inferred oil mass flow rate (Figure 3-7). It was initially believed that these outliers were caused by heat gained from the surroundings, as the condenser heat rate was higher than the compressor input power and frost was observed on the compressor shell. However, the fact that the compressor heat rate is much smaller than the condenser heat rate at these points suggest that heat gained due to low suction temperatures does not tell the complete story. Instead, it is believed that liquid ingestion may have taken place at this point. This liquid refrigerant caused the motor temperatures, oil sump temperature as well as temperature of the compressor shell to drop dramatically. The measured superheat of 3 K is not consistent with the hypothesis because, in a well mixed stream of refrigerant liquid and vapor, the superheat must be zero. Future work will have to address the discrepancy between the apparent and measured superheat.

Chapter 4

Variable Speed Reciprocating Compressor Model

It has been shown experimentally, that some of the benefits of low-lift operation can be realized with a variable-speed scroll compressor. However, it was also shown that reciprocating compressors could be a better choice over scroll compressors because of retained isentropic efficiency at lower pressure ratio. Therefore, this chapter will focus on the development of a model for a variable speed, open-drive reciprocating compressor. Such a model must be able to accurately predict compressor input power as well as refrigerant mass flow rate as a function of inlet (pressure and temperature) and outlet (pressure) conditions. The model must be simple enough to be used within a larger chiller model, but it must also be robust enough to be valid over a wide range of compressor ratios and shaft speeds. In developing a model for a reciprocating compressor there are four states which are of particular interest. It is important to clearly define these states to avoid confusion as the nomenclature may be different in industry or other papers. Figure 4-1 is a schematic of the compression cylinder of a reciprocating compressor just before compression while Figure 4-2 is the cylinder just after compression.

The *inlet* and *outlet* conditions are defined as the state of the refrigerant as it enters and exits the compressor. The pressure of the refrigerant at the inlet and outlet of the compressor are given by p_{in} and p_{out}, respectively. Similarly, the specific

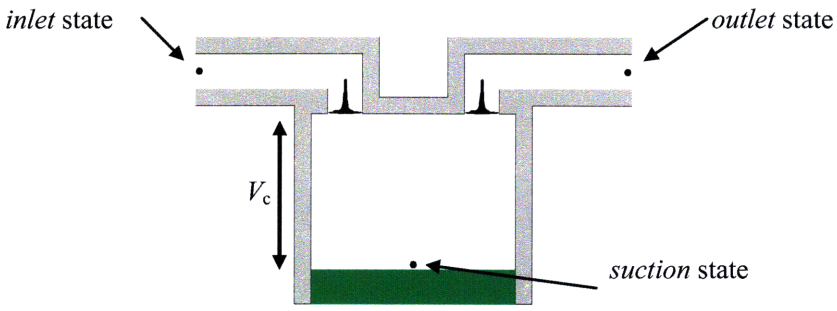

Figure 4-1: Reciprocating compressor cylinder just before compression.

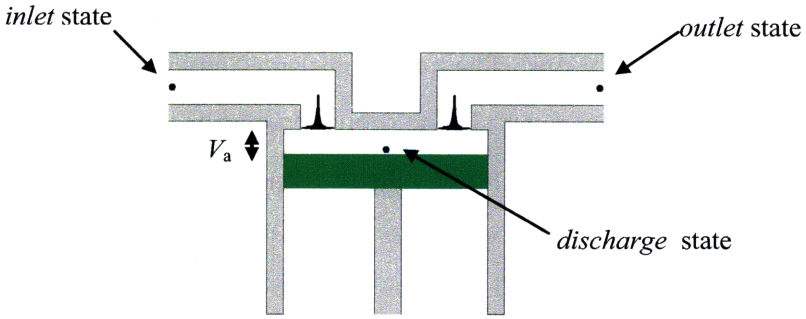

Figure 4-2: Reciprocating compressor cylinder just after compression.

volume of the refrigerant at the inlet and outlet of the compressor are given by ν_{in} and ν_{out}, respectively. The *suction* condition is defined as the state of the refrigerant with the piston at the so-called *bottom dead center* (BDC) position, i.e. the point of maximum cylinder volume. The *discharge* condition is defined as the state of the refrigerant with the piston at the so-called *top dead center* (TDC) position, i.e. the point of minimum cylinder volume. The pressures and temperatures at the *inlet* and *outlet* states can typically be measured directly with the use of thermocouples and pressure transducers installed directly in the pipes on the suction and discharge lines of the compressor. However, obtaining properties at the *suction* and *discharge* states is typically not possible without extensive modifications to the compressor shell. Directly measuring these states becomes even more problematic for hermetic compressors, which have a completely sealed compressor shell. The pressure difference between the *inlet* and *suction* states proves to be quite important in developing a mass flow model for the compressor. Figures 4-3 and 4-4 show the pressure-specific volume and pressure-volume diagrams for an idealized compressor cycle[25]. The refrigerant vapor enters the compressor at state $\mathbf{a}'$. As it passes through the suction valve and into the cylinder there is a drop in pressure bringing the refrigerant vapor to state $\mathbf{b}$. The crankshaft then turns and the piston moves upward, compressing the refrigerant to state $\mathbf{d}$, but, again, as the compressed vapor passes through the discharge valve, there is a drop in pressure leaving the refrigerant vapor at state $\mathbf{d}'$ when it exits the compressor. The pressure drops across the suction and discharge valves are assumed to be adiabatic processes. That is, while the pressure has been reduced, the enthalpy of the refrigerant vapor at the *inlet* state, just upstream of the suction valve, is equal to the enthalpy of the vapor just downstream of the suction valve. Similarly, the enthalpy at the *outlet* state, just downstream of the discharge valve, is equal to the enthalpy of the refrigerant vapor just upstream of the discharge valve. This is important because the enthalpy of refrigerant vapor in the cylinder cannot be easily measured but its *inlet* and *outlet* states can.

The clearance factor, C_1, is defined as the ratio of the clearance volume, V_{a}, to the piston displacement volume, $V_{\text{piston}} = V_{\text{c}} - V_{\text{a}}$, where V_{c} is the total compressor

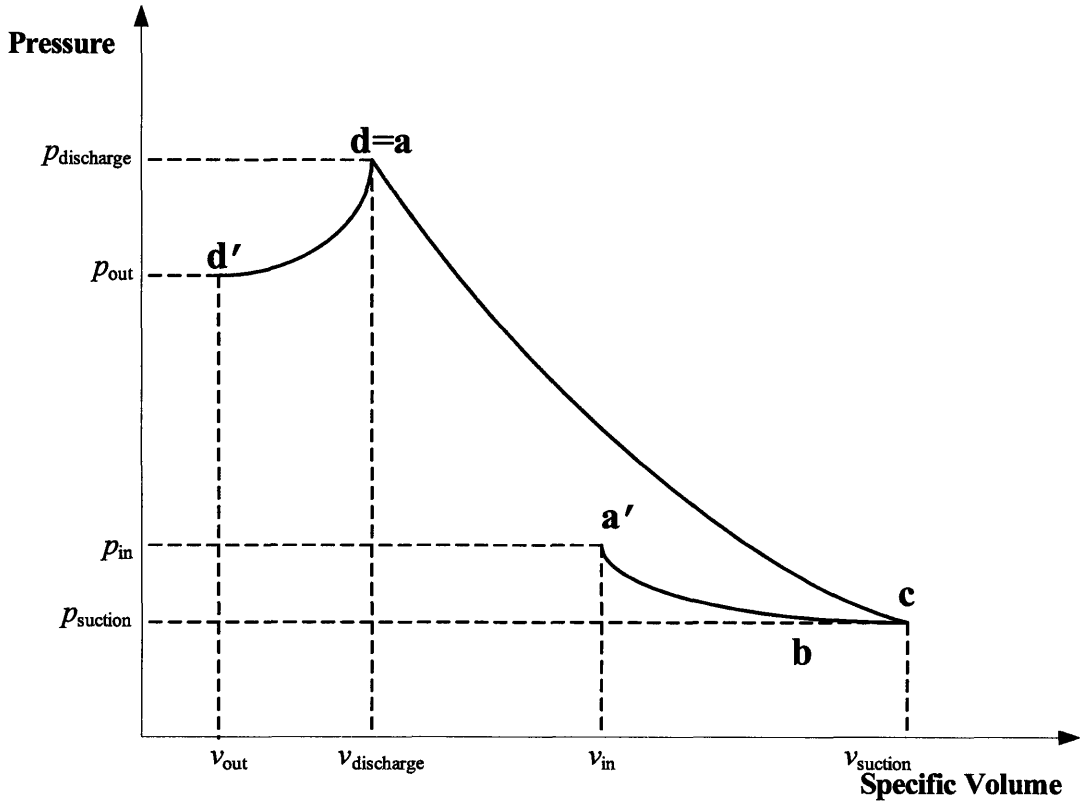

Figure 4-3: Pressure-specific volume for the compression cycle.

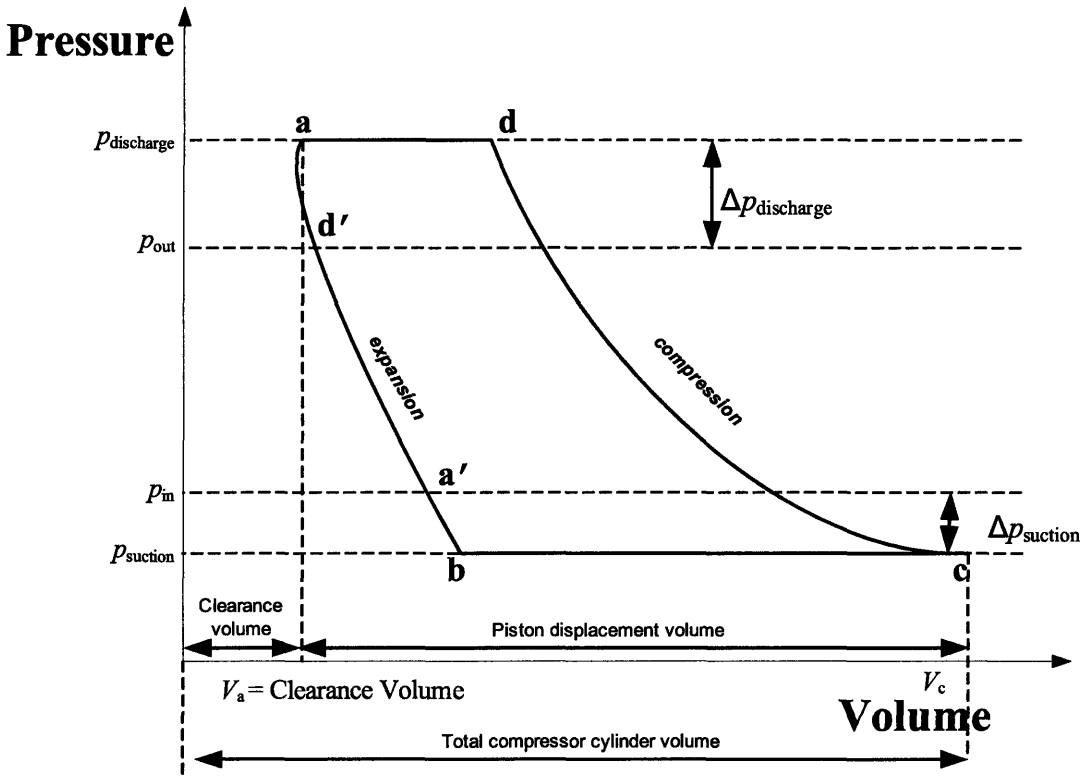

Figure 4-4: Pressure-volume diagram for the compression cycle.

cylinder volume[25]. The clearance volume is the volume of refrigerant left in the cylinder just after the discharge process has been completed. The clearance factor is given by Equation 4.1.

$$C_1 = \frac{V_a}{V_c - V_a} \tag{4.1}$$

The high pressure refrigerant that is left in the cylinder after the discharge of previous cycle must expand to a lower pressure before the suction valve can open and allow refrigerant from the suction line to enter the cylinder. A polytropic expansion process is represented by Equation 4.2,

$$V_b = V_a \left(\frac{p_{\text{discharge}}}{p_{\text{suction}}} \right)^{1/n} \tag{4.2}$$

where n is the polytropic exponent and V_b is the volume of refrigerant in the cylinder after re-expansion. The volumetric efficiency, η_v, can be defined [18] as,

$$\eta_v = \frac{\frac{(V_c - V_b)}{\nu_{\text{suction}}}}{\frac{(V_c - V_a)}{\nu_{\text{in}}}} = \frac{(V_c - V_b)}{(V_c - V_a)} \frac{\nu_{\text{in}}}{\nu_{\text{suction}}} \tag{4.3}$$

where ν_{in} and ν_{suction} are the specific volumes of the refrigerant at the *inlet* and *suction* states, respectively. Equation 4.3 represents the volumetric efficiency as the ratio of the intake refrigerant mass to the refrigerant vapor mass that would be taken in if the intake volume equaled piston displacement and the state of the vapor at the beginning of the compression were equal to the compressor inlet state. The volumetric efficiency can be expressed in terms of the pressure ratio, the clearance factor, and the polytropic exponent by combining Equations 4.1 - 4.3 (See Appendix C for a more detailed explanation).

$$\eta_v = \left\{ 1 - C_1 \left[\left(\frac{p_{\text{discharge}}}{p_{\text{suction}}} \right)^{1/n} - 1 \right] \right\} \frac{\nu_{\text{in}}}{\nu_{\text{suction}}} \tag{4.4}$$

Piston displacement volume can be expressed in terms of $\dot{\forall}_{\text{mfg}}$, which is the displacement volume flow rate through the compressor at some nominal shaft speed (obtained from the manufacturer), the normalized shaft speed (normalized with respect to this nominal shaft speed), w, and the time, t, as shown in Equation 4.5.

$$V_{\text{piston}} = V_{\text{c}} - V_{\text{a}} = \dot{\forall}_{\text{mfg}} w t \tag{4.5}$$

Equation 4.5 can be substituted into Equation 4.3 to obtain another expression for the volumetric efficiency as shown in Equation 4.6,

$$\eta_{\text{v}} = \frac{\nu_{\text{in}}}{\dot{\forall}_{\text{mfg}} w} \frac{V_{\text{c}} - V_{\text{b}}}{t \nu_{\text{suction}}} = \frac{\dot{m}}{\dot{\forall}_{\text{mfg}} w} \nu_{\text{in}} \tag{4.6}$$

where $\dot{m}$ is the refrigerant mass flow rate. Combining Equations 4.4 and 4.6 and solving for the mass flow rate through the compressor, yields Equation 4.7.

$$\dot{m} = \left\{ 1 - C_1 \left[\left(\frac{p_{\text{discharge}}}{p_{\text{suction}}} \right)^{1/n} - 1 \right] \right\} \frac{\dot{\forall}_{\text{mfg}} w}{\nu_{\text{suction}}} \tag{4.7}$$

It should be noted that the mass flow rate, as defined in Equation 4.7, depends on the refrigerant properties at the *suction* and *discharge* states. The actual *suction* pressure is lower than the *inlet* pressure and the *discharge* pressure is actually *higher* than the *outlet* pressure. Determination of these pressure drops is crucial to obtaining an accurate mass flow model. Furthermore, the suction side pressure drop is more critical than the discharge side pressure drop. This can be seen by changing the discharge and suction pressures and observing its effect on the change in the mass flow rate. For the same polytropic exponent, a ten percent drop in suction pressure results in the mass flow rate being reduced by approximately 15% while a ten percent rise in discharge pressure results in the mass flow rate being reduced by approximately 3%. This is somewhat counterintuitive because the refrigerant at the discharge port, which is at a much higher pressure than the suction port, sees a pressure drop which is

much larger in magnitude. The mass flow rate is clearly more sensitive to the suction side pressure drop. It should also be noted that this model is very much compressor dependant, as the clearance factor, C_1 and the displacement volume flow rate, $\dot{\forall}_{\text{mfg}}$, would vary depending on the geometry and design of the compressor.

4.1 Previous Models

Popovic and Shapiro[25] developed a semi-empirical method for modeling reciprocating compressors. Their mass flow rate model is nearly identical to the one given in Equation 4.7. Noting that the suction side pressure drop, $\Delta p_{\text{suction}}$, is the driving force in varying the magnitude of the mass flow rate, they chose to set the two pressure drops equal to each other in order to simplify the problem, so that $\Delta p_{\text{discharge}} = \Delta p_{\text{suction}} = \Delta p$. This expressed in Equation 4.8.

$$\dot{m} = \left\{ 1 - C_1 \left[\left(\frac{p_{\text{out}} + \Delta p}{p_{\text{in}} - \Delta p} \right)^{1/n} - 1 \right] \right\} \frac{\dot{\forall}_{\text{mfg}} w}{\nu_{\text{suction}}} \tag{4.8}$$

Compressor manufacturers are generally reluctant to release the value of the clearance factor, which is dependant on the compressor cylinder geometry, so it is taken as an unknown. Popovic used a program to vary the clearance factor, C_1, as well as the pressure drops, Δp, at each data point to find the values of these two parameters which produced the best agreement with their data set. Their data set consisted of 122 data points which included results for five different refrigerants and two different compressors. The refrigerants investigated were R-134a, R-22, and three refrigerant blends. Blend 1 consisted of 25% R-32 and 75% R-134a. Blend 2 consisted of 30% R-32, 10% R-125, and 60% R-134a. Blend 3 consisted of 23% R-32, 10% R-125, and 57% R-134a. A single data point is defined by measured temperature and pressures at *inlet* and *outlet* conditions; thus the pressure drop was added to the outlet pressure to determine the discharge pressure, while the pressure drop was subtracted from the inlet pressure to determine the suction pressure. With the temperatures and pressures

given at the *inlet* and *outlet* conditions, thermodynamic properties for the refrigerant were determined using the National Institute for Standards and Technology's program for calculating refrigerant properties (REFPROP version 4.0). The pressure drops were assumed to be adiabatic, so that the *inlet* enthalpy was equal to the *suction* enthalpy and the *outlet* enthalpy was equal to the *discharge* enthalpy. Therefore, the refrigerant properties at both the suction and discharge states could be determined. Popovic used Equation 4.9 to compute the polytropic exponent at each data point,

$$n = \frac{\ln\left[\frac{p_{\text{discharge}}}{p_{\text{suction}}}\right]}{\ln\left[\frac{\nu_{\text{suction}}}{\nu_{\text{discharge}}}\right]} \tag{4.9}$$

where ν_{suction} and $\nu_{\text{discharge}}$ are the *suction* and *discharge* specific volumes. Equation 4.9 comes from the definition of a polytropic process, $p\nu^n$ = constant. Therefore $p_{\text{suction}}\nu_{\text{suction}}^n = p_{\text{discharge}}\nu_{\text{discharge}}^n$, and solving for n yields Equation 4.9. The mass flow rate was then calculated for each data point using Equation 4.8. The minimum root-mean-square (RMS) value of the relative errors between the calculated mass flow rate and the actual mass flow rate was used to determine the pressure drops and the clearance factor. Pressure drops and clearance factors were found for each compressor and refrigerant combination. For R-22 in one of the compressors, the clearance factor was found to be 0.0950 and the pressure drop was found to be 59 kPa which yielded a RMS value of 0.12521. Citing Cosling[9], Popovic suggested the functional dependence of the polytropic exponent on the pressure ratio was different for each refrigerant in a particular compressor. Data were fitted to the curve defined by Equation 4.10, to characterize this dependance,

$$n = A_1 + \frac{A_2}{\left(\frac{p_{\text{discharge}}}{p_{\text{suction}}}\right)} + \frac{A_3}{\left(\frac{p_{\text{discharge}}}{p_{\text{suction}}}\right)^2} \tag{4.10}$$

where A_1, A_2, and A_3, are curve-fit coefficients and are unique for each refrigerant and for each compressor. For one of the compressors with R-22, Popovic found A_1 to be 1.2094, A_2 to be -0.2931, and A_3 to be 0.7802. The need for this empirical formula

for the polytropic exponent stems from the simplification of setting the discharge side pressure drop equal to the suction side pressure drop. Since the model doesn't accurately describe the discharge state, Equation 4.10 is used to determine the polytropic exponent, as the curve-fit coefficients ameliorate the effects of this inaccuracy.

Another model for reciprocating compressors was developed by Jahnig, Reindl, and Klein[15]. Their mass flow rate model is similar, and is given by Equation 4.11.

$$\dot{m} = \left\{ 1 - C_1 \left[\left(\frac{p_{\text{out}}}{p_{\text{in}}(1-\delta)} \right)^{1/k} - 1 \right] \right\} \frac{\dot{\forall}_{\text{mfg}} w}{\nu_{\text{suction}}} \tag{4.11}$$

In this model, the polytropic exponent for the compression is taken to be the specific heat ratio, k, which is the ratio of the isobaric to isochoric (c_p/c_v) heat capacities. The specific heat ratio is the polytropic exponent that corresponds to an adiabatic polytropic process of an ideal gas [20]. It can be shown through ideal gas relations that the polytropic exponent in Equation 4.9 reduces to k in the case of isentropic compression of an ideal gas. The δ term is a dimensionless curve-fit parameter which is supposed to capture not only the suction side pressure drop, but also heat transfer effects. Jahnig also noted that the suction side pressure drop was the driving force in varying the mass flow rate, so the discharge side pressure drop was neglected. It should also be noted that the heat capacities and the specific volume, ν_{suction}, are all refrigerant properties taken at the *suction* state. The pressure at the *suction* state is defined as $p_{\text{suction}} = p_{\text{in}}(1-\delta)$. He reports the average relative error for his mass flow rate model to be 1.3%. Jahnig also explored the extrapolative and interpolative capabilities of his model by fitting it to a subset of the data, and then observing how well it works on the rest of the data set. The model had an average relative error of 0.8% over the subset. When extrapolated to regions outside of the training data set, the average relative error increased to 2.1%.

4.2 New Mass Flow Model

The previous two models (Equations 4.11 and 4.8) provide a good starting point but neither model is suitable for a compressor which is operating at various speeds and at a wide range of pressure ratios; particularly those pressure ratios in the low-lift regime. For both Popovic's and Jahnig's models, the empirically determined coefficients would have to be determined for each speed at which the compressor is running. It is desired to develop a model whose parameters remain valid over a wide range of shaft speeds and pressure ratios. The focus of this work is to develop a model that, in its structure, takes into account changes in shaft speed.

4.2.1 Determination of Suction and Discharge States

As the refrigerant passes from the *inlet* state to the *suction* state and again as it passes from the *discharge* state to the *outlet* state there are certainly pressure drops across the valves. The aforementioned models were developed for a compressor operating at a single speed. For a variable speed compressor, the pressure drops will vary with speed as well as the density of the refrigerant as shown in Equations 4.12 and 4.13,

$$p_{\text{suction}} = p_{\text{in}} - C_2 \rho_{\text{in}} \omega^2 \tag{4.12}$$

$$p_{\text{discharge}} = p_{\text{out}} + C_3 \rho_{\text{out}} \omega^2 \tag{4.13}$$

where ω is the compressor shaft speed C_2 and C_3 are curve-fit parameters with units of square meters. These constants are believed to be analogous to the area of the valve plate. The pressure drops are associated with a loss in energy, so the functional form is similar to the relationship for kinetic energy as it has a mass multiplied by the square of velocity. The fluid velocity obviously is not known, so the pressure drop increases or decreases by the square of the shaft speed. This, then, leads to the issue of which density to use: ρ_{in}, ρ_{suction} or some combination of the two. Obviously, determining ρ_{suction} is prohibitive, as its definition is circular in nature; the characterization of

suction state is exactly what is trying to be determined, although it could be solved iteratively. Instead, ρ_{in} is used and the constant, C_2, while related to the compressor geometry, also takes into account the change in refrigerant density. It has already been noted that high side pressure drop, while greater in magnitude than the suction side pressure drop, does not have as significant of an effect on the mass flow rate and compressor power as the low side pressure drop. However, the C_3 term, which is used to characterize the pressure drop on the discharge side, is included in the analysis to ensure that these assertions hold true over a wide range of speed and low pressure ratios.

In addition to the drop in pressure there are also heat transfer effects that may need to be taken into account. Heat is transferred from the hot zones of the compressor, such as the discharge port, to the suction gas which raises its temperature and lowers its density thus negatively impacting the volumetric efficiency. The *discharge* temperature can be well over 100 K hotter than the *suction* temperature. The suction vapor temperature rise is directly related to the temperature difference between the outlet and inlet states as well as the time available for heat transfer to occur. That is, for a large temperature difference (between *suction* and *discharge* states) it would be expected that more heat transfer takes place; therefore the temperature rise of the suction vapor would be greater. The temperature rise is also inversely related to the speed of the shaft. For a faster speed, there is not as much time for the heat transfer to take place resulting in a lower temperature rise than at a slower speed. In reality, both the pressure drop and the heat transfer are happening simultaneously. Figure 4-5 is a pressure temperature diagram describing the process the refrigerant goes through as it moves from the inlet state to the suction state.

A rigorous characterization of the heat transfer effects within the compressor would involve a detailed analysis of all the modes of heat transfer. Most of the heat is carried out by the discharge refrigerant. Some of the heat is transferred from the discharge side to the surrounding ambient air by convection, some heat is transferred directly to the suction side through conduction through the compressor crankcase, and some of the heat from the warmer ambient air is transferred back to

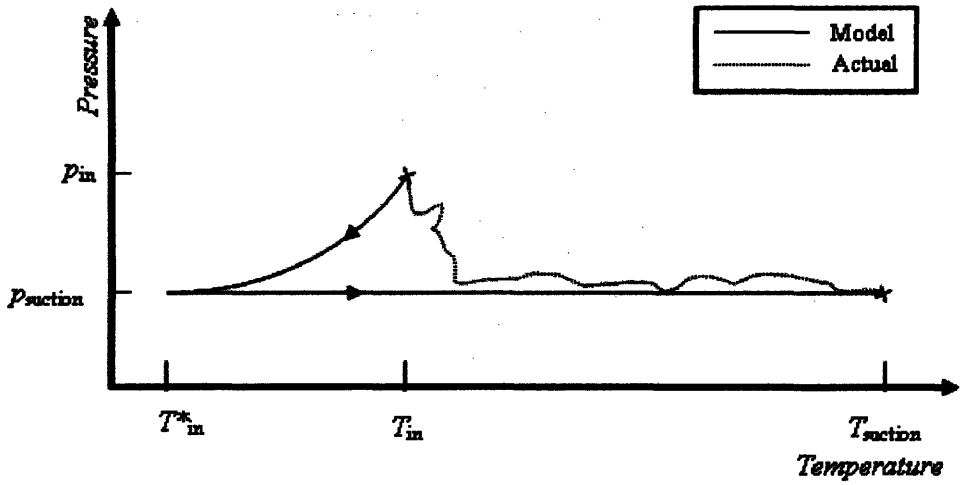

Figure 4-5: Pressure-temperature diagram of suction side pressure drop.

the suction side through convection. However, such an exhaustive approach would introduce several new coefficients and increase the complexity of the model. Recall, that the goal is to develop a fairly simple model that is accurate over a wide range of conditions. To simplify the model, estimated convection heat transfer coefficients and thermal conductivities are not used. Instead, the refrigerant is assumed to first take an adiabatic pressure drop as it passes through the suction valve. The refrigerant is now at a lower pressure, but has the same enthalpy as it had at the *inlet* state. From basic thermodynamics [20], the state of a fluid is defined as function of two of the fluid properties at that state. Thus, $T^*_{in} = F(p_{suction}, h_{in})$. Similarly, on the hot side, $T^*_{out} = F(p_{discharge}, h_{out})$, as the pressure drop across the discharge valve is taken to be adiabatic. This is illustrated in Figure 4-6. It must be emphasized that T^*_{in} and T^*_{out} are not actual measurable temperatures; rather, they represent approximations made by the model. Most of the heat that is not carried off by the refrigerant is lost to the surrounding air, but some of it makes it back to the suction side. In this simplified model, the controlling temperature gradient is $(T^*_{out} - T^*_{in})$. An effort to capture these heat transfer effects is given by Equations 4.14 and 4.15,

$$T_{suction} = T^*_{in} + a\frac{T^*_{out} - T^*_{in}}{w} \tag{4.14}$$

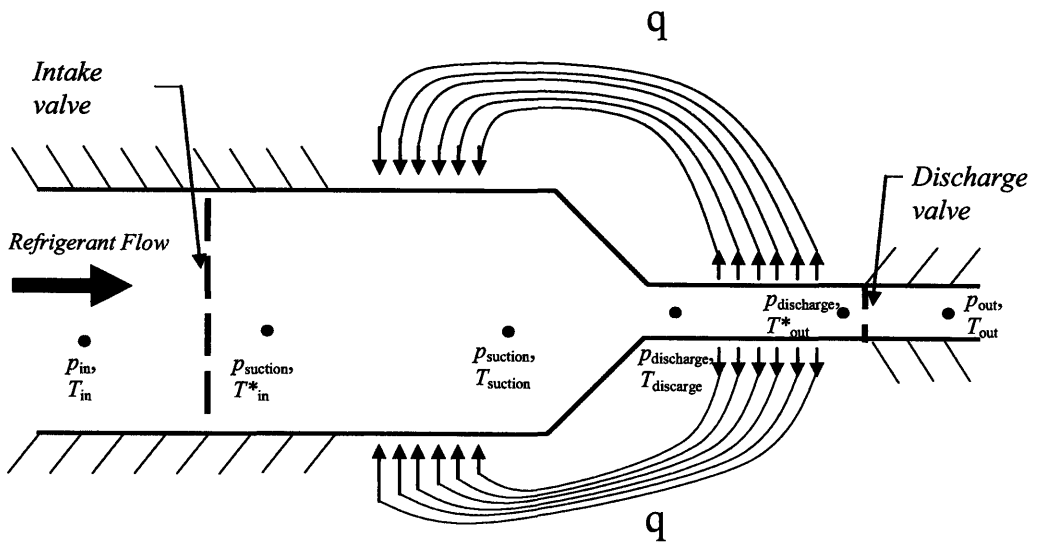

Figure 4-6: Illustration of refrigerant states in compressor model.

$$T_{\text{discharge}} = T_{\text{out}} - b\frac{T^*_{\text{out}} - T^*_{\text{in}}}{w} \tag{4.15}$$

where a and b are curve-fit parameters, and w is the normalized shaft speed.

4.3 Data

Determination of the relevant model parameters (C_1, C_2, C_3, a, and b) requires a data set which provides the compressor power and refrigerant mass flow rate under a variety of different loading conditions. Manufacturers are wary of releasing primary data on compressors, and most of these data sets would not provide the full range of speeds and compression ratios that are desired for low-lift applications. In the absence of primary data from a manufacturer, the Carlyle Compressor Selection Program (Carwin) version 3.0 was used to generate a data set to which a model for a reciprocating compressor would be fitted. This is a program developed by the compressor manufacturer to provide performance data for Carlyle compressors. Performance data are available for single stage, two-stage, and open-drive reciprocating

compressors, for semi hermetic and open-drive screw compressors, and for scroll compressors. There are five choices for refrigerants for which data is presented, R-22, R-407C, R-404A, R-507, and R-134A. A screenshot of the Carwin selection software is shown in Figure 4-7. The Carwin software allows one to input evaporator outlet temperature, saturated suction temperature, saturated discharge temperature and the compressor shaft speed. The software will then compute the input power, evaporator capacity, compressor capacity, condenser heat rejection, economizer load (if used), mass flow rate and compressor discharge temperature. A data set of 500 data points was created for the Carlyle 5F60 compressor with R-22 as the refrigerant. The 5F50 is an open-drive, 6 cylinder reciprocating compressor. The data set is defined by four variables: compressor shaft speed, saturated suction temperature, suction super heat, and saturated discharge temperature. There were five compressor shaft speeds of; 900, 1110, 1330, 1550, and 1750 RPM. There were five saturated suction temperatures; 30, 35, 40, 45, and 50 °F (-1.11, 1.67, 4.44, 7.22, and 10 °C). There were four levels of suction super heat; 0, 5, 10, 20 °F (0, 2.78, 5.56, and 11.11 °C). Finally, there were five saturated discharge temperatures of interest; 80, 90, 100, 110, 130 °F (26.67, 32.22, 37.78, 43.33, and 48.89 °C). This resulted in a data set of 500 points. At each data point, the mass flow rate, discharge temperature, and evaporator and condenser power were manually entered into a spreadsheet. The origins of the Carwin data are not known. It is believed to be the result of model(s) that were fitted to the manufacturer's primary data. Any errors within the data set, with respect to the primary test data, are not reported. Therefore, the need still exists for test data which characterizes compressor performance over a wide range of speed and pressure ratios to which the model developed in this thesis could be tested.

To calculate refrigerant properties, NIST's REFPROP version 8.0 (See Appendix B) was used within Microsoft Excel. The relative error, ε, between the calculated mass flow rate and the actual mass flow rate (as obtained from the Carwin software data) is given by Equation 4.16.

$$\varepsilon = \frac{|\dot{m}_{\text{calc}} - \dot{m}_{\text{actual}}|}{|\dot{m}_{\text{actual}}|} = \left|\frac{\dot{m}_{\text{calc}}}{\dot{m}_{\text{actual}}} - 1\right| \tag{4.16}$$

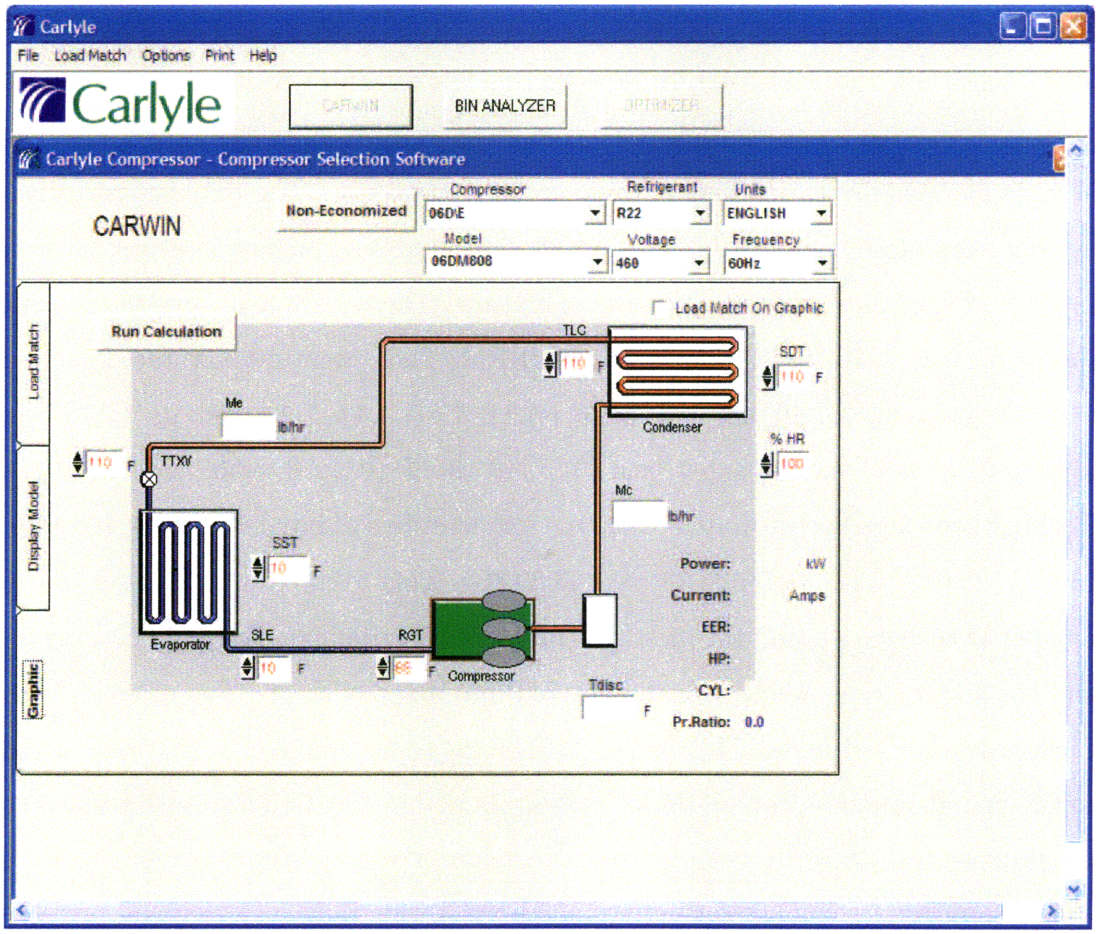

Figure 4-7: Screenshot of Carlyle Compressor Software.

This relative error is calculated for each data point. The RMS of this error is then calculated to determine a goodness of fit as shown in Equation 4.17,

$$RMS = \sqrt{\frac{\sum_{i=1}^{N} \varepsilon_i^2}{N}} \tag{4.17}$$

where N is the number of data points. The Excel Solver add-in was used to minimize the RMS of the relative error between the calculated mass flow rate and the actual mass flow rate. The solver minimizes a target cell by changing user-specified constants, each of which can be bounded to an interval defined by the user.

4.4 Model Performance

4.4.1 Mass Flow Model for the Carlyle 5F60 with R-22

The new model for the mass flow in a variable speed reciprocating compressor, given by Equation 4.18, along with the previous models (Equations 4.8 and 4.11) were fitted to the data generated by the Carlyle software.

$$\dot{m} = \left\{1 - C_1 \left[\left(\frac{p_{\text{out}} + C_3 \rho_{\text{out}} \omega^2}{p_{\text{in}} - C_2 \rho_{\text{in}} \omega^2}\right)^{1/n} - 1\right]\right\} \frac{\dot{\forall}_{\text{mfg}} w}{\nu_{\text{suction}}} \tag{4.18}$$

Equation 4.9 is used to determine the polytropic exponent, n (with p_{suction} and $p_{\text{discharge}}$ defined by Equations 4.12 and 4.13, respectively). It is not necessary to find a functional dependence on the pressure ratio, refrigerant, and compressor model for the polytropic exponent (as done in Equation 4.10) because this model predicts the actual suction and discharge pressures. For the R-22 data in the 5F60 compressor, k (c_p/c_v) ranged from about 1.23 to 1.26 while n (Equation 4.9) ranged from about 1.01 to 1.11. As expected, the isentropic polytropic exponent k is always larger than n, since this exponent is developed for isentropic compression of an ideal gas.

The RMS of the relative errors between the calculated mass flow rate and the actual mass flow rate was minimized to obtain the best fit. Table 4.1 shows the

	Incl. Heat Transfer	Adiabatic
C_1	0.095384921	0.085189
C_2	0.02482108	0.029386
C_3	0	0
a	0.00940063	n/a
b	0.153219821	n/a
RMS	0.42962%	0.47143%

Table 4.1: Results for new mass flow model on the Carlyle 5F60 with R-22 as the working fluid.

ω	900 RPM	1110 RPM	1330 RPM	1550 RPM	1750 RPM	All Data
C_1	0.100975	0.085059	0.073895	0.066121	0.060803	0.076871
δ	6.25%	20.69%	31.08%	38.46%	43.56%	28.28%
RMS	0.47%	0.44%	0.43%	0.41%	0.40%	1.34%

Table 4.2: Jahnig's & Reindl's model, fit to the 5F560 data with R-22.

results for the models using Equation 4.9 for the polytropic exponent and R-22 as the refrigerant over all 500 data points. The model is tested both including the heat transfer effects (Equations 4.14 and 4.15), as well as by assuming the pressure drops across the valves are adiabatic processes.

In the model developed in section 4.2, C_1 is the clearance factor and has a large impact on the volumetric efficiency; C_2 and C_3 are terms used to determine the pressure drop on the suction and discharge sides, respectively, and are analogous to the area of the valve plate; and a and b are terms used to determine the temperatures of the suction and discharge states (Equations 4.14 and4.15). Accordingly a and b are not applicable to the adiabatic case. In both cases, the discharge side pressure drop is zero (i.e C_3 is zero). This implies that either the Carwin software does not account for the discharge side flow losses, the discharge side flow losses are negligible (in terms of how it affects the mass flow rate), or that the effects of the discharge side pressure drop are not accurately accounted for in the Carwin model. The resulting RMS values are low; lower than the RMS values reported by both Jahnig and Popovic, which would be expected since they used actual test data which contain measurement errors. For comparison Popovic's and Jahnig's models were fitted to the Carwin dataset and the results are presented in Tables 4.2, 4.3, and 4.4.

ω	**900 RPM**	**1110 RPM**	**1330 RPM**	**1550 RPM**	**1750 RPM**
C_1	0.08161	0.08282	0.08359	0.0841	0.08452
ΔP **[Pa]**	6,485	12,134	16,222	19,142	21,138
ΔP_{avg}* **[Pa]**	*6,236*	*9,486*	*13,619*	*18,497*	*23,578*
RMS	0.23%	0.36%	0.46%	0.53%	0.59%

Table 4.3: Popovic's & Shapiro's model, fit to the 5F560 data with R-22 - Single Speed.

C_1	0.081778	0.083293
$\Delta P_{@\omega=900\text{RPM}}$ **[Pa]**	16,248	5,257
$\Delta P_{@\omega=1110\text{RPM}}$ **[Pa]**	16,248	11,796
$\Delta P_{@\omega=1330\text{RPM}}$ **[Pa]**	16,248	16,435
$\Delta P_{@\omega=1550\text{RPM}}$ **[Pa]**	16,248	19,710
$\Delta P_{@\omega=1750\text{RPM}}$ **[Pa]**	16,248	21,993
RMS	1.50%	0.46%

Table 4.4: Popovic's & Shapiro's model, fit to the 5F560 data with R-22 - All Speeds.

Jahnig's model fits the data well when it is optimized over single speeds, which is how the model was formulated. However, δ is clearly not a purely physical term as it predicts a pressure drop over 40% at a compressor speed of 1750 RPM which is unrealistic. In comparison, the pressure drops in the mass flow rate model in Equation 4.18 are on average 2.48%, and always fall between 1% and 5%. When taken over the entire range, Jahnig's model performs expectedly worse and still predicts an unreasonably large pressure drop. Jahnig fit his model to several data sets. The pressure drop term was about 1% to nearly 30% across all data sets. He notes that such large pressure drops are unrealistic and, in some case, can be attributed to bad data points. Also, the large variance in C_1 suggests the model is not accurately modeling the clearance factor, which shouldn't vary from speed to speed for a single compressor. In his paper Jahnig notes that both δ and C_1 are curve-fit parameters and while they have some physical meaning, they also account for physical phenomena not directly represented in the model.

Popovic's model fits the data well when it is optimizes over single speeds. Recall that for a given speed, Popovic's model adds/subtracts a constant pressure drop, ΔP, to the discharge/suction pressures. The model in Equation 4.18 has different

	Incl. Heat Transfer	Adiabatic
C_1	0.0.082843578	0.085650673
C_2	0.023443968	0.028911968
C_3	0	0
a	0.038746367	n/a
b	0.046135128	n/a
$\mathbf{RMS}_{\omega=1330/1550/1750\text{RPM}}$	0.30582%	0.45841%
$\mathbf{RMS}_{\omega=900/1110\text{RPM}}$	1.35181%	0.49588%
$\mathbf{RMS}_{\text{total}}$	0.88717%	0.47375%

Table 4.5: Results for new mass flow model on the Carlyle 5F60 with R-22 as the working fluid.

pressure drops at each data point; the average of these pressure drops (ΔP_{avg}*) for each speed is given in Table 4.3 for comparison purposes. Fitting Popovic's model results in similar pressure drops magnitudes as the model in Equation 4.18. Also the values for the clearance factor do not vary as widely over the speed range as it does with the Jahnig model. At 900 RPM, the RMS value is very low, but at higher speeds it gets a bit worse. The relative stability of the clearance factor also suggests that it is doing a better job capturing the physics of the pressure drops and geometric compressor effects on the mass flow rate. Table 4.4 shows how well Popovic's model did at capturing the entire data set. Two approaches in applying the model were taken to gauge its effectiveness. The first approach (column 1) allowed there to be only one ΔP across the entire range. The second approach (column 2) allowed there to be one ΔP for each speed range, while there is only one clearance factor (since this is all with the same compressor). As expected, the first approach had a larger RMS value than the second approach. A constant ΔP across all speeds is certainly a poor assumption. Thus, despite its low RMS value, the problem with Popovic's model is that ΔP, like Jahnig's δ, is not speed dependant; or, rather, its dependency on speed is not modeled, as both researchers carried out their work on single speed compressors. Neither model would be suitable for modeling a variable speed compressor. The new mass flow rate model given in Equation 4.18 does take this speed dependency into account, and the next logical step is to explore the extrapolative capabilities of the model, as shown in Table 4.5.

Since the accurate modeling of a low-speed chiller is desired, the models are optimized over the high range, from 1330 to 1750 RPM, and the RMS value over the low range, from 900 to 1110 RPM is compared to that of the high range. The discharge side pressure drop coefficient, C_3, goes to zero for both models. While the model which attempts to take into account the heat transfer effects has a smaller RMS value than the adiabatic model, its extrapolative features are very poor. The RMS error is over 300% worse in the low speed region, and worse by nearly 200% when compared to the entire data set. For the adiabatic model, there is just an 8% increase in the RMS error when applied to the slow region. The increase in RMS error is just 3% when applied to the entire dataset.

4.4.2 Power Model and Results for the Carlyle 5F60 with R-22

Both Popovic and Jahnig use the same functional form for modeling the compressor power. This model can be found widely in the literature[20] and is given in Equation 4.19,

$$\dot{W}_{\text{comp}} = \dot{m}\left\{\frac{n}{n-1}p_{\text{suction}}\nu_{\text{suction}}\left[\left(\frac{p_{\text{discharge}}}{p_{\text{suction}}}\right)^{\frac{n-1}{n}} - 1\right]\right\} \tag{4.19}$$

where $\dot{W}_{\text{comp}}$ is the work necessary to compress the refrigerant. In a real compressor there are losses which result in the actual work necessary to run the compressor being higher that the work needed to just compress the fluid. These include flow losses as the refrigerant flows through both the suction and the discharge valves as well as losses associated with friction as the piston moves up and down in the cylinder. Flow losses are given by Equations 4.20 and 4.21,

$$\dot{W}_{\text{l,suction}} = \Delta p_{\text{suction}}\dot{m}\nu_{\text{in}} = C_2\omega^2\dot{m} \tag{4.20}$$

$$\dot{W}_{\text{l,discharge}} = \Delta p_{\text{discharge}}\dot{m}\nu_{\text{out}} = C_3\omega^2\dot{m} \tag{4.21}$$

where C_2 and C_3 are are same terms used to determine the pressure drop on the

	Incl. Heat Trans	Incl. Heat Trans	Adiabatic	Adiabatic
	ALL	**Just f**	**ALL**	**Just f**
C_1	0.074098	0.095385	0.081569	0.085189
C_2	0.019944	0.024821	0.021353	0.029386
C_3	0.079236	0	0.072656	0
a	0.037801	0.009401	n/a	n/a
b	0.040237	0.153220	n/a	n/a
f	2.352986	9.736832	3.952455	11.455005
$\mathbf{RMS}_{\dot{m}}$	0.57926%	0.42962%	0.55085%	0.47143%
$\mathbf{RMS}_{\dot{W}}$	3.39079%	6.31670%	3.68531%	5.49936%

Table 4.6: Power model results for the 5F60 with R22.

suction and discharge sides in Equations 4.12 and 4.13, respectively, and are analogous to the area of the valve plate. Frictional loss increases with increasing compressor shaft speed as shown by Equation 4.22,

$$\dot{W}_{\text{l,friction}} = f\omega \tag{4.22}$$

where f is a curve fit parameter constrained to be greater than or equal to zero. The actual compressor power can then be calculated as the sum of the losses and the calculated power as shown in Equation 4.23

$$\dot{W}_{\text{actual}} = \dot{W}_{\text{comp}} + \dot{W}_{\text{l,suction}} + \dot{W}_{\text{l,discharge}} + \dot{W}_{\text{l,friction}} \tag{4.23}$$

The power model depends on the mass flow model, therefore, all of the model parameters (C_1, C_2, C_3, a, b, and f)can be found simultaneously. Alternatively, since the only new parameter is the friction coefficient, f, it is possible to use the optimized flow model and find the value of f that optimizes the power model.

For the adiabatic model, the RMS error for the mass flow rate improves by 16% when the power model is optimized simultaneously, while there is a 34% improvement for the model which includes the heat transfer effect. There is a 33% reduction in the RMS error for the power when all of the parameters are optimized simultaneously as opposed to using the optimal mass flow model and optimizing the friction coefficient separately. Treating the pressure drops across the suction and discharge valves as

adiabatic processes does a fairly good job at predicting data at lower speeds, which was a main goal of this work. However, it is desired to delve in to even lower compressor speeds and lower compression ratios. The compression ratios in the data set used to formulate this model ranged from about 5.03 to 1.65. Low-lift operation would have pressure ratios that approached 1. The model has shown some level of robustness (from its extrapolative capabilities), but actual compressor data at low-lift and low compressor speeds is needed for further validation. Tests taken at several extreme conditions, as well as a few moderate conditions should be enough to identify a model that can accurately predict performance over the range of interest.

Chapter 5

Conclusions and Future Work

In this thesis, a test stand was adapted for the use of generating test points for a variable speed scroll compressor. The goal was to get data in areas with high evaporating temperatures and low condensing temperatures. The motivation for getting data in this region was because under these conditions, the compressor does not have to work as hard which could result in significant energy savings. Compressor manufacturers typically test their compressors at various conditions, but rarely make this data available. Also, such data sets likely would not cover areas of low pressure ratios, low compressor speed, and high evaporating temperatures; a region that is of particular interest for low-lift cooling technologies. Consequently, a previously used de-superheater test stand was used to generate a data set detailing a scroll compressor's performance within these low-lift regions. An extensive overhaul of many of the test stand's equipment and instrumentation was necessary to make it useful in generating the desired data set. Major plumbing changes were made, a variable frequency drive was added, and the data acquisition system was completely replaced. Three stepper-motor control valves had to be properly tuned so that they could control conditions of the refrigerant vapor entering and leaving the compressor. With a properly instrumented and controlled calorimeter, test were able to be conducted on the scroll compressor. A test grid of 57 points was generated. The data set covered 4 different speeds and a variety of different suction and discharge conditions. It was found that, in general, for lower pressure differences between the discharge side and

the suction side of the compressor, the required input power was less. It was also observed that running the compressor at lower speeds can provide significant energy savings. Coupling both low speed operation with low-lift operation saw the most dramatic energy savings, at about 30%. Heat balance checks were also carried out to check the validity of the measurements. The amount of heat rejected by the condenser was always within 7% of the input power.

The isentropic efficiency of the compression process was also considered. It was found that as the compressor approached lower pressure ratios, the isentropic efficiency started to decline rapidly. This, of course, is not desirable, because the low pressure ratio region is of particular interest for this work. This decline in isentropic efficiency at lower pressure ratios is not as profound with reciprocating compressors. It was also found that motor cooling by the refrigerant gas had a significant effect on the settling time of the system.

Both of the foregoing conclusions point to a possible advantage in using an open drive, semi-hermetic reciprocating compressor instead of a scroll compressor for low-lift cooling technologies. To that end, a model for a reciprocating compressor was developed. Unlike previous models, this model is valid over various compressor speeds and pressure ratios. An attempt was made at trying to capture the effects of heat transfer as the pressure drops across the suction and discharge valves, but it was found that assuming an adiabatic, constant enthalpy, pressure drop was more accurate. The mass flow model remains simple, with only 3 parameters, while the power model adds just one extra parameter. The mass flow model performed well, with and RMS error below 0.5%, while the power model had a higher error at 3.7%. The extrapolative capabilities of the mass flow model was also explored. It was found after obtaining the optimal parameters for the mass flow model at the three highest speeds in the data set, this model could still predict the mass flow at the two lower speeds with an RMS error below 0.5%. This is extremely encouraging, as the goal is to have a model that works well at lower speeds.

Future Work

Moving forward, it will be necessary to get data for a reciprocating compressor at low speeds and low pressure ratios. The results from the scroll compressors tests were encouraging in some regards, but also seemed to illustrate that such a compressor is not well suited for low-lift operation. The current test stand is in good shape and could be adapted to test a reciprocating compressor fairly easily. Of concern, however, is the size of the hot gas bypass line piping. In order to achieve low-lift, it is necessary to minimize the magnitude of the pressure drops in the system. A larger hot gas bypass would help with this concern. In performing tests with the VFD, it must be stressed again, that care must be taken to ensure that all control and signal wires are properly shielded and grounded to mitigate the impact of electromagnetic interference. To get an even better heat balance, insulating the compressor itself may also be considered. Two outliers, believed to be caused by liquid ingestion, highlighted the need to get a better mixing device for the hot gas bypass stream and the stream of refrigerant exiting the condenser. A reservoir with the hot gas bypass stream coming from the bottom and flowing through the liquid and out the top would ensure that no liquid would migrate to the compressor. On the modeling front, it would be somewhat unrealistic for most researchers or manufacturers to get 500 data points to determine the parameters of a particular compressor. Instead, care must be taken in formulating a test grid that yields the greatest amount of insight while minimizing the number of test points needed. Consequently, it is necessary to not only look at the extrapolative capabilities of the model, but to also look at the interpolative properties.

Appendix A

Parts List

Pressure Transducers

		Mfg	Model No.	Range
DP	Discharge Pressure	MEAS	MSP-300-01K-P-5-N-1	0-1000 psig
CEP	Condenser Exit Presure	OMEG	PX605-500GI	0-500 psig
SP	Suction Pressure	OMEG	PX305-100AI	0-100 psia

Control Valves

		Mfg	Model No.
TX-VLV	Thermal Expansion Valve	Badger 807	M/N1002GCN36SVXXEEP36
HG-VLV	Hot Gas Bypass Valve	Badger 807	M/N1002GCN36SVXXGEP36
CW-VLV	Condenser Water Valve	Badger 752	M/N1002GCN36SVXXAEP36
Typ of 3	Motor	Airpax	L92411-P1 digital linear actuator
Typ of 3	Bipolar Stepping Motor Drive	IMS	IB462

Flow Meter

	Mfg	Model No.
Discharge Flow Meter	Micro Motion	F050 I239SU
Transmitter	Micro Motion	IFT9701-1-1-N-3-U

Miscellaneous

	Mfg	**Model No.**
Condenser	Packless Industries	CDAX-5032-H-11-176
Filter Drier	Sporlan	C-489-T
Circulation Pump	Grundfos	U15-18-B5
VFD	Baldor	VS1GV210-1B
Wattmeter	Yokogawa	WT230

Appendix B

Refprop 8.0

REFPROP is a program developed by the National Institute of Standards and Technology (NIST) which can be used to determine the properties of a fluid given two properties (i.e. temperature and pressure) of the fluid. It can be used to obtain the density, enthalpy, energy, temperature, pressure, entropy, isobaric heat capacity (cp), isochoric heat capacity (cv), and many other properties. REFPROP can be used within Microsoft EXCEL as well as MatLab. In Excel, the property is obtained by inputting the desired property as a function of the fluid, the two state defining properties, the units base, followed by the values for the two state defining properties. For example, to find the density of R22 in SI units with a temperature of 300 K and a pressure10 MPa, the following would be entered:

=Density("R22", "TP", "SI", 300, 10)

The "SI" designation requires that temperature is given in K, pressure in MPa, density in kg/m3, and enthalpy in KJ/kg, for both inputted values and the outputted values. Similarly, in the following code can be implemented in MATLAB:

PROPERTY('T', 'P', 300, 10000000, 'R22')

In MatLab, the default unit system is standard SI, so that pressure is in Pa and enthalpy is in J/kg.

For more information see: http://www.nist.gov/srd/nist23.htm

Appendix C

Volumetric Efficiency details

The purpose of this appendix is to show, more explicitly, how Equation 4.4 is obtained from combining Equations 4.1 - 4.3. The clearance factor (Equation 4.1) can be written as follows:

$$C_1 = \frac{V_a}{V_c - V_a} \tag{C.1}$$

or

$$\frac{C_1}{V_a} = \frac{1}{V_c - V_a} \tag{C.2}$$

or

$$C_1 V_c = C_1 V_a + V_a \tag{C.3}$$

The volumetric efficiency (Equation 4.3) is given by,

$$\eta_v = \frac{(V_c - V_b)}{(V_c - V_a)} \frac{\nu_{in}}{\nu_{suction}} \tag{C.4}$$

which can be re-written as:

$$\eta_v = \frac{1}{(V_c - V_a)} \frac{(V_c - V_b)}{1} \frac{\nu_{in}}{\nu_{suction}} \tag{C.5}$$

Note, that the first term in Equation C.5 is the right-hand side of Equation C.2, so this leaves us with:

$$\eta_{\mathrm{v}} = \frac{C_1}{(V_{\mathrm{a}})}(V_{\mathrm{c}} - V_{\mathrm{b}})\frac{\nu_{\mathrm{in}}}{\nu_{\mathrm{suction}}} = \left(\frac{C_1 V_{\mathrm{c}}}{V_{\mathrm{a}}} - C_1\frac{V_{\mathrm{b}}}{V_{\mathrm{a}}}\right)\frac{\nu_{\mathrm{in}}}{\nu_{\mathrm{suction}}} \tag{C.6}$$

Recall, that the polytropic expansion (Equation 4.2) can be written as:

$$\frac{V_{\mathrm{b}}}{V_{\mathrm{a}}} = \left(\frac{p_{\mathrm{discharge}}}{p_{\mathrm{suction}}}\right)^{1/n} \tag{C.7}$$

It is clear the the numerator in the first term in Equation C.6 is the left hand side of Equation C.3, and that the second term is equivalent to Equation C.7 multiplied by the clearance factor, C_1. Therefore, the volumetric efficiency can now be written as:

$$\eta_{\mathrm{v}} = \left\{\left[\frac{C_1 V_{\mathrm{a}}}{V_{\mathrm{a}}} + \frac{V_{\mathrm{a}}}{V_{\mathrm{a}}}\right] - C_1\left(\frac{p_{\mathrm{discharge}}}{p_{\mathrm{suction}}}\right)^{1/n}\right\}\frac{\nu_{\mathrm{in}}}{\nu_{\mathrm{suction}}} \tag{C.8}$$

Canceling out the V_{a} terms and re-arranging Equation C.8, yields,

$$\eta_{\mathrm{v}} = \left\{1 - C_1\left[\left(\frac{p_{\mathrm{discharge}}}{p_{\mathrm{suction}}}\right)^{1/n} - 1\right]\right\}\frac{\nu_{\mathrm{in}}}{\nu_{\mathrm{suction}}} \tag{C.9}$$

which is equivalent to Equation 4.4.

Appendix D

CR1000 Program

```
'CR1000 Series Datalogger
SequentialMode

Public PTemp, batt_volt, TrefAM25T
Public k,m,n,i,pulserate,max_pulse
Public TempC(12),AMV(2), Press(3), CompPower, SST,SDT,SCET, ST, Patm, DischargeFlow
Public CWT(2), CW_Kp,CW_Ki,CW_Kd,errSCET_old,errSCET,intgrl,CWcrx,c_off, CW_Kpold, CW_Kiold, CW_Kdold
Public errTsat, errT, errThg_old, errThg, intgl, HG_Kp, HG_Ki, HG_Kd, HGcrx, errTexp_old, errTexp, intg2,
Public LL_Kp, LL_Ki, LL_Kd, LLcrx, c_off2, errSSH ' Sub:
Public HG_Kpold, HG_Kiold, HG_Kdold,LL_Kpold, LL_Kiold, LL_Kdold
Public SST_set,SSH_set,SCET_set,SSH_actual,SST_set_old,SSH_set_old,Tset_old,ST_set
Public HG_pos, LL_pos,CW_pos, al, CWcrx_0, HGcrx_0,LLcrx_0, CWcrx_a, HGcrx_a, LLcrx_a
Public TP, GC, REL, HGmax, LLmax, CWmax, CW_deltaT, ISS, FD_delta_T, Pratio, nn, nn_set, V, Vt, r
Public R_SP, R_DP,R_CEP,R_EP,CW_off,LL_off,HG_off, LL_i, CW_i, HG_i
Public WN_Pwr, PID_trig, LLc, CWc, HGc, TP_old

Alias CWT(1) = CW_T_out_stream 'DT 'AM25T Ch. 1
Alias CWT(2) = CW_T_in_stream'CET 'AM25T Ch. 2

Alias TempC(1) = CW_T_out_stream_old'EconT 'AM25T Ch. 3
Alias TempC(2) = CW_T_in'CW_T_out_stream 'AM25T Ch. 4
Alias TempC(3) = CW_T_mix'MotorT5'AM25T Ch. 5
Alias TempC(4) = MotorT6'CW_T_mix 'AM25T Ch. 6
Alias TempC(5) = DT'CW_T_out 'AM25T Ch. 7
Alias TempC(6) = CET'CW_T_in 'AM25T Ch. 8
Alias TempC(7) = DomeT 'AM25T Ch. 9
Alias TempC(8) = SumpT 'AM25T Ch. 10
Alias TempC(9) = EconT'CW_T_in_stream 'AM25T Ch. 11
Alias TempC(10) = MotorT12  'AM25T Ch. 12
Alias TempC(11) = MotorT13 'AM25T Ch. 13
Alias TempC(12) = MotorT14 'AM25T Ch. 14

'               Patm 'CR1000 Ch. 2
'               ST 'CR1000 Ch. 5
Alias Press(1) = SP ' CR1000 Ch. 6
Alias Press(2) = DP ' CR1000 Ch. 7
Alias Press(3) = CEP ' CR1000 Ch. 8

Const dtt = 1
Const dtt2 = dtt
Const dtt3 = dtt2
Const del = 2000
Const C3=0.3504829222
Const C2=4.5528155289
```

```
Const C1=37.1626340695
Const C0=39.4068892082

DataTable (CntrlData,1,-1)
  DataInterval (0,dtt,Sec,0)
  Sample(1,errSCET,IEEE4)
  Sample(1,SCET_set,IEEE4)
  Sample(1,CW_pos,IEEE4)
  Sample(1,errTexp,IEEE4)
  Sample(1,ST_set,IEEE4)
  Sample(1,LL_pos,IEEE4)
  Sample(1,errThg,IEEE4)
  Sample(1,SST_set,IEEE4)
  Sample(1,HG_pos,IEEE4)
  Sample(1,WN_Pwr,IEEE4)
EndTable' END Table CntrlData

'Define Subroutines
'Sub
'EnterSub instructions here
'EndSub
Sub actvlv(x,y,z)
  If x<0 Then
    PortSet(5,0) 'Close Valve
    PortSet(6,1)
    PulsePort(4,5000)
    If ABS(x) >1 Then' IF STATEMENT # 1
      For i = 1 To (ABS(x) -1)
        PulsePort(4,del) 'Liq Lin TXV - ~2140 Pulses to fullly close
      Next i
    EndIf ' EndIf STATEMENT # 1 ABS(x) > 1
    If ISS = 1 Then' IF STATEMENT # 2
      If LL_pos+x>LLmax ' IF STATEMENT # 3
      LL_pos=LLmax
    ElseIf LL_pos+x<0 Then
      LL_pos=0
    Else
      LL_pos=LL_pos+x
    EndIf ' EndIf STATEMENT # 3 LL_pos
  EndIf ' EndIf STATEMENT # 2 ISS = 1
  x=0
  PortSet(6,0)
  EndIf ' EndIf STATEMENT  x < 0
  If x>0 Then
    PortSet(5,1)
    PortSet(6,1) 'Open Valve
    PulsePort(4,5000)
    If ABS(x) >1 Then ' IF STATEMENT # 1
      For i = 1 To (ABS(x) -1)
        PulsePort(4,del) 'Liq Lin TXV - ~2140 Pulses to fullly close
      Next i
    EndIf ' EndIf STATEMENT # 1 ABS(x) > 1
    If ISS = 1 Then' IF STATEMENT # 2
      If LL_pos+x>LLmax Then' IF STATEMENT # 3
        LL_pos=LLmax
```

```
    ElseIf LL_pos+x<0 Then
      LL_pos=0
    Else
      LL_pos=LL_pos+x
    EndIf ' EndIf STATEMENT # 3 LL_pos
  EndIf ' EndIf STATEMENT # 2 ISS = 1
  x=0
  PortSet(6,0)
EndIf ' EndIf STATEMENT  x > 0
If y<0 Then
  PortSet(5,0) 'Close Valve
  PortSet(7,1)
  PulsePort(4,5000)
  If ABS(y) >1 Then' IF STATEMENT # 1
    For i = 1 To (ABS(y) -1)
      PulsePort(4,del) 'Hot Gas Bypass - ~2160 Pulses to fullly close
    Next i
  EndIf ' EndIf STATEMENT # 1 ABS(y) > 1
  If ISS = 1 Then' IF STATEMENT # 2
    If HG_pos+y>HGmax Then' IF STATEMENT # 3
      HG_pos=HGmax
    ElseIf HG_pos+y<0 Then
      HG_pos=0
    Else
      HG_pos=HG_pos+y
    EndIf ' EndIf STATEMENT # 3 HG_pos
  EndIf ' EndIf STATEMENT # 2 ISS = 1
  y=0
  PortSet(7,0)
EndIf ' EndIf STATEMENT  y < 0
If y>0 Then
  PortSet(5,1) 'Open Valve
  PortSet(7,1)
  PulsePort(4,5000)
  If ABS(y) >1 Then' IF STATEMENT # 1
    For i = 1 To (ABS(y) -1)
      PulsePort(4,del) 'Hot Gas Bypass - ~2160 Pulses to fullly close
    Next i
  EndIf ' EndIf STATEMENT # 1 ABS(y) > 1
  If ISS = 1 Then' IF STATEMENT # 2
    If HG_pos+y>HGmax Then' IF STATEMENT # 3
      HG_pos=HGmax
    ElseIf HG_pos+y<0 Then
      HG_pos=0
    Else
      HG_pos=HG_pos+y
    EndIf ' EndIf STATEMENT # 3 HG_pos
  EndIf ' EndIf STATEMENT # 2 ISS = 1
  y=0
  PortSet(7,0)
EndIf ' EndIf STATEMENT  y > 0
If z<0 Then
  PortSet(5,0) 'Close Valve
  PortSet(8,1)
  PulsePort(4,5000)
```

```
    If ABS(z) >1 Then' IF STATEMENT # 1
      For i = 1 To (ABS(z) -1)
        PulsePort(4,del) 'Condenser Water TXV - ~1220 Pulses to fullly close
      Next i
    EndIf ' EndIf STATEMENT # 1 ABS(z) > 1
    If ISS = 1 Then' IF STATEMENT # 2
      If CW_pos+z>CWmax Then' IF STATEMENT # 3
        CW_pos=CWmax
      ElseIf CW_pos+z<0 Then
        CW_pos=0
      Else
        CW_pos=CW_pos+z
      EndIf ' EndIf STATEMENT # 3 CW_pos
    EndIf ' EndIf STATEMENT # 2 ISS = 1
    z=0
    PortSet(8,0)
  EndIf ' EndIf STATEMENT  z < 0
  If z>0 Then
    PortSet(5,1) 'Open Valve
    PortSet(8,1)
    PulsePort(4,5000)
    If ABS(z) >1 Then ' IF STATEMENT # 1
      For i = 1 To (ABS(z) -1)
      '~96 Turns/Rev
        PulsePort(4,del) 'Condenser Water TXV - ~1220 Pulses to fullly close
      Next i
      EndIf ' EndIf STATEMENT # 1 ABS(z) > 1
    If ISS = 1 Then' IF STATEMENT # 2
      If CW_pos+z>CWmax Then' IF STATEMENT # 3
        CW_pos=CWmax
      ElseIf CW_pos+z<0 Then
        CW_pos=0
      Else
        CW_pos=CW_pos+z
      EndIf ' EndIf STATEMENT # 3 CW_pos
    EndIf ' EndIf STATEMENT # 2 ISS = 1
    z=0
    PortSet(8,0)
  EndIf ' EndIf STATEMENT  z > 0
EndSub 'SUB: actvlv

Sub cond_vlv_cntrl(T_set,T)
  If CW_off=1 Then
    CWcrx_a=0
  Else
    If c_off>0 Then
      If T<50000000000000000000 Then
        errSCET_old=errSCET
        errSCET=T-T_set
        If (ABS(Tset_old-T_set)+ABS(CW_Kp-CW_Kpold)+ABS(CW_Ki-CW_Kiold)+ABS(CW_Kd-CW_Kdold))>0 Then
          intgrl=0 'Reset Intergal term if the setpoint is changed
        EndIf
        CWcrx_0=CW_Kp*errSCET+CW_Kp*(intgrl+dtt*errSCET)/CW_Ki+CW_Kp*CW_Kd*(errSCET-errSCET_old)/dtt
        CWcrx=Round(CWcrx_0,0)+CW_i
        If (CWcrx-CW_pos) > max_pulse Then
```

```
        CWcrx=max_pulse+CW_pos
      ElseIf (CWcrx-CW_pos) < -max_pulse Then
        CWcrx =-max_pulse+CW_pos
      EndIf
      If CWcrx>CWmax Then
        CWcrx=CWmax
        If errSCET < 0 Then
          intgrl=intgrl+errSCET*dtt
        EndIf
      ElseIf CWcrx<0 Then
        CWcrx =0
        If errSCET > 0 Then
          intgrl=intgrl+errSCET*dtt
        EndIf
      Else
        intgrl=intgrl+errSCET*dtt
      EndIf
      CWcrx_a=CWcrx-CW_pos
      CW_pos=CWcrx   'actvlv(0,0,CWcrx)
      Tset_old=T_set
      CW_Kpold=CW_Kp
      CW_Kiold=CW_Ki
      CW_Kdold=CW_Kd
    EndIf
  EndIf
EndIf
EndSub  'SUB: cond_vlv_cntrl

Sub SatTemp(P,Tsat)'Input Pressure in MPa; Outputs Temperature in C
  Tsat=C3*(LN(P))^3+C2*(LN(P))^2+C1*(LN(P))+C0
EndSub  'SUB: SatTemp

Sub liq_hot_gas_vlv_cntrl(Tsetpoint_sat_suc,Superheat_set)
  If SP*ST<9000000000000000000 Then
    If c_off2>0 Then
      ST_set = Tsetpoint_sat_suc + Superheat_set
      errTsat = Tsetpoint_sat_suc-SST
      errT = ST_set-ST
      errSSH=Superheat_set-(ST-SST)
      errThg_old = errThg    'errThg = errSSH + errT
      errThg = errTsat 'SST
      errTexp_old = errTexp   'errTexp = errSSH-errT
      errTexp = errT
      If ABS(SST_set_old-Tsetpoint_sat_suc)>0  Then'Reset intergral term
        intgl=0 'HG integral
      EndIf
      If ABS((SST_set_old+SSH_set_old)-(Tsetpoint_sat_suc+Superheat_set))>0  Then'Reset intergral term
        intg2=0 'TXV/LL integral
      EndIf
      If (ABS(HG_Kp-HG_Kpold)+ABS(HG_Ki-HG_Kiold)+ABS(HG_Kd-HG_Kdold))>0 Then
        intgl=0
      EndIf
      If (ABS(LL_Kp-LL_Kpold)+ABS(LL_Ki-LL_Kiold)+ABS(LL_Kd-LL_Kdold))>0 Then
        intg2=0
      EndIf
```

```
If HG_off=1 Then
  HGcrx_a=0
  intgl=0
  errThg=0
Else
  HGcrx_0 = HG_Kp*errThg + HG_Kp*(intgl+errThg*dtt)/HG_Ki + HG_Kp*HG_Kd*(errThg-errThg_old)/dtt
  HGcrx=Round(HGcrx_0,0)+HG_i
  If (HGcrx-HG_pos) > max_pulse Then'2
    HGcrx=max_pulse+HG_pos
  ElseIf (HGcrx-HG_pos) < -max_pulse Then
    HGcrx =-max_pulse+HG_pos
  EndIf'2
  If HGcrx>HGmax Then'3
    HGcrx=HGmax
    If errThg < 0 Then
      intgl = intgl+errThg*dtt
    EndIf
  ElseIf HGcrx<0 Then
    HGcrx=0
    If errThg > 0 Then
      intgl = intgl+errThg*dtt
    EndIf
  Else
    intgl = intgl+errThg*dtt
  EndIf'3
  HGcrx_a=HGcrx-HG_pos
  HG_pos=HGcrx
EndIf'1
If LL_off=1 Then
  LLcrx_a=0
  intg2=0
  errTexp=0
Else
  If nn=nn_set Then
    LLcrx_0 = LL_Kp*errTexp + LL_Kp*(intg2+errTexp*dtt)/LL_Ki + LL_Kp*LL_Kd*(errTexp-errTexp_old)/dtt
    LLcrx=Round(LLcrx_0,0)+LL_i
    If (LLcrx-LL_pos) > max_pulse Then
      LLcrx=max_pulse+LL_pos
    ElseIf (LLcrx-LL_pos) < -max_pulse Then
      LLcrx =-max_pulse+LL_pos
    EndIf
    If LLcrx>LLmax Then
      LLcrx=LLmax
      If errTexp > 0 Then
        intg2  = intg2+errTexp*dtt
      EndIf
    ElseIf LLcrx<0 Then
      LLcrx=0
      If errTexp < 0 Then
        intg2  = intg2+errTexp*dtt
      EndIf
    Else
      intg2 = intg2+errTexp*dtt
    EndIf
    LLcrx_a=LLcrx-LL_pos
```

```
        LL_pos=LLcrx
        nn=0
      ElseIf nn>nn_set Then
        nn=0
        LLcrx_a=0
      Else
        nn=nn+1
        LLcrx_a=0
      EndIf
    EndIf
    SST_set_old=Tsetpoint_sat_suc
    SSH_set_old=Superheat_set
    HG_Kpold=HG_Kp
    HG_Kiold=HG_Ki
    HG_Kdold=HG_Kd
    LL_Kpold=LL_Kp
    LL_Kiold=LL_Ki
    LL_Kdold=LL_Kd
  EndIf
EndIf
EndSub  'SUB: liq_hot_gas_vlv_cntrl

Sub runpgm(TestPnt)
  If TestPnt=1 Then
    SCET_set = 55.83
    SST_set =-6.67
    SSH_set = 11.11
    c_off=1
    c_off2=1
    cond_vlv_cntrl(SCET_set,SCET)
    liq_hot_gas_vlv_cntrl(SST_set,SSH_set)
    TestPnt = 99
  ElseIf TestPnt=2 Then
    SCET_set = 63.4
    SST_set = -23.33
    SSH_set = 11.11
    c_off=1
    c_off2=1
    cond_vlv_cntrl(SCET_set,SCET)
    liq_hot_gas_vlv_cntrl(SST_set,SSH_set)
    TestPnt = 99
  ElseIf TestPnt=3 Then
    SCET_set = 36.78
    SST_set = -28.89
    SSH_set = 11.11
    c_off=1
    c_off2=1
    cond_vlv_cntrl(SCET_set,SCET)
    liq_hot_gas_vlv_cntrl(SST_set,SSH_set)
    TestPnt = 99
  ElseIf TestPnt=4 Then
    SCET_set = 50
    SST_set = 0
    SSH_set = 5
    c_off=1
```

```
    c_off2=1
    cond_vlv_cntrl(SCET_set,SCET)
    liq_hot_gas_vlv_cntrl(SST_set,SSH_set)
    TestPnt = 99
  ElseIf TestPnt=5 Then
    SCET_set = 50
    SST_set = 0
    SSH_set = 5
    c_off=1
    c_off2=0
    cond_vlv_cntrl(SCET_set,SCET)
    liq_hot_gas_vlv_cntrl(SST_set,SSH_set)
    TestPnt = 99
  ElseIf TestPnt = 99 Then'Manual Mode
    c_off=1
    c_off2=1
    cond_vlv_cntrl(SCET_set,SCET)
    liq_hot_gas_vlv_cntrl(SST_set,SSH_set)
  ElseIf TestPnt=0 Then
    c_off=0
    c_off2=0
    intgr1=0
    intg1=0
    intg2=0
    TestPnt=0
  Else
    c_off=0
    c_off2=0
    intgr1=0
    intg1=0
    intg2=0
    TestPnt=0
  EndIf
EndSub   'SUB: runpgm

Sub ActuateValves(TestPoint)
  If TestPoint > 0 Then
    actvlv(LLcrx_a,HGcrx_a,CWcrx_a)
  EndIf
EndSub    'SUB: ActuateValves

'Main Program
BeginProg
  'PID_trig=1
  k=10 'Liq Lin/ TXV
  m=0 'Hot Gas Bypas
  n=0 'Condenser Water
  CW_Kp=80 '80
  CW_Kpold=CW_Kp
  CW_Ki=14 '9
  CW_Kiold=CW_Ki
  CW_Kd=1 '2.25
  CW_Kdold=CW_Kd
  HG_Kp=35 '
  HG_Kpold=HG_Kp
```

```
HG_Ki=5 '
HG_Kiold=HG_Ki
HG_Kd=0.1 '
HG_Kdold=HG_Kd
LL_Kp=-15 '-8
LL_Kpold=LL_Kp
LL_Ki=30 '30
LL_Kiold=LL_Ki
LL_Kd=7.5 '7.5
LL_Kdold=LL_Kd
LL_i=340
HG_i=1000
CW_i=900
HGmax=2100
LLmax=2100
CWmax=1220
LL_pos=340
HG_pos=1000
CW_pos=900
nn_set=0
'Vt=1
pulserate=(1000000*0.5/del)
'[Hz] 'The Delay is half of the period devided by the pulse rate (in Hz); del=1000000*0.5/pulserate
max_pulse=Floor((0.9*pulserate*dtt/3))-25 'Since there are three valves running
PortsConfig (&B11111000,&B11111000) 'Config Ports 4 - 8 to Outputs
R_SP=12.11
R_DP=12.02
R_CEP=12.09
R_EP=12.09
Scan (dtt,Sec,0,0)
  PanelTemp (PTemp,_60Hz)
  Battery (Batt_volt)
  actvlv(k,m,n)
  TCDiff (ST,1,mV7_5,5,TypeT,PTemp,True ,0,250,1.0,0)
  VoltDiff (Press(),3,mV250,6,True ,0,250,1.0,0)
  VoltDiff (Patm,1,mV250,2,True ,0,250,1.0,0)
  'multi_WN=(300/R_WN)*0.6=18
  PulseCount(WN_Pwr,1,2,0,1,18,0) ' Power in [Watts]
  Patm=(Patm-4*12.23)*25/(16*12.23*0.145037738)' R = 12.23 ohms
  CEP = (CEP-4*R_CEP)*500/(16*R_CEP*0.145037738)
  CEP = CEP+Patm ' Convert gauge pressure to absolute pressure
  SP = (SP-4*R_SP)*100/(16*R_SP*0.145037738) ' R = 12.04 ohms
  DP = (DP-4*R_DP)*1000/(16*R_DP*0.145037738)
  DP = DP+Patm ' Convert gauge pressure to absolute pressure
  'Pratio=DP/SP
  SatTemp(SP/1000,SST)
  SatTemp(DP/1000,SDT)
  SatTemp(CEP/1000,SCET)
  SSH_actual=ST-SST
  runpgm(TP)
  CallTable CntrlData
  ActuateValves(TP)
NextScan
SlowSequence
  DataTable (HTData,1,-1)
```

```
    DataInterval (0,dtt,Sec,0)
     'Sample(1,TP,FP2)
     Sample(1,CompPower,IEEE4)
     Sample(1,DischargeFlow,IEEE4)
     Sample(1,CW_T_in_stream,IEEE4)
     Sample(1,CW_T_out_stream,IEEE4)
   EndTable 'END table: HTData

   Scan(dtt,sec,0,0)
     AM25T(CWT(),2,mV7_5,1,1,TypeT,TrefAM25T,1,2,Vx1,True,0,_60Hz,1,0) 'AM25T Ch. 1-2
     AM25T(DischargeFlow,1,mV250,20,1,-1,TrefAM25T,1,2,0,True,0,_60Hz,1,0) 'AM25T Ch. 20
     AM25T(CompPower,1,mV2500,22,1,-1,TrefAM25T,1,2,0,True,0,_60Hz,5.4099,0) 'AM25T Ch. 22
     DischargeFlow=(DischargeFlow-4*35.93)*125*60/(16*35.93*2.20462262) 'Flow in kg/h
    CallTable HTData
   NextScan
 EndSequence

 SlowSequence
   DataTable (SlowData,1,-1)
     DataInterval (0,dtt2,Sec,0)
     Sample(1,TP,FP2)
     Sample(1,Patm,FP2)
     Sample(1,DT,IEEE4)
     Sample(1,SDT,FP2)
     Sample(1,DP,FP2)
     Sample(1,ST,FP2)
     Sample(1,SST,FP2)
     Sample(1,SP,FP2)
     Sample(1,CET,IEEE4)
     Sample(1,SCET,IEEE4)
     Sample(1,CEP,FP2)
     'Sample(1,EconT,IEEE4)
     Sample(1,CW_T_in,IEEE4)
     Sample(1,CW_T_out_stream_old,IEEE4)
     Sample(1,CW_T_mix,IEEE4)
     Sample(1,DomeT,IEEE4)
     Sample(1,SumpT,IEEE4)
     Sample(1,MotorT12,IEEE4)
     Sample(1,MotorT13,IEEE4)
     Sample(1,MotorT14,IEEE4)
   EndTable 'END table: SlowData
  Scan(dtt2,sec,0,0)
     AM25T(TempC(),12,mV25,3,1,TypeT,TrefAM25T,1,2,Vx1,False,0,_60Hz,1,0) 'AM25T Ch. 3-18
    CallTable SlowData
  NextScan
 EndSequence
EndProg
```

Bibliography

[1] Afjei, Th., P. Sutz, and D. Favra. 1992. Experimental analysis of an inverter-driven scroll compreesor with liquid ingestion. Proceedings of the International Compressor Engineering Conference, Purdue.

[2] ASHRAE. 2008. Compressors. *ASHRAE Handbook: HVAC Systems and Equipment*, Ch. 37.

[3] ARI. 1999. *ANSI/ARI 540-1999(R2002), Positive Displacement Refrigerant Compressors And Compressor Units.* Air Conditioning and Refrigeration Insittute.

[4] Armstrong, P., W. Jiang, D. Winiarski, S. Katipamula, and L.K. Norford. 2009. Efficient low-lift cooling with radiant distribution, thermal storage and variable-speed chiller controlsPart II: Annual energy use and savings estimates. *HVAC&R Research* 15(2):402-433.

[5] Armstrong, P.R., W. Jiang, D. Winiarski, S. Katipamula, L.K. Norford, and R.A. Willingham. 2009. Efficient low-lift cooling with radiant distribution, thermal storage and variable-speed chiller controls Part I: Component and subsystem models. *HVAC&R Research*15(2):366–401.

[6] Cuevas, C. and J. Lebrun. 2009. Testing and modelling of a variable speed scroll compressor. *Applied Thermal Engineering* 29(2) 469-478.

[7] Choi, J.M. and Y. C. Kim. 2002. The effects of improper refrigerant charge on the performance of a heat pump with an electronic expansion valve and capillary tube. *Energy* 27(4):391–404

[8] Conroy, C.L. and S.A. Mumma, 2001. "Ceiling radiant cooling panels as a viable distributed parallel sensible cooling technology integrated with dedicated outdoor-air systems." *ASHRAE Transactions.* 107(1).

[9] Cosling, C.T. 1980. Applied air conditioning and refrigeration, 2d ed. London: Applied Science. Comparison of three steady-state heal pump computer models. *ASHRAE Transactions* 96(2): 191–205.

[10] DOE. 2008. Buildings energy database. United States Department of Energy. <http://buildingsdatabook.eren.doe.gov>. (April 29, 2009).

[11] Finney, D. 1988. *Variable Frequency AC Motor Drive Systems.* IEE Power Engineering Series 8. London: Peter Peregrinus Ltd.

[12] Grace, I.N., D. Datta, and S.A. Tassou. 2004. Sensitivity of refrigeration system performance to charge levels and parameters for on-line leak detection. *Applied Thermal Engineering* 25(4):557–566.

[13] Gopal, M. 2008. *Control Systems: Principles and Design.* New York: McGraw-Hill.

[14] Incropera, F.P., D.P. DeWitt, T.L. Bergman, and A.S. Lavine. 2007. *Fundamentals of Heat and Mass Transfer, 6th Edition.* Hoboken, NJ: Wiley.

[15] Jahnig, D.I., D.T. Reindl, and S.A. Klein. 2000. A semi-empirical method for representing domestic refrigerator/ freezer compressor calorimeter test data. *ASHRAE Transactions* 106(2).

[16] Kulakowski, B.T., J. F. Garner, and J.L. Shearer. 2007 *Dynamic Modeling and Control of Engineering Control Systems.* 3rd Edition. New York: Cambridge Univeristy Press.

[17] Leung, Patrick Cheong-Yu,"Thermal Analysis of an Oil and R-22 Cooled Compressor Motor", Masters Thesis, Department of Mechanical Engineering, Massachusetts Institute of Technology, 1994

[18] McQuiston, F.C., J.D. Parker, and J.D. Spitler. 2005. *Heating, Ventilation, and Air Conditioning: Analysis and Design, 6th Edition.* Hoboken, NJ: Wiley.

[19] Mumma, S.A. 2002. Radiant Cooling Panel Cooling Systems. *ASHRAE*, Winter 2002. ASHRAE: Atlanta, GA

[20] Moran, M.J., and H.N. Shapiro. 2004. *Fundamentals of Engineering Thermodynamics, 5th Edition.* Hoboken, NJ: Wiley.

[21] Nanigian, Jake. 2003. From Where Do Errors Stem? *Process Heating* November 1, 2003. <http://www.process-heating.com/CDA/Archives/338d34329f268010VgnVCM100000f932a8c0> (May 12, 2009)

[22] National Institute of Standards and Technology. 2008. NIST ITS-90 Thermocouple Database. <http://srdata.nist.gov/its90/main/its90_main_page.html> (May 18, 2009)

[23] Otten, David. 2001. *Experimental Setup for Testing Refrigeration Scroll Compressors.* Unpublished.

[24] Qureshi, T.Q. ans S.A. Tassou. 1996. Variable speed capacity control in refrigeration systems. *Applied Thermal Engineering.* 16(2) 103-113.

[25] Popovic, P., and H.N. Shapiro. 1995. A semi-empirical method for modeling a reciprocating compressor in refrigeration system. ASHRAE Transactions 101(2):367-382.

[26] Purvis, E. 1987. Scroll compressor technology. Heat Pump Conference, New Orleans.

[27] Siegel, J.A. and C.P. Wray. 2002. Refrigerant Charge Diagnostics for Residential Cooling Systems. *ASHRAE Transactions.* 108(2).

[28] Tassou, S.A., and K.M. Lau. 1998. Low Energy Cooling Technologies - A Review. *Low-Energy Cooling Technologies For Buildings* Suffolk, UK: Professional Engineering Publishing Limited.

[29] Threlkeld, J.L. 1970. *Thermal Envrionmental Engineering, 2nd Edition.* Edgewood Ciffs, NJ: Prentice-Hall, Inc.

[30] Tojo, K. 1992. Performance analysis of hermetic scroll compressors. Proceedings of the International Compressor Engineering Conference, Purdue.

[31] Vargaraftik, N.B., Y. K. Vinogradov, and V.S. Yargin. 1996. *Handbook of Physical Properties of Liquids and Gase - Pure Substances and Mixtures.* 3rd Edition. New York: Begel House. 1277.

[32] Winandy, E., C. Saaverda, and J. Lebrun. 2002. Experimental analysis and simplified modelling of a hermetic scroll compressor. *Applied Thermal Engineering* 22(2) 107-120.

[33] Wulfinghoff, D.R. 1999. *Energy Efficiency Manual.* Wheaton, Md.: Energy Institute Press